

A method to develop patient-specific models for FE analysis of aortic root dilatation

Yachen Zhao (Master student of BME)

A thesis submitted to the School of Computer Science, Engineering and Mathematics in
the Faculty of Science and Engineering in total fulfilment of the requirements of the
degree of Master

Supervisor: Prof Karen Reynolds

Co-Supervisor: Dr Melissa Ryan

Flinders University of South Australia, Australia

Submitted October 2016

Contents

List of figure	III
List of table	X
Abstract	XI
Declaration	XII
Acknowledgement.....	XIII
Chapter 1 Background.....	1
1.1 Aortic dilatation and current treatment	1
1.2 Cardiovascular diseases computation	2
1.3 Aim and outline of project.....	3
Chapter 2 Introduction.....	4
2.1 physiology of aortic root and aortic aneurysm	4
2.1.1 Anatomy of the heart and aortic root	4
2.1.2 Cardiac cycle and mechanical change of aortic valve	7
2.1.3 Aortic aneurysm and influences.....	9
2.2 Introduction of FEA.....	11
2.2.1 FEA theory and application in FEA software	11
2.2.2 Environment selection.....	12
2.2.3 Decompose object.....	13
2.2.4 Assign boundary condition.....	13
2.2.5 Solve global equation	13
2.2.6 Supplementary calculation.....	13
2.3 Cardiac simulation	14
2.3.1 Cardiac simulation and medical application.....	14
2.3.2 History of aortic root model and patient specific modelling	14
2.4 Mechanical consideration in aortic root FEA model	15
2.4.1 Stress and strain	15
2.4.2 Young's module and shear module.....	15
Chapter 3 geometry reconstruction.....	17
3.1 Introduction.....	17
3.2 Aortic root segmentation	19
3.2.1 Image processing.....	19
3.2.2 Smoothing solid model.....	22
3.3 Surface model reconstruction	27
3.3.1 Aortic root reconstruction.....	28

3.3.2 Aortic leaflet rebuilding.....	31
Chapter 4 Material properties and boundary condition.....	41
4.1 Material properties	41
4.1.1 Material property of aortic root in other thesis.....	41
4.1.2 Determine element type	44
4.1.3 Coordinate system for aortic root model.....	46
4.1.4 Thickness	50
4.2 Boundary condition.....	51
4.2.2 Fixing.....	58
4.2.3 Loading	60
4.3 Mesh refinement.....	60
4.3.1 Intensive mesh in important place.....	61
4.3.2 Topology capture.....	61
4.3.3 Sizing and Mapping	61
4.2.4 Mesh connection.....	62
Chapter 5 Results.....	64
5.1 Results of model building	64
5.1.1 Image processing validation	64
5.1.2 Geometry validation.....	65
5.1.3 Mesh quality checking	69
5.1.4 Element normal checking.....	74
5.1.5 Contact	75
5.2 Mechanical results checking.....	79
5.2.1 Converge.....	79
5.2.2 Maximum stress and strain	81
Chapter 6 Discussion	86
6.1 Geometry.....	86
6.2 Material property and boundary condition	86
6.3 Model convergence.....	88
6.4 Mechanical results.....	92
6.4.1 Aortic leaflet	92
6.4.2 Aortic root	93
Chapter 7 Conclusion	94
7.1 Method of geometry reconstruction.....	94
7.2 Method of simulation assignment	95
Reference	96

List of figure

Figure 1. Normal aortic root (left) and aortic root having disease of an aortic aneurysm (right)	1
Figure 2 Aortic root aneurysm (left) and surgery procedure (right).....	2
Figure 3. The anatomy of heart.....	4
Figure 4. The anatomy of aortic root.....	5
Figure 5. The front view of aortic leaflet	5
Figure 6. The aortic root includes aortic wall and aortic leaflets. The sinutubular junction and annulus is two important rings combining three hinge lines define the crown geometry of the aortic root main features (Sievers and Schmidtke, 2007)	7
Figure 7. Aortic valve open at the begin of systole and close at the end of diastole, which corresponding the top of R wave and end of T wave signal in the ECG respectively (Wong et al., 2010).....	8
Figure 8. Valve status during diastole and systole of the cardiac circle.....	9
Figure 9. Saccular aneurysm (left) and fusiform (right).....	10
Figure 10 Aortic root patient specific 3D solid model image.....	15
Figure 11 typical stress -strain curve formed by two parts. The first part is elastic region. During this region, stress value increases as strain enhancing. This part of the curve has constant slope value which named 'Young's modulus'. Elastic region finish at yield strength. After experiencing a small decrease, the stress value re-increase till ultimate strength and the curve end at material fracture point. The region form yield strength to fracture point is called non-linear region.....	16
Figure 12 Patient aortic root model with three leaflets connected to interactive triangle and sinus connected to aortic ascending (Jermihov, 2013).....	17
Figure 13 Patient specific model with continuous geometry from aortic root to interactive triangle	17
Figure 14 Picture shows the location of aortic root at the CT data image	19

Figure 15 Using different window filter to modify back ground	20
Figure 16 Aortic root after the 'Fill' image processing	21
Figure 17. Edge segmentation process of the aortic root.....	22
Figure 18 RC leaflets before smooth (left) and after smooth (right)	22
Figure 19 A mask filling all the work space.....	23
Figure 20 An inverse mask of aortic root was generated (picture at left shows the side cross section view of mask, and picture at right shows the top view of mask).....	23
Figure 21. Fine smooth at hinge line in cross section view	24
Figure 22. Sharp angle of two mask in cross section view.....	24
Figure 23 there is a large gap between aortic leaflets at the initial segmentation (picture A, B, C). After one pixel enlargement of the mask, the gap was filled. (picture D, E, F).....	25
Figure 24 Boolean to remove the overlap volume (Boolean three leaflets follow the order of clockwise or anticlockwise. An example shows in yellow arrow in Figure 24).....	26
Figure 25 The smoothing of the mask reduces mask outline (the non-smoothed leaflet at yellow, the smoothed leaflet at light blue)	26
Figure 26 Picture A and B illustrate the side view and bottom view of the non-smoothed aortic root, and C shows the top view of the non-smoothed three leaflets. Picture D and F illustrate the side view and bottom view of smoothed aortic root, and F shows the top view of the smoothed three leaflets.....	27
Figure 27. Low curvature at aortic leaflet but gap in the hinge line.....	27
Figure 28 Importing setting of the geometry. Noticed that the operation is 'add Frozen'; both Solid body column and surface body column are 'yes'.	29
Figure 29 Side view of Aortic root solid body after importing to the ANSYS 15.0.....	29
Figure 30 Solid body of aortic root (side view at left and top view at right)	30
Figure 31 select all the surface at the side which represent aortic root geometry.....	30

Figure 32 generate a surfaced body formed only surfaces	30
Figure 33 Virtual faces reducing multi-faces to three faces. Each of the faces contains one sinus	31
Figure 34 Mesh before virtual body (left). Generating mesh is limited by the initial faces. Mesh after the virtual body (right) generates mesh depending on geometry surface feature.....	31
Figure 35 Pick two hinge line button at XZ plane and assign the line formed by those two points to the new Y Axis. Repeat this process in the YZ plane of the image data. Pick hinge line bottom but assign to the new X Axis this time	32
Figure 36 Central line of the aortic root can help define the three tips of aortic leaflet and other important parameters.....	33
Figure 37 the land mark of three button points of hinge line (red), two ostium (blue), three leaflet tips (yellow), and three commissures (green) during the diastole of the cardiac circle	33
Figure 38 (a) The three commissure (red point) of aortic root formed a ring geometry, and the three bottom point of hinge ling formed another ring geometry. The plate of two rings does not need parallel. (b) the aortic root ...	34
Figure 39 Three solid bodies which donates to three leaflets separately	34
Figure 40 Find hinge line and reduce the solid leaflets body mask begin at the hinge line (hinge line located at the transient change of green and blue colour from this picture).....	35
Figure 41 Aortic leaflets were directly selected from the solid IGES model	36
Figure 42. Aortic root and aortic leaflets are on different surfaces, the gap between them are filled by new surface	36
Figure 43 Failed model with geometry (left) and mesh (right)	37
Figure 44. Yellow curves highlight in the picture show the free edge of the aortic leaflet (top) and hinge line (bottom).....	37
Figure 45 Top view of aortic leaflets and aortic root.....	38
Figure 46. Side view of aortic leaflets. Noticed that those aortic leaflets are not fully repeated the feature of aortic leaflets at the diastole of the cardiac circle	38

Figure 47. The fitting leaflets compare to the normal solid leaflets (front view at left and back view at right).....	38
Figure 48 Top view of aortic three leaflets after importing to ANSYS 15.0 with leaflets initial position (left) and moved position (right)	39
Figure 49 Side view of single leaflet generation process. Firstly, fitting curve along with the surface of aortic leaflet (left). Secondly, using curves to create new surface to represent the surface of aortic leaflet (right)	40
Figure 50. Front view (right) and top view (left) of fitting leaflet and the initial solid geometry (high light in the yellow colour).....	40
Figure 51. Front view of single fitting leaflet	40
Figure 52. Three layers of aortic leaflets which are ventricularis and fibrosa at the two outsides and spongios tissue at the middle. (Vesely and Noseworthy, 1992)	41
Figure 53. Definition of circumferential and radial orientation for Aortic leaflet (Vesely and Noseworthy, 1992).....	42
Figure 54. Stress – strain curve illustration transition, pre-transition and post transition mechanics (Helsen and Missirlis, 2010).....	43
Figure 55. Fibre orientation at the aortic leaflets.....	43
Figure 56 Shell element with four nodes (left) and with three nodes (right). In the four nodes element, node I, J, K, L locate at the four angles top of the rectangular geometry. In the three nodes shell elements, nodes K and L reduce to one node.....	44
Figure 57 Shell element 181. The element has four nodes. L and K node constrain to one node when we use triangle element. Local coordinate system X, Y, and Z are shown in the picture	45
Figure 58 Shell joint at the Ansys software	46
Figure 59. Different types of coordinate systems in ANSYS 15.0 (a) Cartesian coordinate system with components in X, Y, Z (b) Cylindrical coordinate system with components in R, θ , Z orientations (c) Spherical coordinate system with components R, θ , ϕ orientations d) Cylindrical coordinate system with components R, θ , Y orientations (ANSYS, 2013).....	47
Figure 60. Aortic root in the simulation in the cylinder coordinate system. Aortic wall is in circumferential orientation. The aortic root aligns to	

longitudinal orientation. The aortic leaflet is located in the radial orientation from the contact point of three leaflets point to the aortic wall.....48

Figure 61. Cylinder system which shows longitudinal component z , radial component x and circumferential component y 49

Figure 62 X, Y, and Z component in ANSYS workbench Cartesian coordinate system (left) and in Cylinder coordinate system (right).....49

Figure 63. Local shell coordinate system is a Cartesian coordinate system with three component alignment orthogonal directions (left). The shell coordinate system alignment during aligning the shell element to the cylinder system (right). Local shell element y -axis transpose to the global longitudinal component; Local shell element x -axis transpose to the circumferential element; local z -axis aligns to a radial orientation.50

Figure 64 Movement of contact bodies causes different iteration. The two bodies can stay in small contact (situation shown in the left), push away from each other (situation shown in the middle), or generate large penetration (situation shown in the right). Iteration value is the results of applying iterative method. Iterative method helps increasing surface converge ability when solving FE problems. More details of this method can be found in Oysu (2007).....53

Figure 65 when coarse mesh body be the target body (left), the 'contact' is recognized properly. When the coarse mesh body be the contact body (right), the 'contact' dose not be detected properly.54

Figure 66 Different methods use different gap algorithm56

Figure 67 Integration detection method detect contact from integration points (left) while nodal detection method detect contact by the nodes at mesh (right)57

Figure 68 contact is detected when the contact body close to the target body57

Figure 69 Loading circle of aortic root (modified from Grande et al, 1997)60

Figure 70 Typical mesh connection.....62

Figure 71 Mesh connection method combine two separated geometries when meshing63

Figure 72 The leaflet volume that connecting to commissure is reduced significant during smoothing.....65

Figure 73. Position of Cusp- Commissure (solid line) and Cusp- Cusp measurement (dash line)	66
Figure 74 Relative value at aortic leaflet when STJ diameter is 1 (note where is the value A, and B)(Nataf and Lansac, 2006)	67
Figure 75 Relative value at aortic root when STJ diameter is 1 (note where is α and φ , those two angles are measured in the table 6)(Nataf and Lansac, 2006)	68
Figure 76 Button view of the aortic root. The aortic wall is outside body and the three leaflets are inside bodies.....	70
Figure 77 Front view of aortic leaflets	70
Figure 78 Error increase as aspect ratio far away from 1	72
Figure 79 Small blue arrows show element normal. All the element normal point to the outside of the aortic root.....	74
Figure 80 Inner alignment of element normal at the aortic root model (cutting half view). Small green arrows represent element Y axis and small red arrow point to element X axis. Element normal aligns uniform along the aortic root.	74
Figure 81 The alignment of aortic leaflet shows that the main orientation of small red arrows along at circumferential orientation	75
Figure 82 Vector of element shows similar alignment as in element normal....	75
Figure 83. Real loading process in the model simulation	77
Figure 84. Penetration over the whole process.....	77
Figure 85 Penetration when the loading achieves maximum (at 125.5s)	78
Figure 86 Overall process displacement residual converge	79
Figure 87 Force residual converge of aortic root model in 50 points view.....	80
Figure 88 Displacement residual converge of aortic root model in 50 points view.....	81
Figure 89. Moment residual converge of aortic root model in 50 points view .	81
Figure 90 Aortic leaflets and their maximum stresses (A. RC leaflet B. NC leaflet C. LC leaflet Unit: MPa)	83

Figure 91 Aortic leaflets and their maximum strains (A. RC leaflet B. NC leaflet C. LC leaflet)	83
Figure 92 Stress (left) and strain (right) distribution at the surface of the non-coronary sinus.....	84
Figure 93 Stress (left) and strain (right) distribution at the surface of the right coronary sinus.....	85
Figure 94 Stress (left) and strain (right) distribution at the surface of the left coronary sinus.....	85
Figure 95 Aortic root with cylinder coordinate system. The original point of the aortic root is located at the central point of button plane of the whole aortic root.....	87
Figure 96 Stress – strain curve in aortic leaflet (Wang et al., 2012)	87
Figure 97 Contact status at leaflet including three leaflets view.....	88
Figure 98 Contact status of single leaflet view	89
Figure 99 Low quality mesh located at leaflet attachment and the hinge line of aortic root.....	90
Figure 100 initial overlapping body in the second model.....	90
Figure 101 Initial contact body assignment in second geometry model have a lot of warnings. Even though all the warning is accessible, the figure shows the assemble are not in a desire contact status.....	91
Figure 102 Second model can run when leaflets do not detect contact (left) and the aortic leaflet simulation failed with high stress at contact parts of two leaflets (right)	92
Figure 103 The initial geometry of commissure(left) and the meshed bodies at commissure (right)	93

List of table

Table 1. Material property from Grande et al. (1997)	44
Table 2 Review of thickness for aortic root and leaflets	50
Table 3 Assignment of aortic root in ANSYS scope and definition part.....	59
Table 4. Data comparison of before and after soothing	64
Table 5 Aortic root measurement	66
Table 6 Aortic root geometry validation.....	68
Table 7. Surface area of aortic root.....	69
Table 8 Aortic root mesh quality checking	73
Table 9 initial contact table.....	76
Table 10 Overall process contact checking	78
Table 11 Maximum and minimum aortic leaflet stress and strain value	81
Table 12 Maximum stress and strain value of aortic wall	84

Abstract

Risk evaluation for surgery in aortic aneurysm disease should be considered fully. Patient-specific model increases the accuracy of simulation results by rebuilding mathematical models from real patients CT Scan images. Patient-specific model for dilatation of the aortic root has been studied by Grande et al. (1997), however, little information is provided with regards to the methods for the model development. A standardised methodology would allow a streamlined process for developing patient specific models that may be used for pre-operative planning, or in the decision making of when to operate.

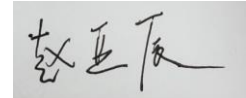
In this study, a patient specific model method for dilatation aortic root study was developed. This method generating a model from CT image data. Then, the initial model was smoothed and generated in ScanIP. After creating aortic leaflets in ANSYS, combine the leaflets and the aortic wall in ANSYS DesignModeler to have a complete aortic root model. Finally, the aortic root model is simulated in ANSYS and validated by previous studies.

The maximum stresses are 0.864 MPa at Right-Coronary leaflet, 1.03MPa at Left-Coronary leaflet, while the Non-Coronary leaflet has the largest value 1.19MPa. Right-Coronary leaflet has an extreme maximum strain value of 0.404, which is followed by Non-Coronary leaflet (0.273 maximum strain). Left-Coronary leaflet has 0.228 maximum strain.

This method contributes to feature patient specific model building. It is a dilated aortic root from real patient rather than a dilatation aortic root model simulated from normal aortic root.

Declaration

I certify that this work does not incorporate without acknowledgment any material previously submitted for a degree or diploma in any university, and that to the best of my knowledge and belief it does not contain any material previously published or written by another person except where due reference is made in the text.

A rectangular box containing a handwritten signature in Chinese characters, which appears to be '赵亚辰' (Zhao Yachen).

Date: 2017.03.27

Acknowledgement

I would like to offer my special thanks to my supervisor Professor Karen Reynolds and Dr. Melissa Ryan introduce me join in this fantastic project. Thanks for all your help and because of your help I can achieve what I have so far. Karen, thanks for your time, your hearing, and your supports. I always can get energy from talking with you. Mel, you are a so kind, and you are my strong support. I am so lucky to have you always there. Thanks for help from Mr. James Edwards Edwards (Ashford Hospital), Dr. Jason Varzaly (Ashford Hospital). We cannot start this project without your image data support. Thanks for your patient, your understanding, and your high capability in problem solving. I also would like to thanks for technical help from Professor Mark Taylor and Dr. Saulo Martelli. Thanks for your technique help in this project.

Next, I would like to thanks all my friends who helped me with the project. I could not finish the review without your help. The last but not latest, I would like to thanks my family. Thanks for the support from my husband, my mum, and my dad. I would not go this far without you. I love you all.

It is a challenge to study in a country with totally different cultural and language. There are some periods I need passing through along after initial curiosity gone. I am pride for myself for choosing this way and I am lucky to experience so many kindnesses in a lovely city.

Chapter 1 Background

1.1 Aortic dilatation and current treatment

The cardiac disease is one of the critically important problem in the human diseases. The number of people died as a result of cardiac disease has increased during last decades (Tu et al., 2015). Aortic aneurysms have become the 13th high risk disease that results of death in the western countries (Bickerstaff et al., 1982). Dilation of the aortic root is one type of aortic aneurysms (Nataf and Lansac, 2006), which results in an increase of aortic diameter. The result of this is aortic valves that do not fully close at diastole. The non-closed valve cannot stop blood flow back to heart efficiently, which can lead to other heart conditions (Schwartz et al., 2004, Roman et al., 1987, Chong et al., 2006). Studies have shown that aortic root dilatation is related to annulo-ectasia, Marfan syndrome, Bicuspid aortic valve and other diseases (Isselbacher, 2005). An aortic aneurysm can be identified via medical CT by resembling a pear shape (Figure 1).

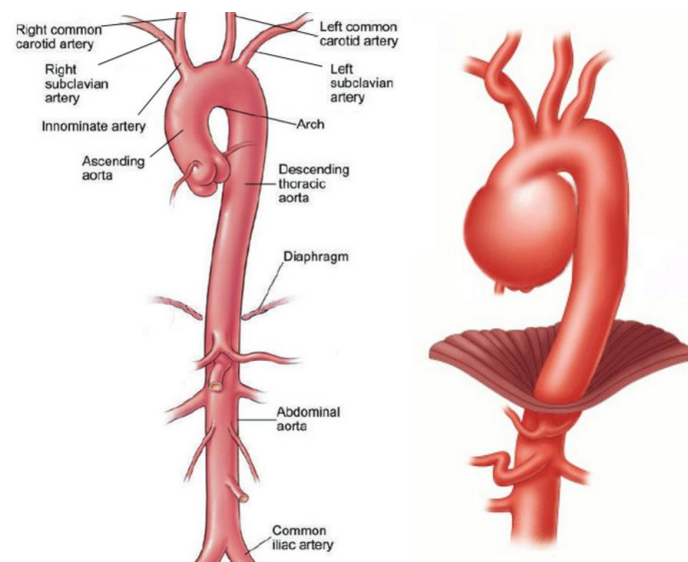


Figure 1. Normal aortic root (left) and aortic root having disease of an aortic aneurysm (right)

One of the treatments for aortic root dilatation is valve-sparing aortic root replacement. The basic procedure of treatment includes excising aortic valve and replacing it with artificial tissue such as Dacron (Figure 2).

Trimarchi et al. (2004) reported the outcome of type A aortic dissection is highly related to individual, which confirmed the importance of the guideline.

Surgery risks are highly dependent on patients' family disease history, living habits, age, and current health situation (Brown et al., 2009). Since the risks of surgery vary from person to person, (Guideline) classified dangerous level and suggested to do surgery when the benefits of surgery are highly over risks.

However, the classification of aortic aneurysm in Guideline does not have sufficient medical evidence. It has been questioned by Leyh et al. (2002) about extreme failure rate in acute type A aortic dissection. On the other side, Kerendi et al. (2010) proved that the safety of valve-sparing aortic root replacement surgery with acute dissection and reoperations.

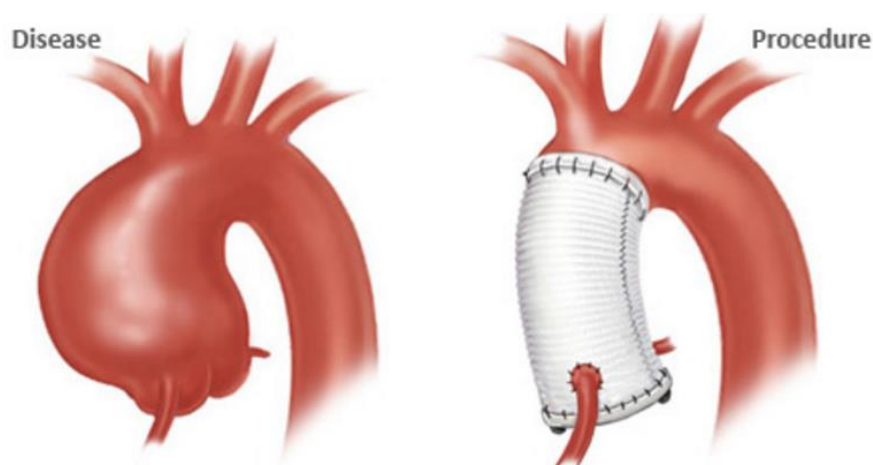


Figure 2 Aortic root aneurysm (left) and surgery procedure (right)

1.2 Cardiovascular diseases computation

With increasing computational technology in recent years, the ability of computation increases rapidly. It is possible to perform complex numerical calculations, such as mechanical movement of human tissue. Numerical model can help researchers to predict the behaviour of tissues. The main applications of the biomedical simulation are academic researches and training surgeons (Krummen et al., 2010). The study of aortic root disease also can acquire numerical simulation method.

Patient specific model is a branch of biomedical simulation which rises in recent years. The aim of the patient specific model is building a model with accurate geometry. The model usually develops from CT, MRI or ultrasound imaging (Krummen et al., 2010).

1.3 Aim and outline of project

This purpose of this study includes:

1. Develop the method of establishing patient – specific model from CT image
2. Assignment consideration of finite element model in ANSYS 15.0

The results will contribute to further studies and analysis which provides evidence to help understand risks, classification of aortic dilatation and help doctors have a medical diagnosis.

This thesis is divided into eight chapters. The first chapter illustrates the aim outline of this thesis. The second chapter provides an introduction to the anatomy and function of the aortic root. The third chapter explains the mechanical and finite element theory. The fourth chapter gives information about image processing and geometry building. The fifth chapter shows the methodology of FEA model establishment. The sixth chapter collect results from finite element model solver. The following chapter discusses the FE analysis. The final chapter concludes this projects and outlines future works.

Chapter 2 Introduction

2.1 physiology of aortic root and aortic aneurysm

2.1.1 Anatomy of the heart and aortic root

Heart supports body function by delivering oxygenated blood to all the organs and collect all the de-oxygenated blood back to the lungs. The oxygenated blood is delivered by coronary circulation, which is pumped by the left half of the heart. On the other hand, de-oxygenated blood is expelled by the pulmonary circulation, which is controlled by the right side of the heart. The heart is divided in to two sides and each side is separated into two cavities by the mitral valve and tricuspid valves respectively (Figure 3).

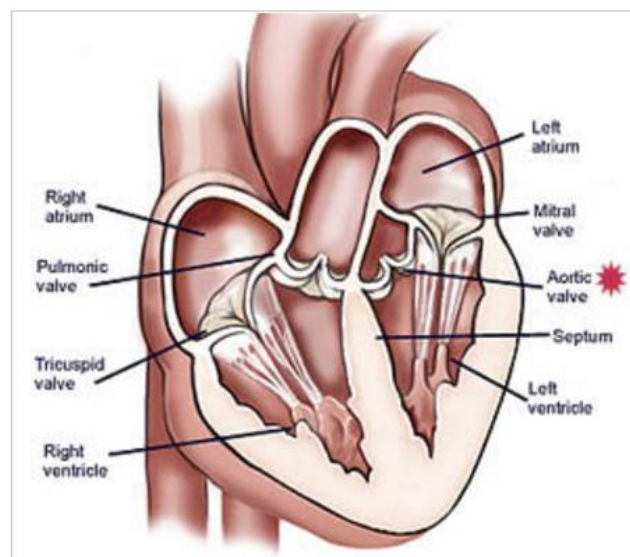


Figure 3. The anatomy of heart

Note the position of aortic valve and aortic root in the cardiac system (aortic valve is highlight with red point)

The aortic root is located at the connection between the aorta and the left ventricle. The aortic valve connects the aortic root to the heart, and separates the spaces of the aorta and left ventricle. The main geometry of aortic root includes ascending of the aorta, three sinuses, inter-leaflet triangle and three leaflets in the sinuses (Figure 4).

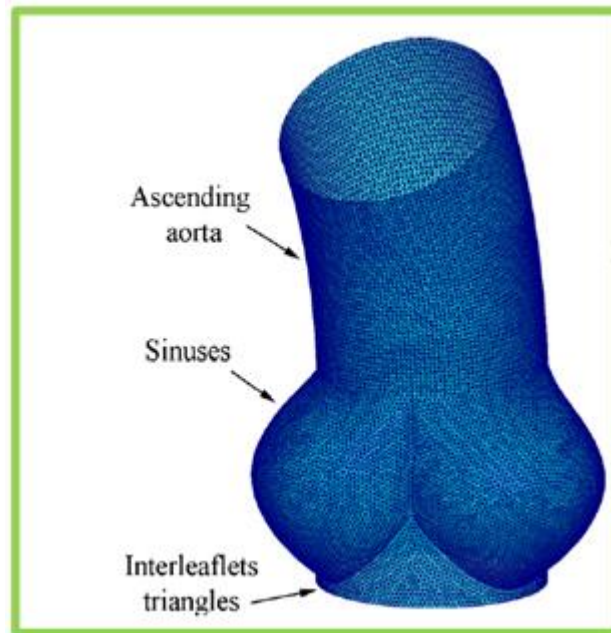


Figure 4. The anatomy of aortic root

From top to bottom, aortic root includes aortic ascending, sinuses, valves (in the sinuses), and interleaflets triangle

Leaflets of aortic root are named by the associated coronary arteries. The three leaflets are left coronary (LC), right coronary (RC) and non-coronary (NC) leaflets. Each leaflet of the aortic root is divided into four parts (figure 5). Free margin is at the top of the aortic leaflets. Coaptation area allocated at the region below the free margin. Belly is at the lower parts of the aortic leaflets, combining coaptation area, and those two parts account most area of aortic valves. The last part is attachment area, which is a region that connects leaflet to the aortic wall.

Coaptation area will attach to other leaflets during the diastole of the cardiac cycle, while belly area only undergoes blood pressure.

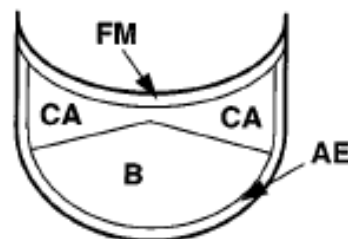


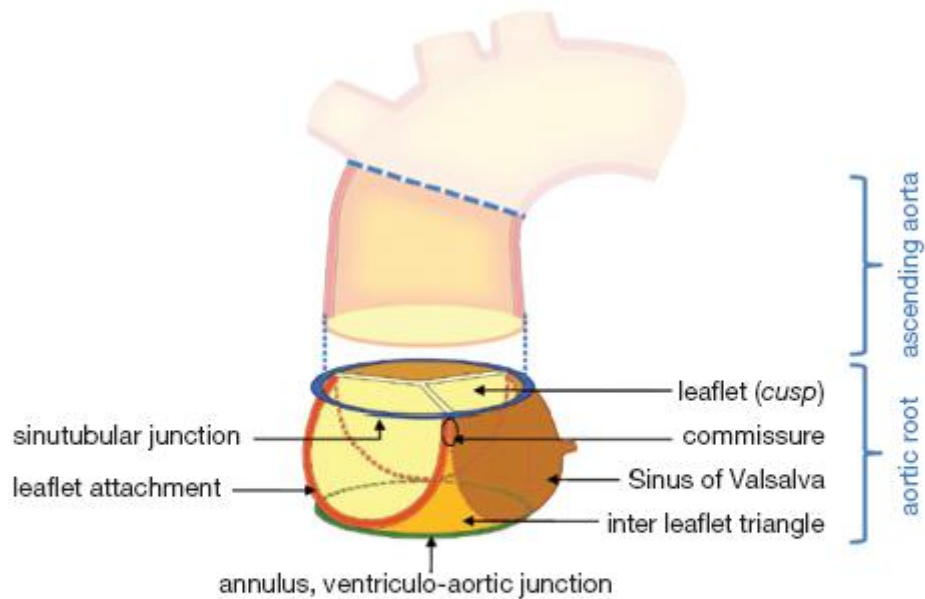
Figure 5. The front view of aortic leaflet

free margin (FM), coaptation area (CA), belly (B), and attached edge (AE)
(Grande et al., 1997)

Coronary ostium is the connection part of sinus and coronary arteries. Since ostium only exists at left and right coronary sinus, ostium makes three sinus has different anatomies. However, the functional aspect of three sinus shows that they have identical mechanics (Saremi, 2011).

Leaflets of the aortic root and corresponding aortic wall form Valsalva sinuses. Three sinuses are named as the same as aortic valves which are left coronary sinus, right coronary sinus, and non-coronary sinus.

There are two important cross sections at the aortic root. The cross sections are encountered to the clinic consideration of geometry of aortic root. They are annulus and sinutubular junction. 'Annulus' located at the bottom of hinge line of three sinuses. The length of the annulus is Indicator to determine an aortic aneurysm. Sinutubular junction is a ring geometry address at begin of the aortic root and the end of aortic ascending (Figure 6). The diameter of STJ can help recheck the measurement of the rest part of the aortic root.



aortic valve:	Three leaflets only
aortic root:	All components (<i>Sinuses of Valsalva, inter leaflet triangles, sinutubular junction, leaflet attachments, leaflets, annulus</i>)

Figure 6. The aortic root includes aortic wall and aortic leaflets. The sinutubular junction and annulus is two important rings combining three hinge lines define the crown geometry of the aortic root main features (Sievers and Schmidtke, 2007)

Commissures are the combination of leaflet attachment line (Figure 6). The position of commissure indicates the height of valves, which is crucial for the fitting valve.

2.1.2 Cardiac cycle and mechanical change of aortic valve

Cardiac cycle describes the series of events during one pump of heart. A normal heart rate for an adult commonly is 60–90 beats/min (bpm). In general, one cardiac cycle comprises systole and diastole phases, which correspond to the contracting and relaxing process of myocardial tissue (Tu et al., 2015).

The function of aortic root and coronaries are crucial in cardiac system and the cardiac system is one of the most important systems of human body. People's

body function is support by oxygen in the blood, and aortic root domains blood pumping. The key thing of operation of blood cycle is sufficient blood pump out from the left ventricle.

The aortic valve opening in the systole and closing at diastole depends on the pressure change in the ventricle and the artery (Figure 7 & Figure 8). During diastole the three valve contact to each other. The contact area of aortic valves is called coaptation area (refers to Figure 5), and the state of valves at coaptation is called coaptating. Closed aortic leaflets prevent blood flowing back to the heart and make sure sufficient blood enters bodies circulation.

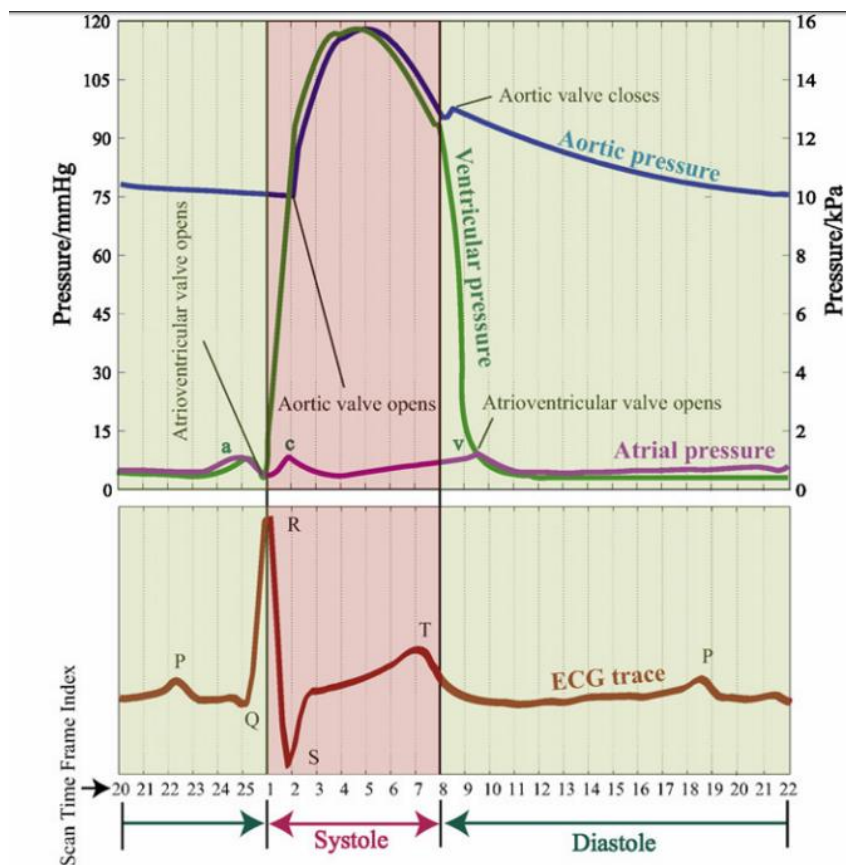


Figure 7. Aortic valve open at the begin of systole and close at the end of diastole, which corresponding the top of R wave and end of T wave signal in the ECG respectively (Wong et al., 2010)

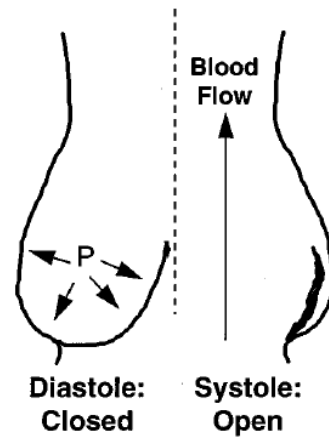


Figure 8. Valve status during diastole and systole of the cardiac cycle.

Aortic pressure higher than the ventricular pressure during diastole, which causes aortic valve closed. Aortic pressure smaller than the ventricular pressure which pushes the aortic leaflet open at the systole of the cardiac cycle. (Grande et al., 1997)

2.1.3 Aortic aneurysm and influences

Aortic aneurysm mainly results from atherosclerosis, hypertension, aging, marfan syndrome and bicuspid aortic leaflet. Abnormal aortic root means that three aortic valves cannot coaptate together. Therefore, Blood leak from the artery to the ventricle. The leakage changes the pressure of ventricle and causes heart diseases.



Figure 9. Saccular aneurysm (left) and fusiform (right)

Saccular or fusiform are two categories of aneurysms (Figure 9). Those two types are defined by their geometry. Aortic aneurysm commonly results in an increase of diameter by 5 mm ~ 20 mm. Saccular aneurysms are extra lumen of spherical shape. This type of disease affects a small length of the blood vessel. Alternatively, the fusiform aneurysm is spindle - shape cavity which has a influence of larger length at the blood vessel. Aortic dilatation generally is a fusiform type disease (Tu et al., 2015).

The degeneration of aortic aneurysms results of severe bleeding and other complications. Additional severe disease may lead to death. However, aortic aneurysms are very common in the older population. Meirelles et al. (2007) illustrated that almost 8.9 percent of the population who is 65 years and over 65 years suffering from this disease. Patients generally do not display any symptoms, so the main treatment would be the non-surgical method if the risk of rupture remains low, as determined by surgeons. Maximum diameter criterion is the most general method to evaluate risks in the aortic dilatation surgery (Hiratzka et al., 2010). Patients are recommended to undergo surgery if the growth rate of the aneurysm is higher than 10mm per year (Hiratzka et al., 2010).

2.2 Introduction of FEA

2.2.1 FEA theory and application in FEA software

Finite element method is a procedure of solving physical problem by establishing the numerical model. It is a method of using an approximation value to represent unknown information. In engineering, it helps simplify real world problem. The results of solution can predict numerical data for engineering analysis. The initial analysis of FE model is for the structural problem and their application now has extended to fluid, thermal, electronic, and the combination of multi-phase analysis.

Mathematically, the basic theory of establishing model can be divided into several steps:

First, an object is broken down into micro pieces which called element. The behaviour of elements determined by the interaction function of nodes which are defined by the user.

An individual matrix, then, was using to illustrate the numerical relationship of nodes in each element. For instance, static mechanical model is looking for displacements and the load distributions of the structure. the approximate value of individual matrix can be given from:

$$[k]_e \{\delta\}_e = \{F\}$$

where $[k]_e$ represents individual stiffness matrix, $\{\delta\}_e$ represents vector of nodal deflation and $\{F\}$ is force in different orientations of local coordinate system. It can be observed that the essential of finite element methods is displacement calculation.

In a continuum, individual matrixes are assembled to global matrix. The combination process depends on the location of elements addressing in the global coordinate. Then, boundary conditions of the assembling are required to obtain further constraint.

Finally, an external force is applied on the model and the mathematical calculation is solved by a computational machine. Results return possible approximate stress and displacement values for each node. Apart from stresses, additionally information, such as strain energy, average stress, and strain, stresses and strains distribution at one plane, also can be given by further calculations.

FEA software represents all the processes in three phases: pre-processing, solving, and post-processing. Third party software embeds all the mathematical calculation processes in the solver. Pre-processing requires users to assign all the known information of models, which include material properties, boundary conditions and formulations for solving a model. Post-processing includes some further calculation and visualization of results. Hence, to ensure commercial software solving a problem correctly and validly, researches should assign proper information to the pre-processor. All in all, the essential steps of building finite element model must include:

- Environment selection
- Decompose object
- Determine element properties
- Assign proper boundary condition
- Solve global equation
- Supplementary calculation

2.2.2 Environment selection

As mentioned before, FEA can be applied in the multiple environments. Features and formulations vary in different environments. The most basic environment is steady state. Steady state is good for solid body movement studies. For linear material, material properties do not change as the variation of temperature.

The other environments can solve further problems such as physical field changing and interaction of solid and fluid. Multi-environment problems are not required for current study, so we do not have to illustrate details of them.

2.2.3 Decompose object

ANSYS workbench simulation base on the model structure, which means geometry should be provided before simulation. Geometry building process briefly performed real world problems in the ways that can be solved by FEA software.

The geometry can be built in surface bodies, solid bodies or both. Surface model focus on studying mechanical change at the surface, such as share force and strain change, while the solid model provides the deformation of solid volume and interaction between parts and assemblies. Aortic root is a cylinder model which is formed by thin soft tissue, so surface model can well explain the mechanical at the aortic root.

2.2.4 Assign boundary condition

Boundary condition refers to forces and constraints in the FE model. The boundaries of the geometry are main positions to assign constrains. The external and internal object that stopping movement of parts also provides boundary. For example, contact and fixed supply are the boundaries of models.

2.2.5 Solve global equation

The ANSYS 15.0 Workbench and ANSYS APDL have the same solver during dealing with problems of steady structure. Various information can be track during ANSYS 15.0 solver.

2.2.6 Supplementary calculation

Supplementary calculation is post processing. This calculation using informed data to provide further information such as the maximum and minimum value of stresses and strains. Moreover, it helps people visual results and directly observe variable distribution at bodies.

2.3 Cardiac simulation

2.3.1 Cardiac simulation and medical application

The main application of computational image and visualization technology in medical area have two different aspects. The diagnosis of cardiovascular diseases has vastly improved due to the advancement of imaging techniques (Banerjee et al. 2000). Apart from directly using the computationally technique in medical diagnose, the high function of image processing ability also is used in prediction of cardiac failure and hemodynamic movement behavior studies.

Cardiac simulation studies use image-based models to simulate the behavior of heart during the cardiac cycle. Studies aim to analyses and diagnose disease and failing process of heart pumping. To simulate a model, we firstly need a geometry. Then, the model is explained and formed by micro points. After that, particular constraints and parameters are assigned to the model. The basic cardiac simulation includes three areas of knowledge which are: Medical imaging and computer aided design, the basic concept of FEA, computational capability.

2.3.2 History of aortic root model and patient specific modelling

Most previous models assumed that three aortic valves were identical (Labrosse et al., 2006). At the same time, they build valve in symmetrical objects and simulate the function of the aortic valve in a straight tube. The real dynamic function of the aortic leaflet is far away from identical valves model. The asymmetrical property of the leaflet has been well recognized (Lansac et al., 2005). Grande and their teams built a patient specific model with an asymmetrical aortic valve (Grande et al., 1997, Grande et al., 2000, Grande-Allen et al., 2001a, Grande-Allen et al., 2000). Different stresses and strains value was found in individual valves. This method has been proved by Conti et al. (2010b).

Recent decades, patient specific modelling has raised as a new branch of medical modelling.

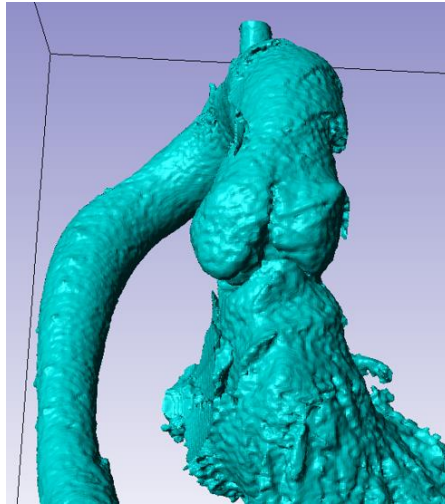


Figure 10 Aortic root patient specific 3D solid model image

2.4 Mechanical consideration in aortic root FEA model

2.4.1 Stress and strain

Stress and strain use to predict the behavior of materials, and return ultimate state results. Moreover, strain - stress curves are widely regard to important mechanical properties of materials. In this study, we observe the strain and stress distribution vary with addresses and time to analyses and predict the behavior of aortic leaflets.

2.4.2 Young's module and shear module

Young's modulus (E) refers to the slope of stress - strain curve. For elastic materials, the value of Young's module does not change with time, while for the nonlinear model, the slope of stress - strain curve varies with strain or stress value changing. Young's module can be given by:

$$E = \frac{\sigma}{\varepsilon}$$

Hooke's Law describes the stiffness of material. Stiffness is positively proportional to Young's module. The increase of stiffness makes materials harder, while the decrease of stiffness change materials softer. Hard material has a high tolerance of bending force. On the contrary, soft materials such as aortic roots are compatible with large force distribution.

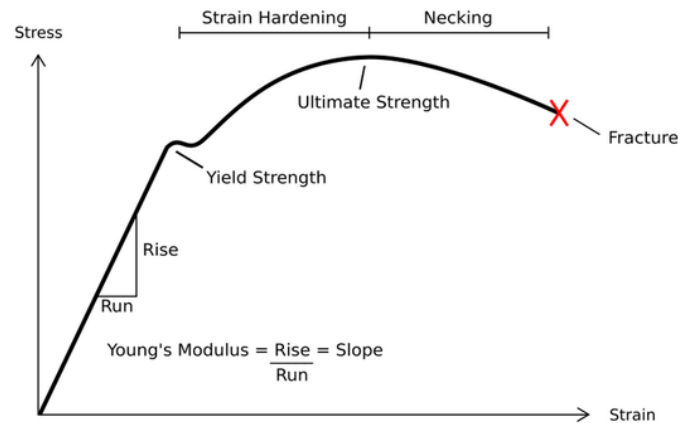


Figure 11 typical stress -strain curve formed by two parts. The first part is elastic region. During this region, stress value increases as strain enhancing. This part of the curve has constant slope value which named 'Young's modulus'. Elastic region finish at yield strength. After experiencing a small decrease, the stress value re-increase till ultimate strength and the curve end at material fracture point. The region form yield strength to fracture point is called non-linear region.

Apart from Young's modulus which defines mechanical property in tension and compression direction, shear modulus (G) defines mechanical properties in shear direction. Shear strain (γ) indicates the rotation of object, which equals to θ . The relationship of shear module, shear strain, and shear stress (τ) is

$$\tau = G\gamma$$

Poisson's ratio (ν) illustrates transverse strain over axial strain. It represents a small expansion in the compressive direction.

Aortic roots and aortic leaflets are soft tissues undergoing pressures from inner body environment and blood pressure in the aorta.

Chapter 3 geometry reconstruction

3.1 Introduction

There are two methods to build patient specific aortic root geometry model. The first method is building aortic root into the aortic root and aortic leaflets parts. The aortic root parts include sinuses and ascending aorta, and the rest parts are the aortic leaflets and interactive triangle. The second method establishes aortic root wall and interactive triangle into one surface and connects three leaflets to the aortic wall.

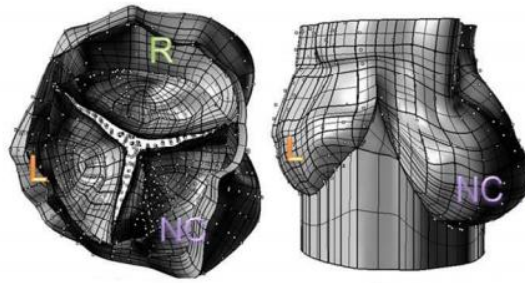


Figure 12 Patient aortic root model with three leaflets connected to interactive triangle and sinus connected to aortic ascending (Jermihov, 2013)

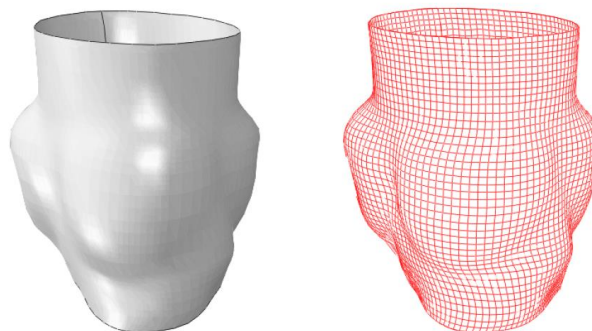
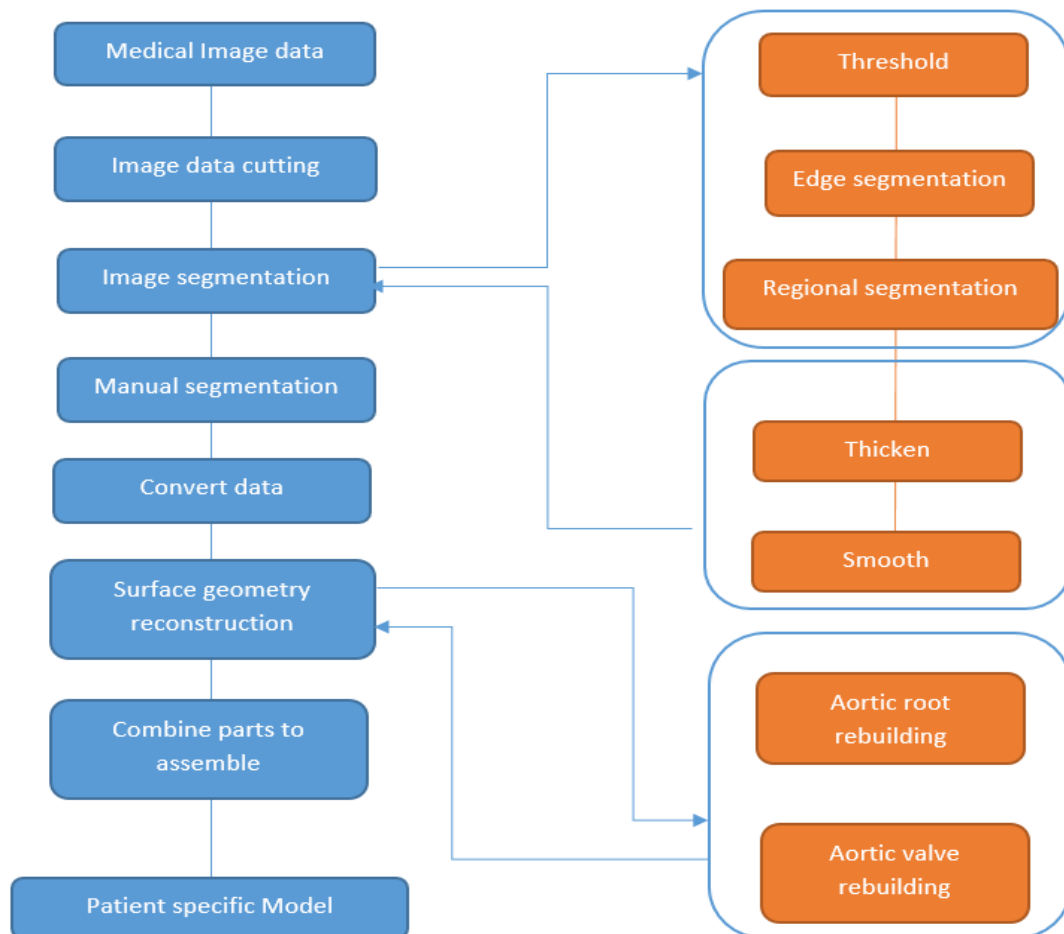


Figure 13 Patient specific model with continuous geometry from aortic root to interactive triangle

The first method is more representative of the real situation of the aortic valve, but mesh setting in the aortic root is hard to control. The second method creates a more uniform mesh at the surface.

Generally, a geometry model reconstruction in medical researches separates into four phases, which are Image capture, data conversion, image segmentation, and surface model reconstruction.

The first stage requires medical image from medical image devices. Generally, these images pack information in the 3D matrix, and the information is represented by voxels elements. The anatomy of tissue is illustrated by greyscales. In terms of extracting useful information from the pixel image, different image processing methods are applied to the next stage of studies.



Form up to down, blue blocks show the process that segment out model from the CT image data; top groups of orange blocks show the image processing method details; the bottom group of orange blocks illustrates two parts of surface geometry rebuilding.

There are three main image processing techniques requires in this study which are thresholding, edge segmentation, and regional segmentation. Pixel based segmentation identifies useful position by the greyscale value of initial image data. Edge based segmentation determines the edge of geometry by the significant change at the outline of geometry. Regional segmentation is given by the group of similar pixels. The whole process is showed in blocks above.

3.2 Aortic root segmentation

3.2.1 Image processing

Primary CT image is given from real dilated patient. The resolution of image data is 0.5 mm, and pixel information in each slide is 512 X 512. This patient is 31 years old male. The weight and height are 80Kg and 170cm respectively.

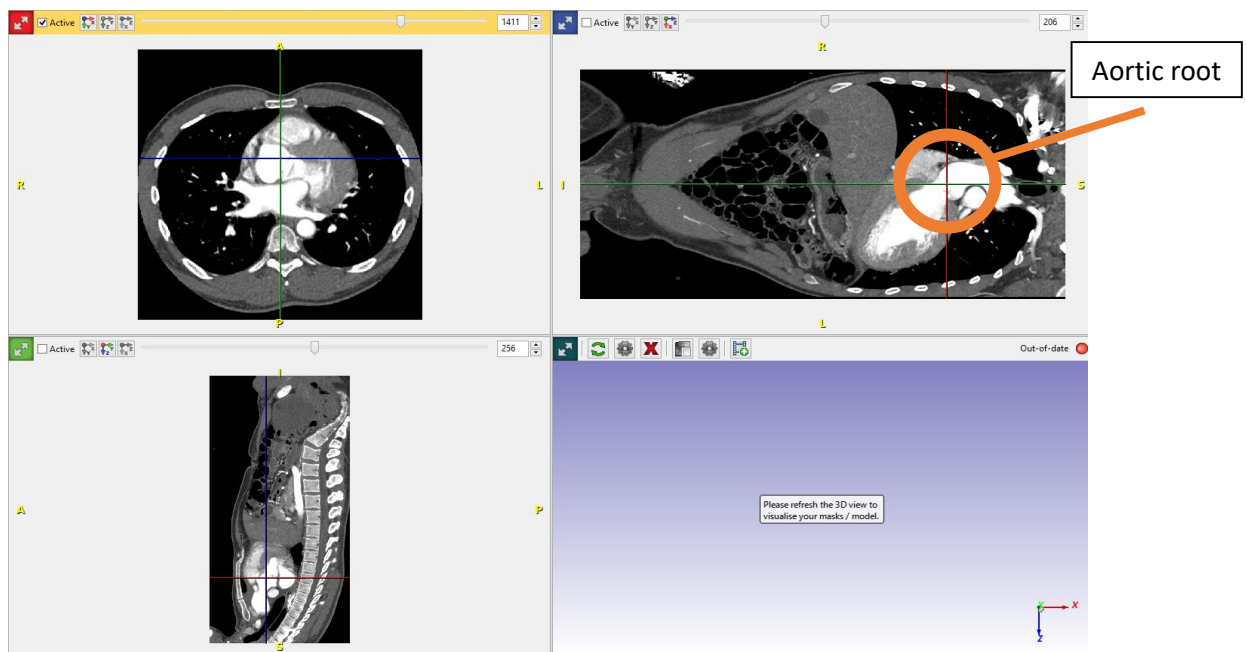


Figure 14 Picture shows the location of aortic root at the CT data image

Threshold means pick up certain image grey scale and make upper and lower grey scale images change to same grey value. After the threshold has been chosen, the grey scale of aortic root was picked out. It is achieved by defining a filter which has certain window centre and window width in a certain frequency. The filtered image only remains frequency in the window, and reset the information to black if they are located outside the window frequency. This filter

enhances important greyscale information and ignores other irrelevant tissues such as stomach, bone, and skin. Different means of the threshold have been used in this process. The effect of image processing is shown in Figure 15.

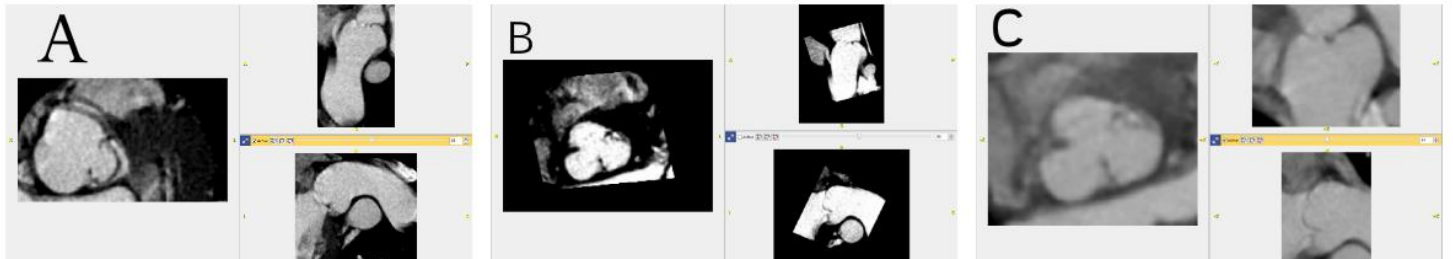


Figure 15 Using different window filter to modify back ground

(A) is background look when the filter window is 644.34 and filter level is 422.74. (B) is background look when the filter window is 322.17 and filter level is 422.74. (C) is background look when the filter window is 1208.13 and filter level is 382.47. (all value is frequency)

Then, we pick up the image data in a certain scale of the histogram and ensure that all the aorta is included in the mask.

Then irrelevant part and the connection between the useful part and the useless part were deleted. The final mask is in figure 16. This image processing method has been repeated with different thresholds, but the bottom of the image is still difficult to segment.

Before doing further smoothing, the mask should be cleaned up and the other tissues except aorta are unselected.

Edge segmentation has been also given from selecting grey value in the histogram. Compared with selecting a threshold, this method selects regions where have large transient changes in the grey data value. This method extracts the outline of subjects from the dramatic change of grey scale of the outline. In our model, most parts of aortic root model have clear outline. However, the middle bottom of aortic root does not generate any outline in any threshold (see detail in Figure 17). The outline of this model is between lower value of 81 and upper value of 111.

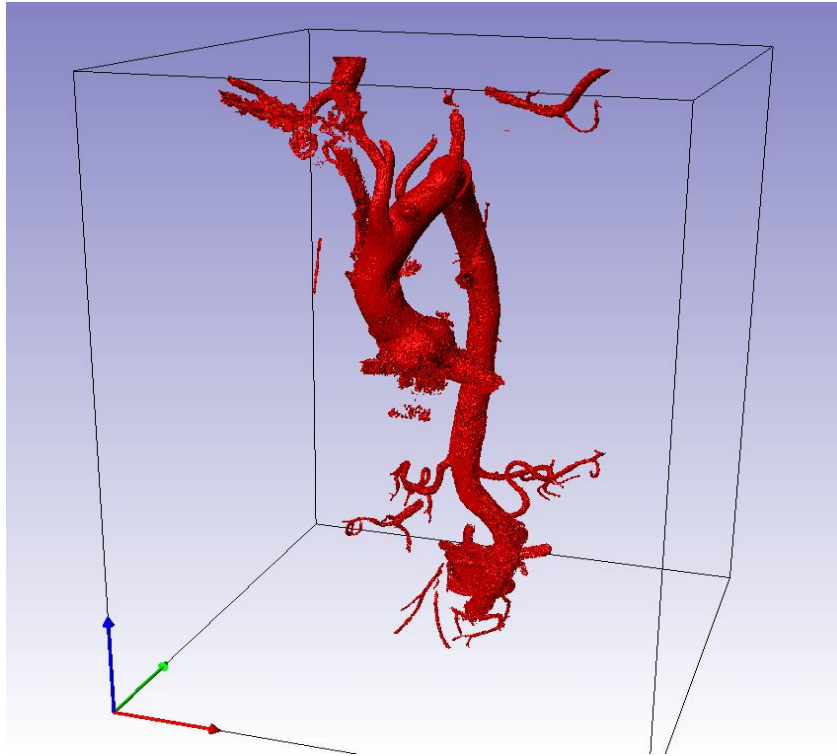


Figure 16 Aortic root after the 'Fill' image processing.

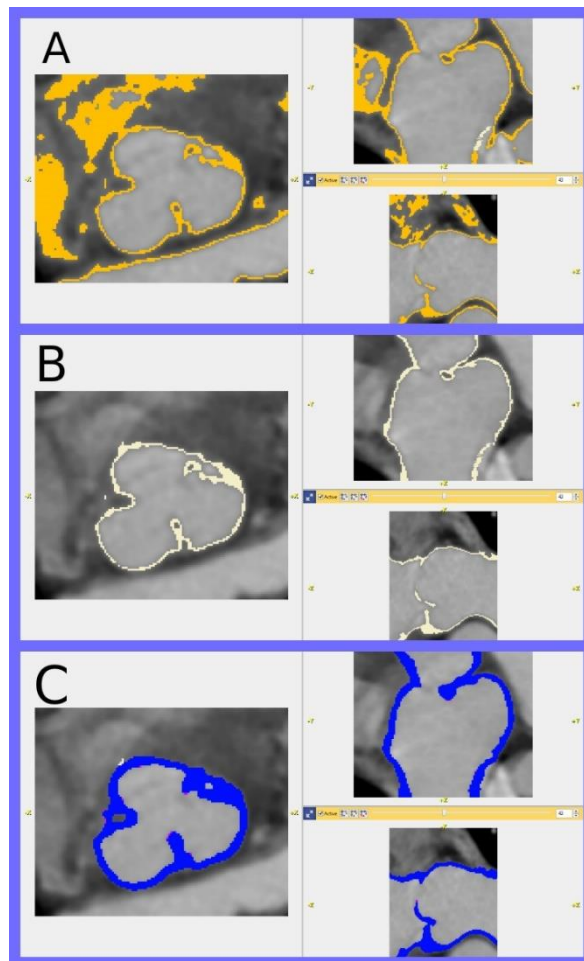


Figure 17. Edge segmentation process of the aortic root

(A) The edge of aortic root is picked out by choosing a certain level of grey scale. (B) modify mask and delete the useless information. (C) thicken the outline to make the unconnected part in thin outline became connected.

3.2.2 Smoothing solid model

The most important step for aortic root segmentation is smooth. The primary image data is not ideal due to resolution and other factors which affecting image quality. Image smoothing prevents errors that given from initial model and prepares further modification in following finite element analysis.

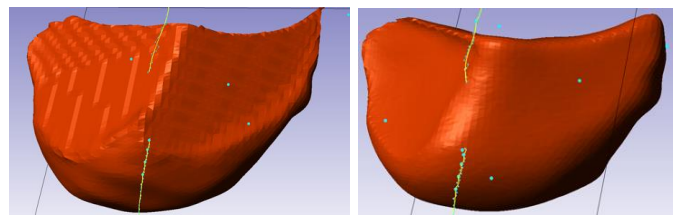


Figure 18 RC leaflets before smooth (left) and after smooth (right)

3.2.2.1 Smooth to have good hinge line and connection between aortic leaflet and aortic wall

This method aims to generate a surface with smooth transient at the connection between leaflets and aortic wall.

A mask that fills all the space is generated (Figure 19). Using this mask Boolean with the initial aortic solid body to have a new mask with empty inside (Figure 20). This mask now has the complete geometry outline of the aortic root and it is only used to adjust the shape of aortic root and leaflet. All the further smoothing process are given from the constraining of this outline mask.

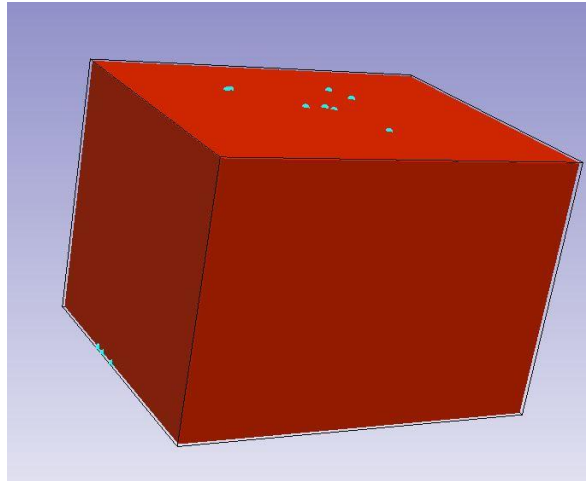


Figure 19 A mask filling all the work space

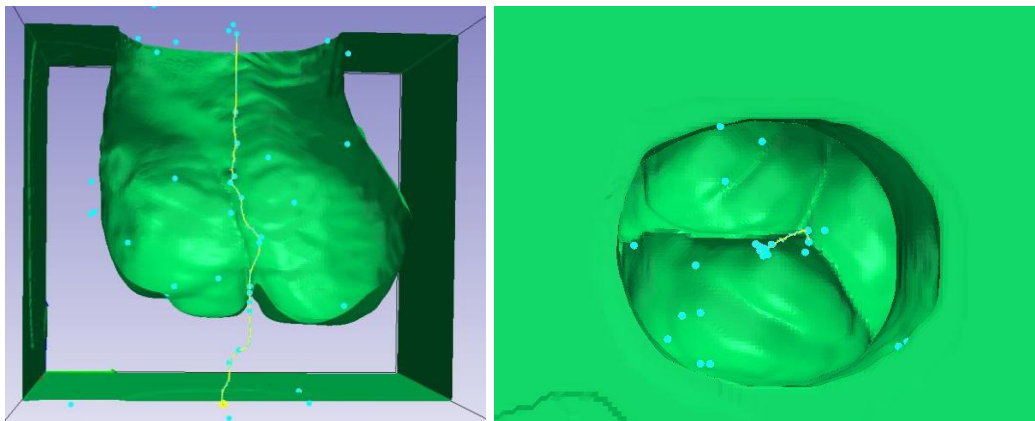


Figure 20 An inverse mask of aortic root was generated (picture at left shows the side cross section view of mask, and picture at right shows the top view of mask)

This method gives smoothing connection between the aortic leaflet and the aortic wall (figure 21). However, a sharp angle is also generated at the contact of any two leaflets (figure 22) since the algorithm of smoothing tries to fill all the holes in the middle of the leaflet and to match the outline to the shape of background at the same time.

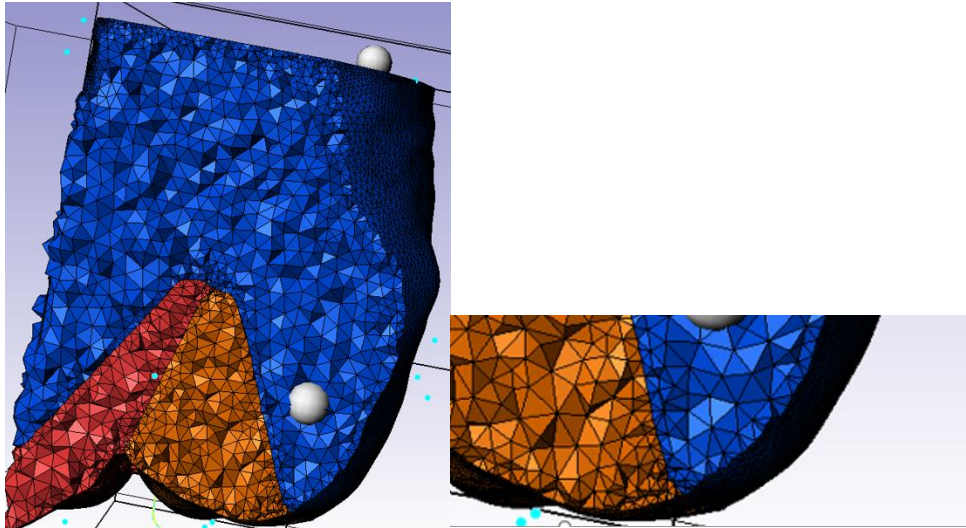


Figure 21. Fine smooth at hinge line in cross section view
 (see the blue and orange colour at the right bottom)

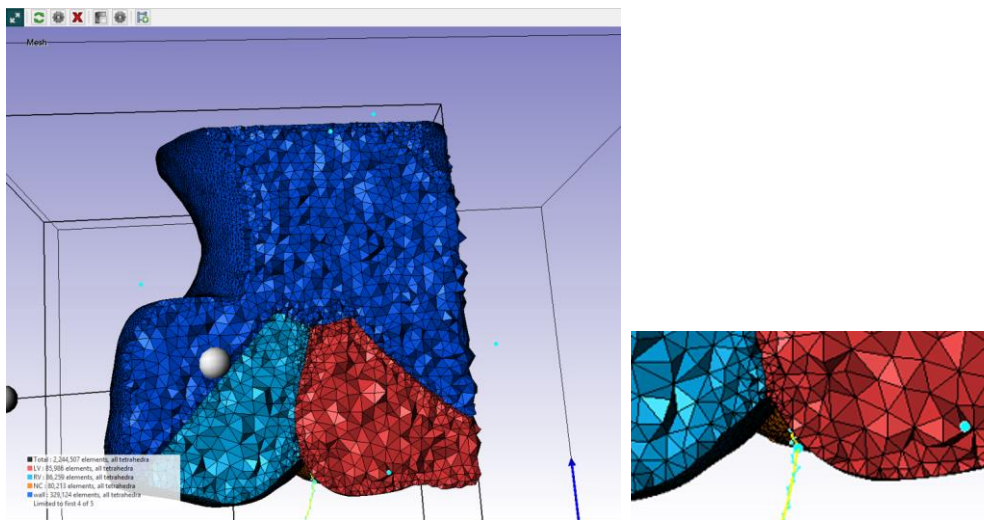


Figure 22. Sharp angle of two mask in cross section view
 (see bottom of light blue mask and red mask)

This method provides a more specific model in the performance of real leaflets since the aortic root and the three leaflets are fully connected. However, the sharp angle at the leaflets contacts results in hard to generate a surface in ANSYS 15.0 DesignModeler. The difficulties in generating surfaces are extreme angle can not achieve the tolerance in ANSYS 15.0.

3.2.2.2 Method to have smooth curvature at aortic leaflet

For the purpose of generating a smooth surface from the valve, the model of different leaflets and the model of aortic wall are smoothed and generated separately. The smoothing process reduces connection from a sharp angle to smooth angle, since the algorithm of smooth only is applied on single leaflets and ignores the relationship between leaflets. Nevertheless, this method brought the gap between leaflets and aortic wall (figure 27). The details of smooth are shown below.

At first, the selected mask is enlarged one pixel before three pixels Gaussian smoothing (Figure 23), since smooth will reduce and change the outline of the object. After that, two pixels smooth on each mask was applied (Figure 25). Then, apply Boolean operation in three leaflets to subtract from one to another (Figure 24). All the overlap at the leaflets can be deleted in this process. Finally, models were generated in the individual surface model. All the solid body were exported as IGES files.

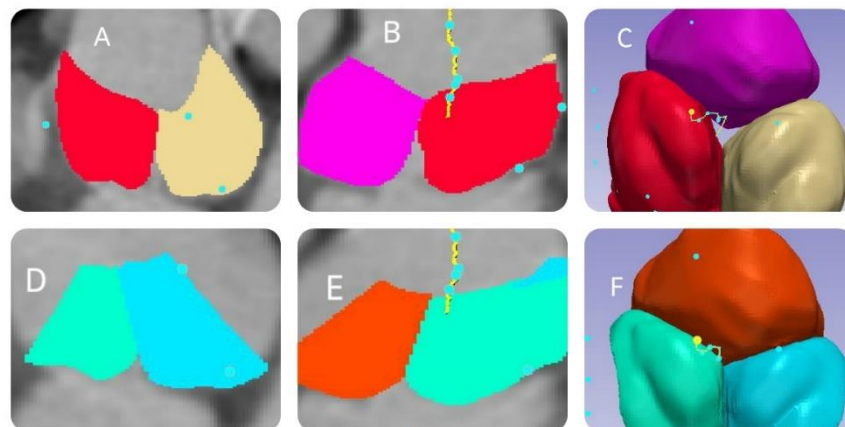


Figure 23 there is a large gap between aortic leaflets at the initial segmentation (picture A, B, C). After one pixel enlargement of the mask, the gap was filled. (picture D, E, F)

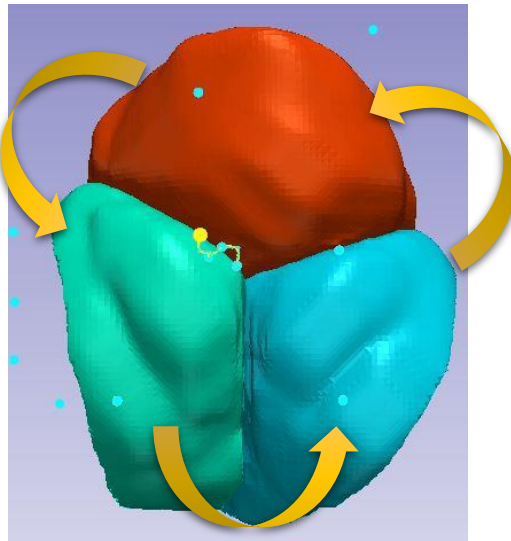


Figure 24 Boolean to remove the overlap volume (Boolean three leaflets follow the order of clockwise or anticlockwise. An example shows in yellow arrow in Figure 24)

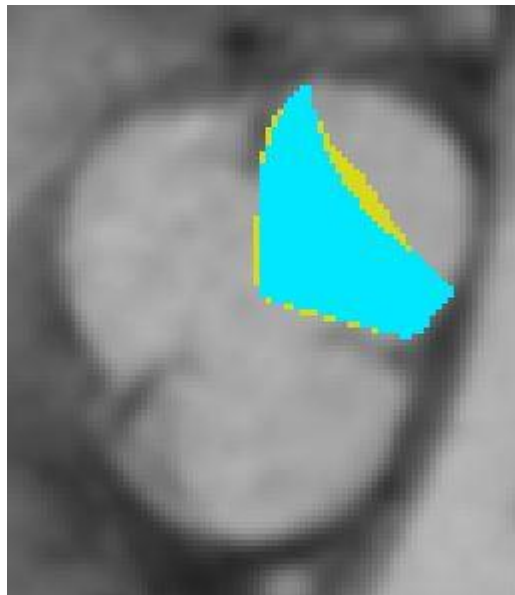


Figure 25 The smoothing of the mask reduces mask outline (the non-smoothed leaflet at yellow, the smoothed leaflet at light blue)

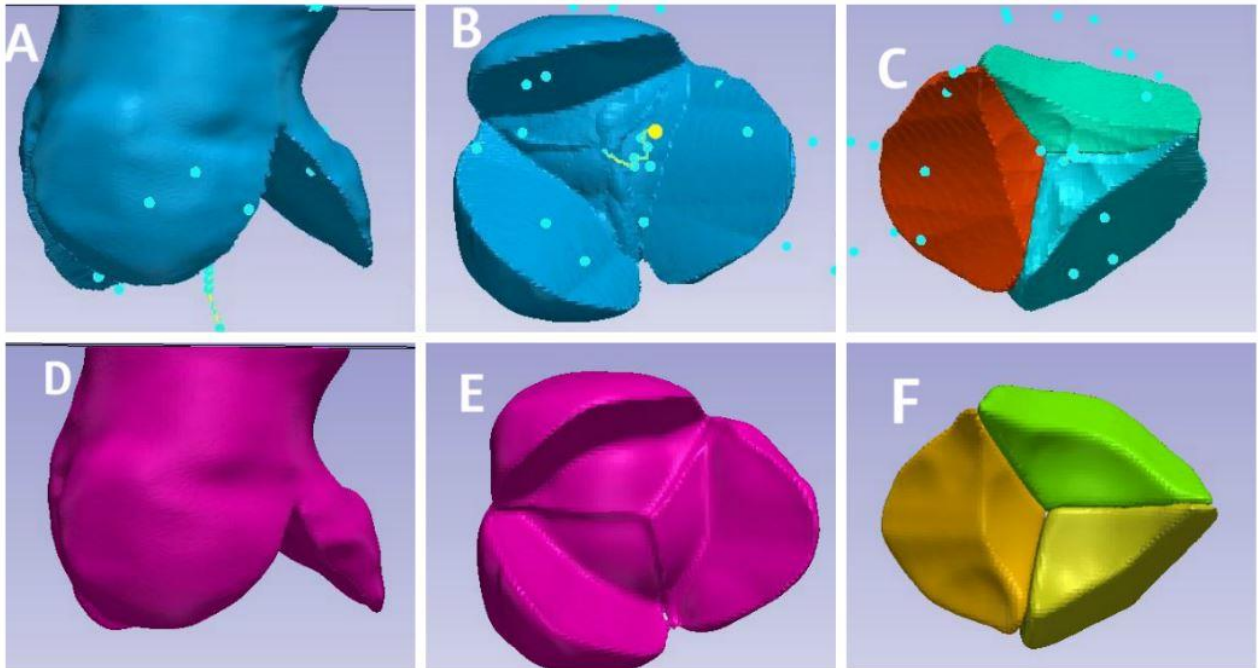


Figure 26 Picture A and B illustrate the side view and bottom view of the non-smoothed aortic root, and C shows the top view of the non-smoothed three leaflets. Picture D and E illustrate the side view and bottom view of smoothed aortic root, and F shows the top view of the smoothed three leaflets

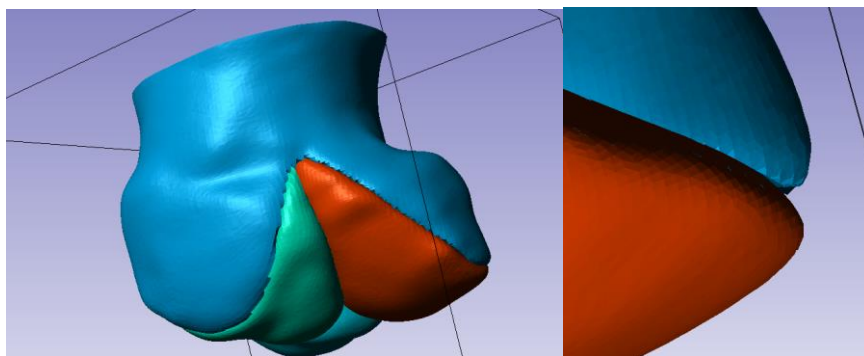


Figure 27. Low curvature at aortic leaflet but gap in the hinge line

3.3 Surface model reconstruction

CT scan has limited resolution for soft tissue. The thickness of aortic leaflets is close to 0.5mm (according to table 2) and the resolution of CT image in this study is 0.5mm as well. Hence, the position and geometry of aortic leaflets are hard to observe from this CT image.

To deal with aortic leaflet geometry, the geometry of aortic valve should be given by key points of leaflets tips, commissures, and hinge line.

The surface can be given easily with NURBS type of format. However, STL and IGES are normally what we have after exporting the model from image processing software. The main feature of these two types of formats is multi-faces instead of the single smooth surface. The multi-faces geometry has a large amount of edges and small surfaces which enhance the complexity of the modification process.

ANSYS Workbench is a software that established meshing and other calculation depending on the geometry, so mesh quality and mesh algorithm are related to the initial body curvature. It is much harder to change and adjust the geometry in the ANSYS. Hypermesh, which can generate mesh freely ignoring initial geometry, is more simple to modify multi-faces body.

In this study, we develop a model in ANSYS, so the valve geometry modification is the main things should conquer before any simulation. Due to the limitation, the surface model reconstruction of the aortic root is divided into two parts which are aortic root reconstruction and aortic leaflet rebuilding.

3.3.1 Aortic root reconstruction

Aortic root surface model can be easily given by solid model aortic root. The methods are illustrated in the followed steps:

Step 1 Importing model into ANSYS 15.0 DesignModeler

Importing model with both solid body and surface body. This importing method serves the multi- surfaces as a whole topology, which ensures that the face can be selected by multi face selection in ANSYS DesignModeler. The final solid body is shown in picture 23

Details of Import3	
Import	Import3
Source	F:\Mel\Yachen\New DICOM04.08.2016.igs
Base Plane	XYPlane
Operation	Add Frozen
Solid Bodies	Yes
Surface Bodies	Yes
Line Bodies	No
Simplify Geometry	No
Simplify Topology	No
Heal Bodies	Yes
Clean Bodies	Normal
Stitch Surfaces	Yes
Tolerance	Normal
Replace Missing Geometry	No
Refresh	No

Figure 28 Importing setting of the geometry. Noticed that the operation is 'add Frozen'; both Solid body column and surface body column are 'yes'.

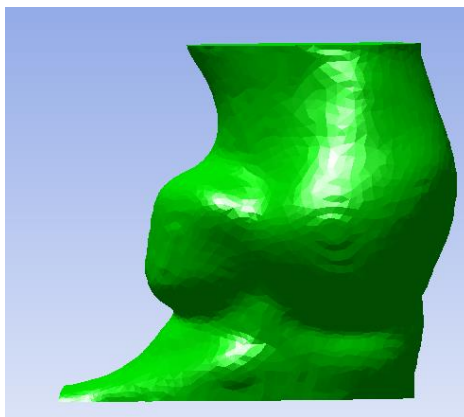


Figure 29 Side view of Aortic root solid body after importing to the ANSYS 15.0

Step 2. Generate new surface

Selecting one small surface at the aortic wall from the solid body surface, and expanding the surface selection to the limit (figure 30). This option returns the whole surface of aortic wall except the top and the bottom faces. Generating a new surface from selected faces (figure 31). This new surface should represent all the feature of the aortic root.

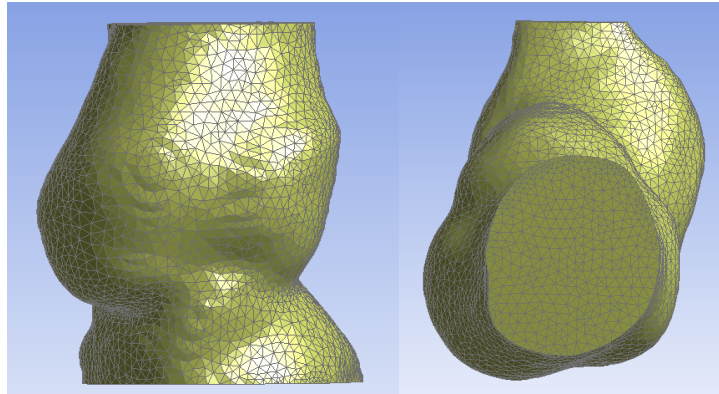


Figure 30 Solid body of aortic root (side view at left and top view at right)

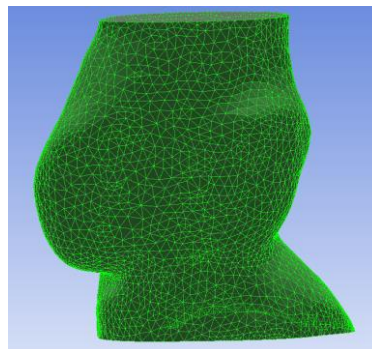


Figure 31 select all the surface at the side which represent aortic root geometry

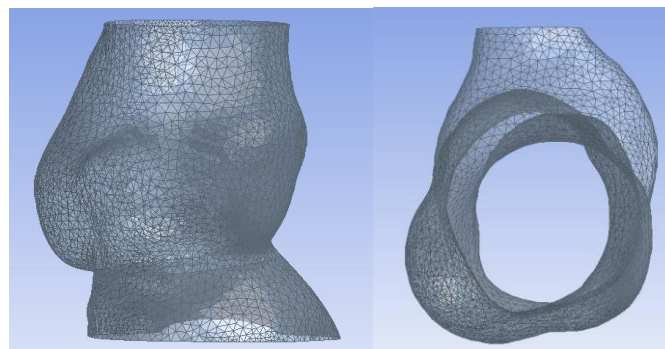


Figure 32 generate a surfaced body formed only surfaces

Step 3. Adjusting surface model

If the central line of the aortic root is not vertically orientated, it is recommended to change the whole geometry to the orientation that the central line is almost aligned with Z - direction. The bottom of the model is a plane which is located at the lowest point of three hinge line. Therefore, some redundant geometry can be deleted in this step.

Step 4. Build virtual surface

The initial multi-surface body is not suitable for mesh generation since the new mesh element is limited in each face. The virtual body should be generated before creating meshes. Thus, three virtual bodies were generated to represent the three sinuses (Figure 33).

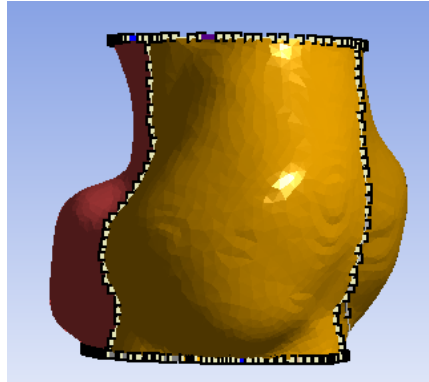


Figure 33 Virtual faces reducing multi-faces to three faces. Each of the faces contains one sinus

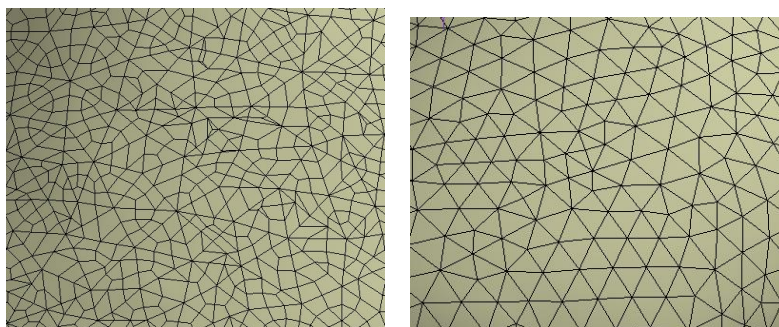


Figure 34 Mesh before virtual body (left). Generating mesh is limited by the initial faces. Mesh after the virtual body (right) generates mesh depending on geometry surface feature.

3.3.2 Aortic leaflet rebuilding

It is important to ensure leaflets have uniform edges, which is easy to mesh controlling in the following steps. If ANSYS Workbench is the main software in the study, this is extremely important. Most previous patient specific studies do not have the leaflets from the image processing (Wang et al., 2012), since the valve thickness is too small and it has a large displacement at a small period of time.

The fitting valves highly depend on the initial valve geometry, so it is important to have a roughly outline of the geometry at first.

The following steps are included in leaflet geometry building:

Step 1. Change alignment of whole geometry to almost along as vertical direction

The alignment changing is preparing steps for the central line generation. Once the model aligns to with the z orientation, the central line of the z direction represents the central of the aortic root. The centre of the aortic root is the/an important reference for aortic leaflet generation. We first change the slides' curser to the slide where we can observe the bottom of hinge line of two sinuses at the same time.

Two points of hinge line bottom were chosen. Changing the parameter to move the line to located in at the desire XZ plane. Repeat the same process to the other two sinuses in YZ observe window.

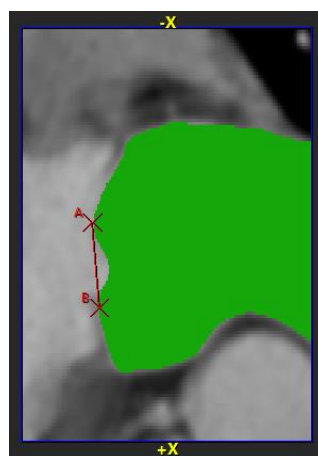


Figure 35 Pick two hinge line button at XZ plane and assign the line formed by those two points to the new Y Axis. Repeat this process in the YZ plane of the image data. Pick hinge line bottom but assign to the new X Axis this time

If the aortic root still does not look in the vertical direction, repeating the process above in plane XZ plane image view.

Step 2. Define central line of aortic root

The central line can be easily given by generating a central line in the z direction if the alignment has been modified.

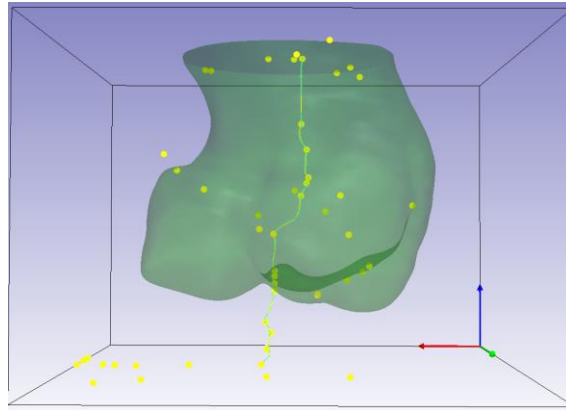


Figure 36 Central line of the aortic root can help define the three tips of aortic leaflet and other important parameters

Step 3. Define the tips and hinge line of aortic root

The leaflet is defined by tips and hinge line. To address the tips in the model, the relevant value of geometry of leaflet is required. Since the leaflet is closed in this study, the position of the leaflet is similar in picture 31.



Figure 37 the land mark of three button points of hinge line (red), two ostium (blue), three leaflet tips (yellow), and three commissures (green) during the diastole of the cardiac cycle

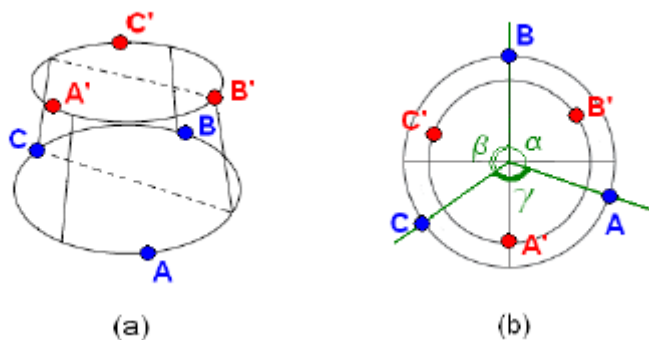


Figure 38 (a) The three commissure (red point) of aortic root formed a ring geometry, and the three bottom point of hinge ling formed another ring geometry. The plate of two rings does not need parallel. (b) the aortic root

From side view in figure 37, each commissure is located in the middle of the vertical line of two hinges.

Step 4. Using three solid bodies to illustrate leaflet

We then find aortic commissures, and three button points of the hinge line. From the solid model of the aortic root, three other solid models were extracted out with a Boolean operation. These three solid parts contained the leaflets (figure 39).

Swanson and Clark (1974) illustrated the tips of the aortic leaflets are located at 5-7 mm above the middle of coaptation. From tips and hinge line, the three leaflets are extracting from the aortic root solid model separately (figure 40). The location of leaflet and hinge line was justified by experts.

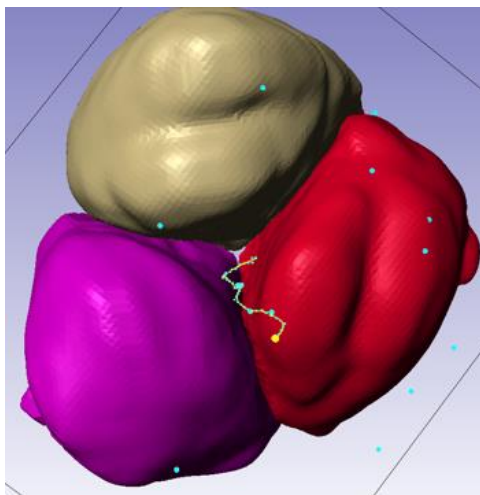


Figure 39 Three solid bodies which donates to three leaflets separately

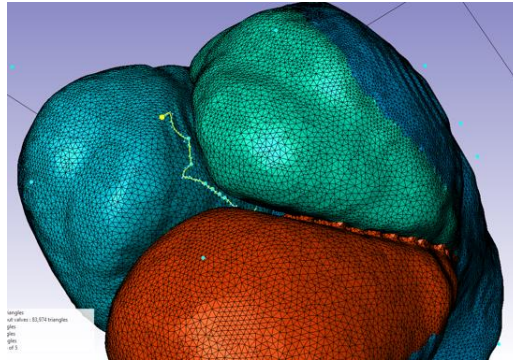


Figure 40 Find hinge line and reduce the solid leaflets body mask begin at the hinge line (hinge line located at the transient change of green and blue colour from this picture)

Step 5. Smooth and export as IGES surface model

Since the resolution of current CT image is 0.5 mm, smoothing one pixel results in 1 mm gap between two leaflets. However, it is noticed that the thickness of aortic leaflets is near 0.5 mm. The error of position change at aortic leaflets may exist during smoothing process.

Step 6. Import into ANSYS and modify to generate a new surface to fitting and replace current multi-faces body

The aortic leaflets are thin surfaces and preload to the diastole position in this study. The leaflet in the diastole initially should close in the real situation. However, third party software generates contact matrix to represent the contact. The contact matrix is similar to a spring which increases reaction force due to displacement and internal coefficient. Hence, the contact will be detected once the two parts are in a certain distance of gap. Therefore, the more penetration in the two bodies, the more possibility of the getting no converge results due to the large penetration creating dramatic stress at the contact areas. In this study, three methods are applied in the leaflets surface generation.

- Creating surface from IGES Multi – faces
- Roughly fitting leaflets depending on leaflets tips, leaflets hinge line, and aortic root commissures
- Specific generating leaflets depending on the aortic leaflets IGES solid model

(1) Creating surface from IGES Multi – faces

'solid model' was assigned to the leaflets when importing three aortic leaflets to ANSYS. Then, surface models for aortic leaflets was generated. Model generation can uses the similar method in the aortic root model generation. Finally, it should manually choose some faces from aortic leaflets solid mode and generate a new surface model with selected faces.

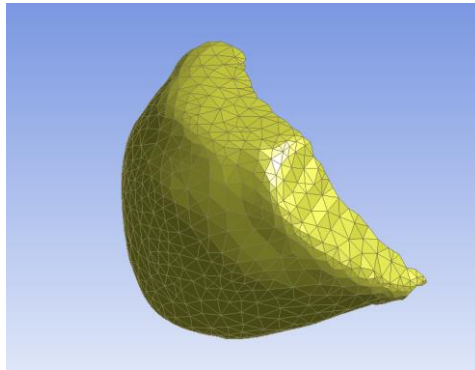


Figure 41 Aortic leaflets were directly selected from the solid IGES model

There is a gap between the aortic leaflets and the aortic root, since their surfaces are generated from different solid bodies. Using new surfaces to connect aortic wall and leaflets can fill the gap. However, the edges of connecting surfaces are not uniform and smooth surfaces, since aortic root and aortic leaflets edges are not smooth. Non-smooth edges also result of large curvature change at the connection surface. Finally, curvature changes caused connection surface difficult to mesh (figure 42 and 42).

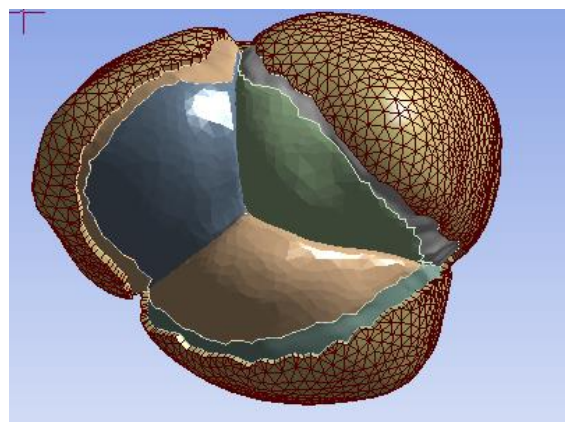


Figure 42. Aortic root and aortic leaflets are on different surfaces, the gap between them are filled by new surface

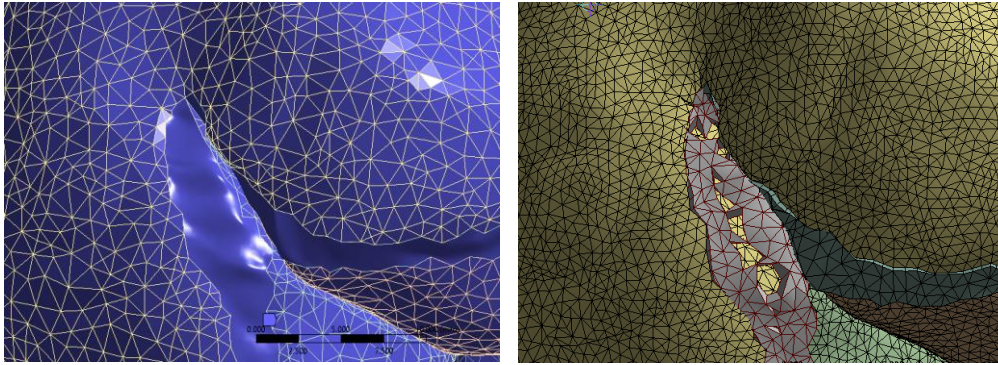


Figure 43 Failed model with geometry (left) and mesh (right)

(2) Roughly fitting leaflets depending on leaflets tips, leaflets hinge line, and aortic root commissures

Since aortic leaflets are hard to modify and generate meshes in the ANSYS 15.0, the leaflets are fitted out and connected to the aortic root.

The leaflets are given from the aortic leaflets solid model by selecting some key points from the solid model and fitting a surface to represents leaflets in the ANSYS 15.0 DesignModeler.

The model can be given from landmarks method. All the landmarks for generating aortic root are tips, hinge line, and commissures (Grande-Allen et al., 2001b).

free edges and hinge line of the aortic leaflet are presented by curves. Generating leaflets depends on those curve lines.

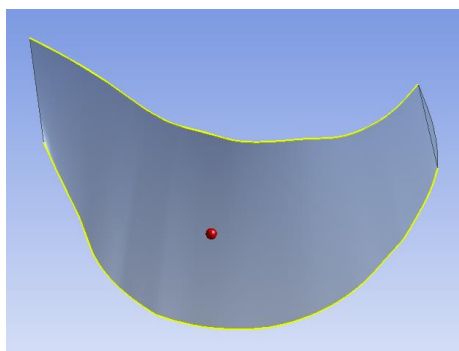


Figure 44. Yellow curves highlight in the picture show the free edge of the aortic leaflet (top) and hinge line (bottom)

The leaflets surface will large decrease since the leaflet geometry does not fully repeat the leaflets at the diastole position.

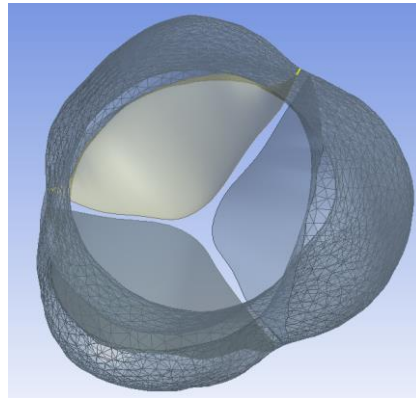


Figure 45 Top view of aortic leaflets and aortic root

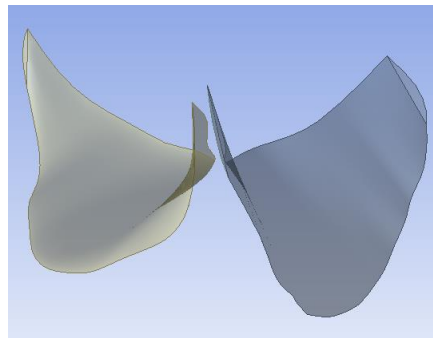


Figure 46. Side view of aortic leaflets. Noticed that those aortic leaflets are not fully repeated the feature of aortic leaflets at the diastole of the cardiac circle

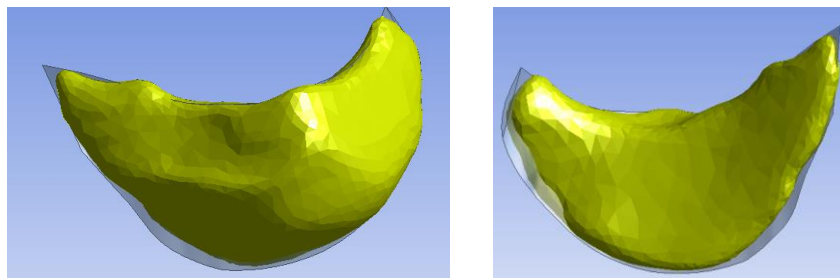


Figure 47. The fitting leaflets compare to the normal solid leaflets (front view at left and back view at right)

All the leaflets should be contacted after applying pressure to the aortic root, but simulation stops before setting end time reached and results showed that the model was not converge. A single leaflet connected to a fixing end can work properly under the small pressure, but this model does not run under the large pressure and multi leaflets situation.

This model is hard to converge when pressure increasing at leaflet, since large stress generates at the contact of edges. The two leaflets have a trouble of recognizing each other and generating contact stiffness matrix between contacts leaflets.

(3) Specific generating leaflets depending on the aortic leaflet IGES solid model

Since the contact between leaflets is not easily to be recognized by ANSYS 15.0, a more precise leaflet fitting model is generated.

Since the initial solid leaflets is smoothing and exported from Scan IP separately, there are some initial contact parts at the initial state. It will cause initial overlap after creating leaflets depending on the surface features. Therefore, the solid leaflets should be moved away from each other about 1mm to reduce prevent the generated leaflets surface from penetrating to each other.

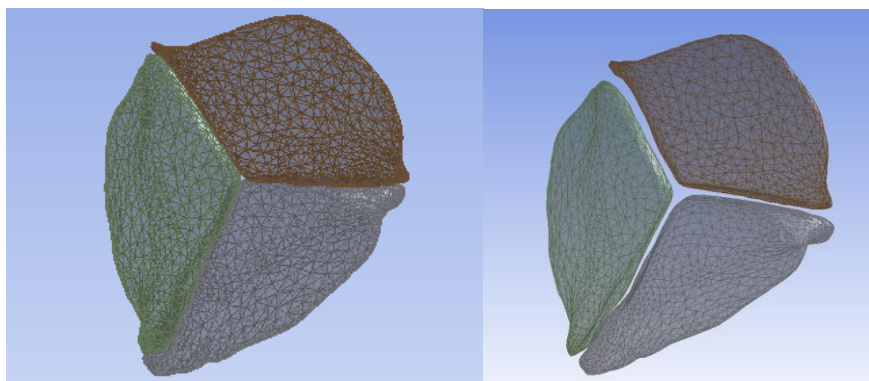


Figure 48 Top view of aortic three leaflets after importing to ANSYS 15.0 with leaflets initial position (left) and moved position (right)

Several points are chosen at the surface of the solid body. Making sure these points are located at the important places where can modify splines curve to desire orientation. Then, generating curves depends on the spline body. During this process, being aware of having a smooth boundary of the connection between the leaflets and aortic root. If penetration is generated at this step, it is important to ensure that the penetration is in the tolerance.

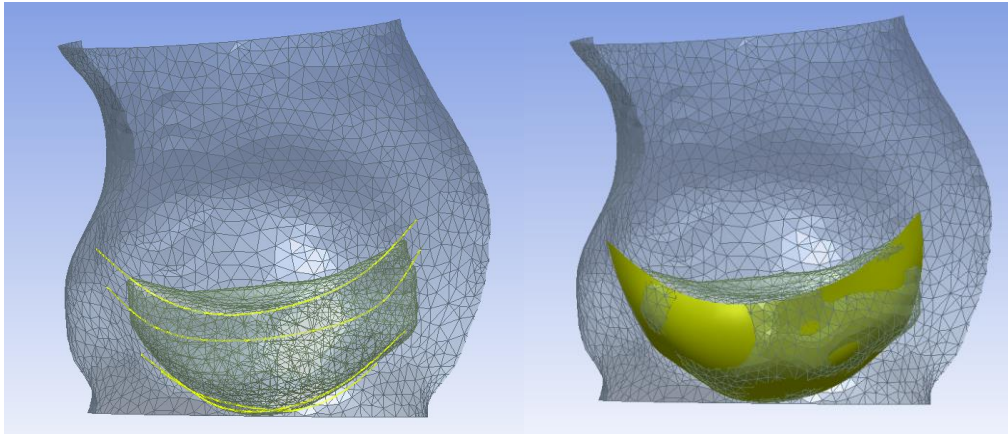


Figure 49 Side view of single leaflet generation process. Firstly, fitting curve along with the surface of aortic leaflet (left). Secondly, using curves to create new surface to represent the surface of aortic leaflet (right)

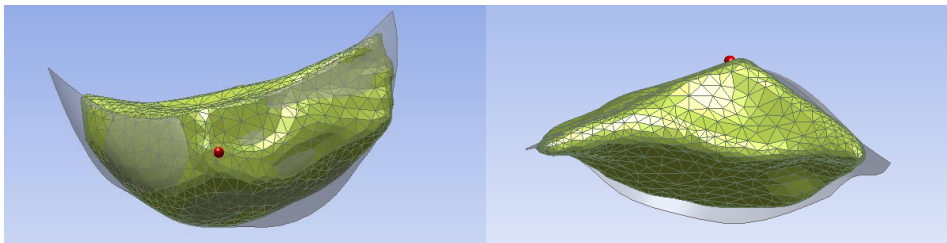


Figure 50. Front view (right) and top view (left) of fitting leaflet and the initial solid geometry (high light in the yellow colour)

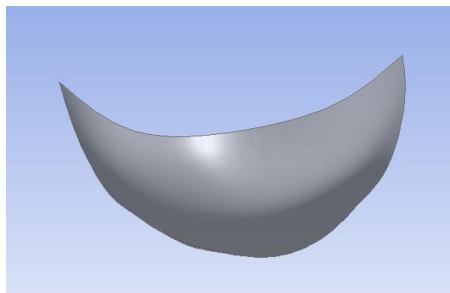


Figure 51. Front view of single fitting leaflet

Chapter 4 Material properties and boundary condition

4.1 Material properties

4.1.1 Material property of aortic root in other thesis

In micro-scale studies, the aortic leaflet is recognized as a composite material with three layers, which from top to bottom are ventricularis, spongios, and fibrosa. Ventricularis and fibrosa both have certain mechanical properties and spongios is an intermediate filling material with low density. Vesely and Noseworthy (1992) test the leaflets' tension and stress strain curves of the top and bottom parts.

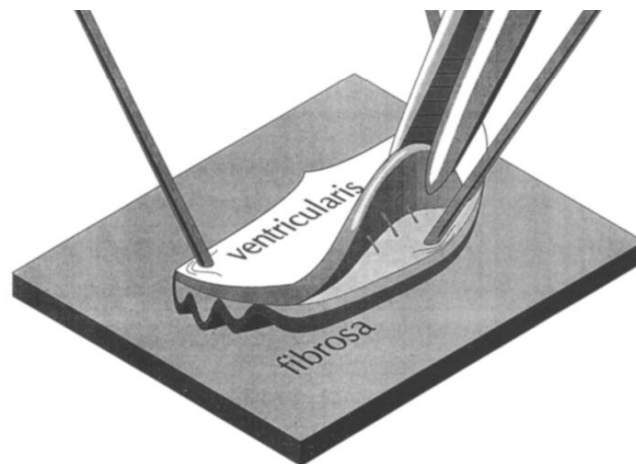


Figure 52. Three layers of aortic leaflets which are ventricularis and fibrosa at the two outsides and spongios tissue at the middle. (Vesely and Noseworthy, 1992)

Results showed that ventricular tissue has remarkably higher Young's modulus in the radial orientation and fibres present similar material properties in the radial and circumferential directions.



Figure 53. Definition of circumferential and radial orientation for Aortic leaflet (Vesely and Noseworthy, 1992)

Consequently, aortic leaflets have the ability to undergo large deformation in the radial direction. The material properties of aortic wall have similar modulus in both longitudinal and circumferential directions (Nicosia et al., 2002).

The researches from He and Roach (1994) and Raghavan et al. (1996) proved that heterogeneous and bi-phasic properties are the basic biomechanical feature of the aortic root. However, to reduce the sophisticated mathematical process of modelling such material models, aortic material was assumed isotropic in the studies by Soncini et al. (2009a) and Gnyaneshwar et al. (2002). Similar material properties were also used by other studies in the following years. The stress layered structure of aortic leaflets has been performed anisotropic behaviors.

In this study, aortic leaflets are at the position that almost contacts to each other, which means experiment begins at the end of systole. When an aortic valve enters diastole phases, leaflets are closed and the mechanical property of the leaflet tissue reaches close to post-transition elastic moduli during diastole (Figure 54).

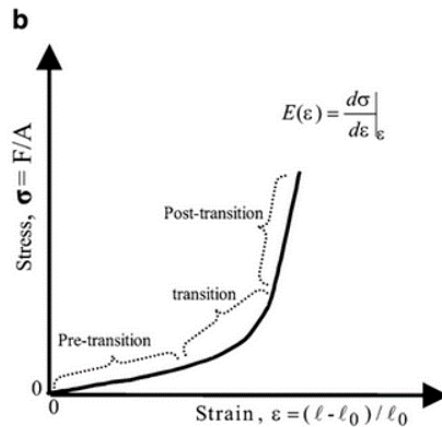


Figure 54. Stress – strain curve illustration transition, pre-transition and post transition mechanics (Helsen and Missirlis, 2010)

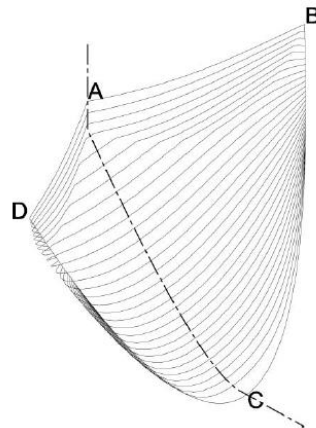


Figure 55. Fibre orientation at the aortic leaflets
(Li et al., 2001)

The material properties of aortic leaflets are highly related to fibre orientation. Grande et al. (1997) assigned leaflets modules in the independent coordinate system by the fibre orientations and built orthotropic leaflets. This method was later simplified by Mohammadi et al. (2009). To have a more specific model and achieve the performance of the real functions of leaflets, we adopted record data from Grande et al. (1997). The detail of assignment was illustrated as Table 1.

Table 1. Material property from Grande et al. (1997)

	Young's modulus (MPa)			Poisson's ratio			Shear modulus (MPa)		
	E _{circ}	E _{rad}	E _{long}	v _{xy}	v _{yz}	v _{xz}	G _{xy}	G _{yz}	G _{xz}
Aortic leaflet	6.885	1.624	NA	0.106	0.106	0.45	1.121	1.121	0.56
Aortic wall	0.334	NA	0.35	0.45	0.45	0.429	0.119	0.115	0.119

Modulus in the longitudinal direction of aortic leaflets and radial orientation of aortic wall refers local z component of shell element local coordinate system. The material property in the z orientation do not effect this study too much, most of the studies not provide this value. However, this value is compulsory for simulation. According to ANSYS reference material, the value of z modulus can be assigned ten times lower than the smallest value between the x or y modulus.

4.1.2 Determine element type

There are different types of elements in FEA for mesh model. The term 'mesh' in finite element means using a small element to approximate represent assemble. Shell element is a a small micro triangle and rectangular elements. (Figure 56)

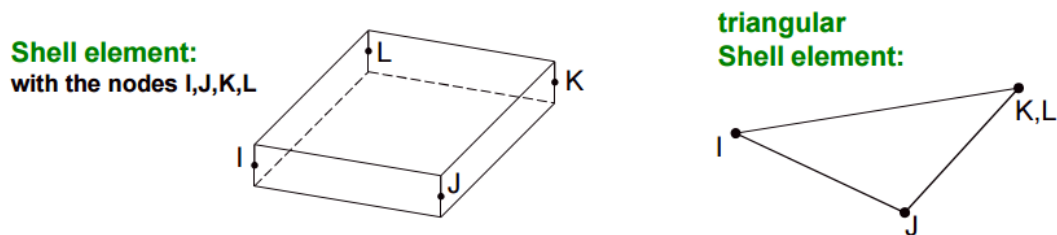


Figure 56 Shell element with four nodes (left) and with three nodes (right). In the four nodes element, node I, J, K, L locate at the four angles top of the rectangular geometry. In the three nodes shell elements, nodes K and L reduce to one node.

Aortic root and aortic leaflets formed by thin soft tissues and their thicknesses are represented in the unit of millimetre. Shell element is widely used in cardiac

tissue, especially aortic root, modelling (Soncini et al., 2009b, Smuts et al., 2011, Conti et al., 2010a, Astorino et al., 2012). ANSYS 15.0 will generate shell 181 automatically in ANSYS workbench. The Similar element type can be found in ABAQUS such as S3R and S4R elements, which has been used in Soncini et al. (2009b) and Conti et al. (2010a) for modelling aortic root and leaflets.

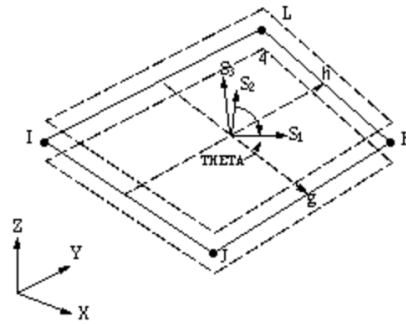


Figure 57 Shell element 181. The element has four nodes. L and K node constrain to one node when we use triangle element. Local coordinate system X, Y, and Z are shown in the picture

Our project uses shell 181 for the surface model system. Shell 181 is a four node shell system, and it can be reduce to three nodes once the K and L node combine together. Triangle element is good to apply at curve body, since the geometry is more is be captured by triangle rather than four nodes element. Thus, triangle element can ensure the performance as the same as the real leaflets when aortic leaflets undergoing large displacement and the deformation and have nonlinear anisotropic material properties.

Orthotropic material properties are defined by the orthotropic stiffness matrix. There are nine parameters should be pronounced in the orthotropic stiffness matrix, which includes Young's modulus, Poisson's ratios, and shear modulus in x, y, and z directions respectively. E_x , E_y and E_z represent Young's modulus in the local x, y and z orientation. ν_{xy} , ν_{yx} and ν_{xz} indicate possion's ratio in xy plane, xy plane and xz plane respectivele. G_{yz} , G_{zx} , and G_{xy} refer to shear modelus in xy plane, yz plane and xz plane. The orthotropic stiffness matrix as followed:

$$\begin{bmatrix} \varepsilon_{xx} \\ \varepsilon_{yy} \\ \varepsilon_{zz} \\ \varepsilon_{yz} \\ \varepsilon_{zx} \\ \varepsilon_{xy} \end{bmatrix} = \begin{bmatrix} \frac{1}{E_x} & -\frac{\nu_{yx}}{E_y} & -\frac{\nu_{zx}}{E_z} & 0 & 0 & 0 \\ -\frac{\nu_{xy}}{E_x} & \frac{1}{E_y} & -\frac{\nu_{zy}}{E_z} & 0 & 0 & 0 \\ \frac{\nu_{xz}}{E_x} & -\frac{\nu_{yz}}{E_y} & \frac{1}{E_z} & 0 & 0 & 0 \\ 0 & 0 & 0 & \frac{1}{2G_{yz}} & 0 & 0 \\ 0 & 0 & 0 & 0 & \frac{1}{2G_{zx}} & 0 \\ 0 & 0 & 0 & 0 & 0 & \frac{1}{2G_{xy}} \end{bmatrix}$$

Where $\frac{\nu_{yx}}{E_y} = \frac{\nu_{zy}}{E_z}$, $\frac{\nu_{zx}}{E_z} = \frac{\nu_{xz}}{E_x}$, $\frac{\nu_{xy}}{E_x} = \frac{\nu_{yx}}{E_y}$.

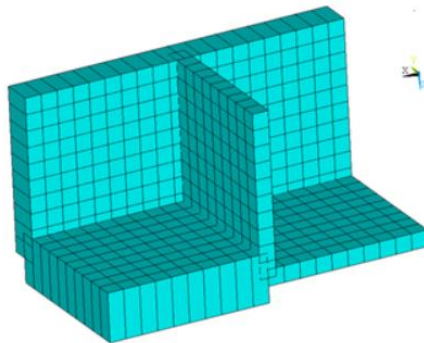


Figure 58 Shell joint at the Ansys software
(the dashed line shows the overlap)

Moreover, shell 181 has an inherent problem of overlapping in joint (figure 58). The stress of the joint will be located in the mid-plane, which reduces the stiffness of the objects. Offsetting the shell can reduce this shortage. However, this disadvantage can not be alleviated in this study.

4.1.3 Coordinate system for aortic root model

The directions of forces are highly related to the assignment of the global coordinate system or local coordinate system. Global coordinate system is the initial coordinate system for assemble. Local coordinate system is the other

coordinate systems which can assign to selected parts. The selective bodies are not restricted to a single object or multiple parts or even the whole bodies. Shell coordinate system is default ANSYS surface meshing.

There are four local coordinate systems in ANSYS 15.0 (figure 59). Default global coordinate system is the orthogonal coordinate system.

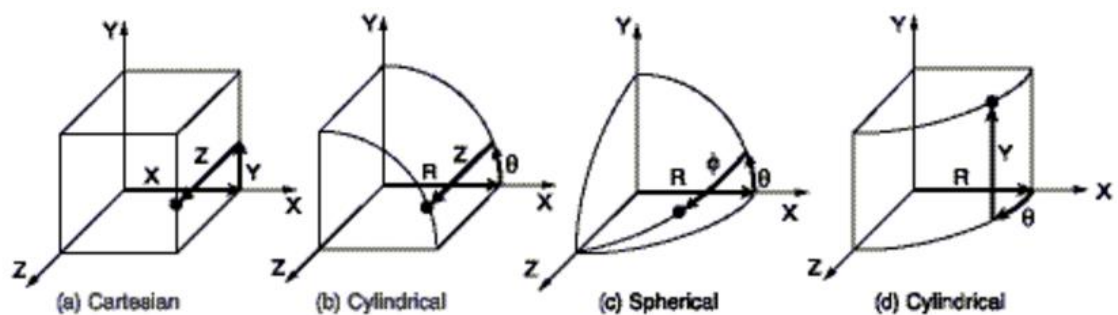


Figure 59. Different types of coordinate systems in ANSYS 15.0 (a) Cartesian coordinate system with components in X, Y, Z (b) Cylindrical coordinate system with components in R, θ , Z orientations (c) Spherical coordinate system with components R, θ , ϕ orientations (d) Cylindrical coordinate system with components R, θ , Y orientations (ANSYS, 2013)

The geometry of aortic root is similar to a tube, so cylinders coordinate system is the optimal coordinate system to assign material properties and forces. The aortic root aligns in the longitudinal direction. Original points located at the button of central of the aortic root. Aortic wall address in the circumferential direction.

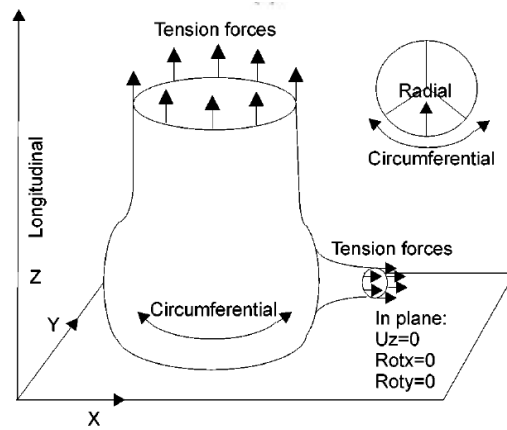


Figure 60. Aortic root in the simulation in the cylinder coordinate system. Aortic wall is in circumferential orientation. The aortic root aligns to longitudinal orientation. The aortic leaflet is located in the radial orientation from the contact point of three leaflets point to the aortic wall.

It can be found that longitudinal force determines the changes in aortic root and ascending. Radial force determines the aortic root deformation of enlarging at the diastole and shrinking during systole. The circumferential force presents the interaction of the aortic root tissues.

The three axis of cylinder system is longitudinal, radial and circumferential direction respectively (figure 61). Longitudinal orientation aligns in the tube extending direction. Radial component represents the orientation that from the central of tube cross-section pointing to the nearest point of the tube wall. A circumferential component refers to the angle that from zero radial component to the certain value.

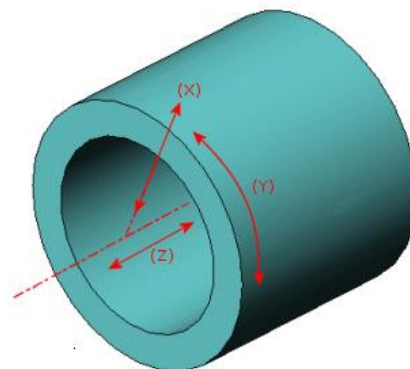


Figure 61. Cylinder system which shows longitudinal component z , radial component x and circumferential component y

In the ANSYS workbench 15.0, the default cylinder coordinate system alignment changes the y component of Cartesian coordinate from orthogonal directions to the circumferential orientation. The orientation of component x and component z stays in the same orientation (figure 62).

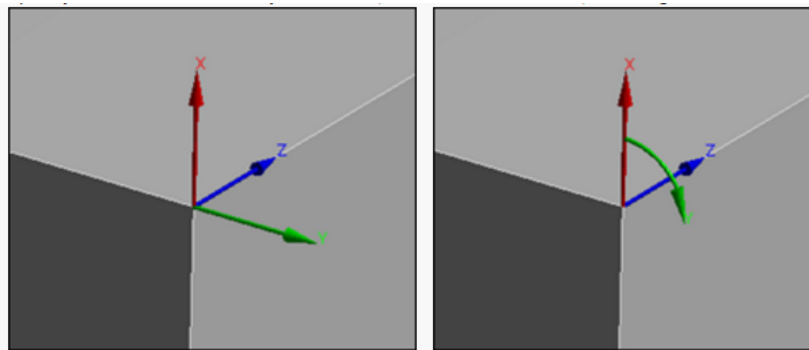


Figure 62 X, Y, and Z component in ANSYS workbench Cartesian coordinate system (left) and in Cylinder coordinate system (right)

Local shell element has a Cartesian coordinate system, and the default material property for the shell element is orthotropic.

In order to ensure the mechanical properties assigned to the correct component, we should give proper material properties in the local shell coordinate system. After transporting the local shell coordinate system to the new Cylinder coordinate system, the alignment of the materials should correspond desire component in the global coordinate system.

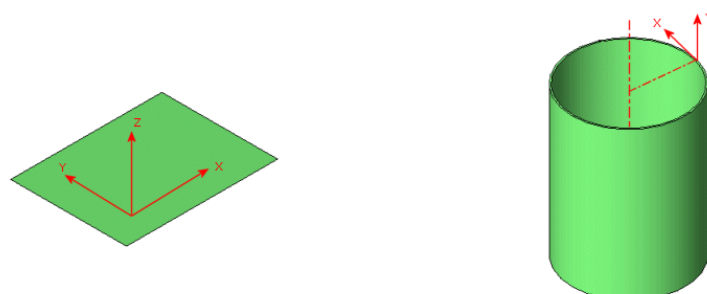


Figure 63. Local shell coordinate system is a Cartesian coordinate system with three component alignment orthogonal directions (left). The shell coordinate system alignment during aligning the shell element to the cylinder system (right). Local shell element y-axis transpose to the global longitudinal component; Local shell element x-axis transpose to the circumferential element; local z-axis aligns to a radial orientation.

There are default rules for transposing local shell Cartesian coordinate system to global Cylinder coordinate system in the ANSYS workbench. At first, local element Cartesian Y-direction changes to longitudinal orientation. Then, local Cartesian X-component transposes to circumferential component and stays at the initial x orientation. Finally, local Cartesian Z axis refers to the radial component (Figure 63).

The aortic root material properties in provides circumferential, radial and longitudinal orientation. Grande et al. (1997) also mentioned that local x and local y correspond to circumferential and radial orientation in the global coordinate system for the aortic leaflet. In terms of aortic root, Grande et al. (1997) assigned local x to circumferential and local y to longitudinal orientation respectively.

4.1.4 Thickness

Aortic root varies thickness at the different parts. Different people record different aortic root thickness value in their article.

Table 2 Review of thickness for aortic root and leaflets

	aortic leaflet(mm)			aortic wall(mm)	
Grande		RC,LC	NC	sinus near leaflet attachment	0.6-1.977
	attachment edge	1.16	0.155	sinus near sino-tubular junction	1.824-2.138
	belly	0.18-0.58	0.18-0.58	Sino-tubular junction	2.142
	coaptation area	0.68-1.29	0.68-1.65	ascending aorta	2.128-2.137
	free margin	1.53	1.96		
	nodules of aranti	2.06	2.75		
Carlo A. Conti	attachment edge	1.16	1.55	aortic duct	2.3
	belly	0.25	0.25	Valsalva sinuses	1.6
	coaptation area	0.99	1.17	Inter-leaflet triangles	2.3
	free margin	1.53	1.96		
Mohammadi	0.8				

Monica Soncini	0.71	aotia	2.13
		Valsalva sinuses	1.64
		interleaflet triangles	2.3
A.N. Smuts	0.25		
Carlo A. Conti, MD	as Grande		
A. Ranga	0.5	1.5	

This study reduces thickness of aortic root to 1.5 mm and the aortic leaflet is 0.5 mm.

4.2 Boundary condition

The duration and contact type should be assigned at the contact face and bodies when two different parts are connected to each other. Different types of mechanical contacts are used in leaflets simulation (Humphrey & Yin 1987). ANSYS has a different method for contacts assignment between two geometries. Aside from the contact types, algorithm and symmetry of contact types can also be defined in ANSYS. A proper contact assignment is crucial for an accurate model simulation.

The aortic root movement simulation includes two types of main contact.

The first type of contact is the aortic root and the aortic leaflets. The aortic root and leaflet are fixed. Therefore, the edges of the aortic root and the aortic leaflets have a bonded contact. An asymmetric behavior is assigned to the contact face because the moduli of the aortic root and that of the aortic leaflet are significantly different in material property assignment.

The second type of contact is the leaflets contacting to each other in the diastole. Grande et al. (1997) assigned the contact face as frictionless. Some studies assumed a frictional contact between the leaflets and assigned

a contact coefficient of 0.05 (Conti et al., 2010b, Soncini et al., 2009b, Conti et al., 2010a). However, other studies defined the contacts as frictionless in reducing the slip between the contact faces (Dellimore et al., 2013, Grande-Allen et al., 2001a, Astorino et al., 2009, Carmody et al., Lim et al., 2004). The friction of the leaflet and the dynamic fluid has a significant effect at the systole (Dellimore et al., 2013), but the friction between the leaflets is negligible.

- Contact definition in FE simulation and assignment of contact pairs

The contact forces in FEA is given by a virtual stiffness matrix. This stiffness matrix generated when two bodies are close to a certain gap value, and once the virtual stiffness matrix created, the two bodies are defined “contacted”. Once contact was detected, the solver uses the contact stiffness matrix to provide pressures and forces. This method reduces the calculation effort by generating a new small matrix instead changing the whole stiffness matrix of two contact bodies.

The contact detection is governed by the pinball region. All the nodes assigned to the potential contact will generate a sphere space with a certain radius. The system automatically creates a new contact matrix at the middle of the two bodies once the nodes find any other body entering this region. the contact matrix calculates the reaction force by the displacement in the pinball region. This reaction force provides strain results, showing a reduced contact gap, or in some cases, pushes the contact bodies away from each other (Figure 64).

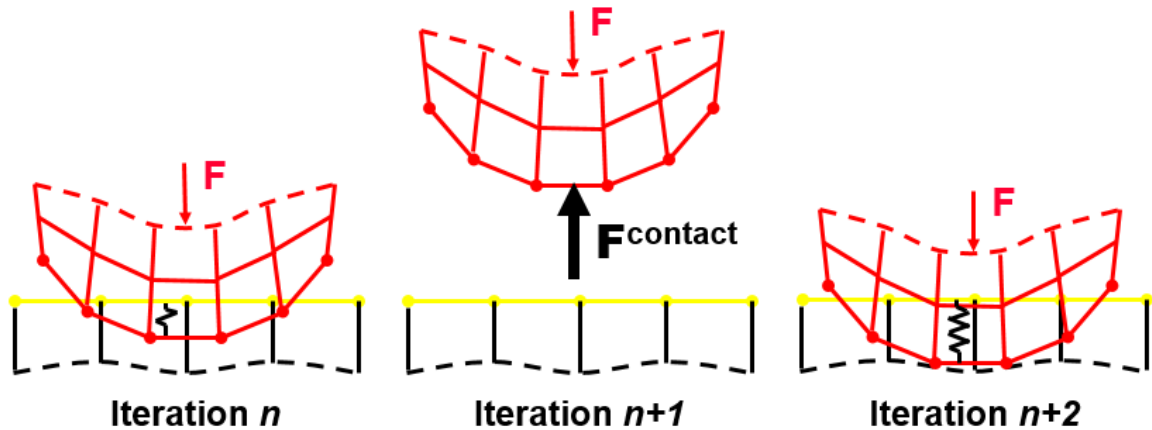


Figure 64 Movement of contact bodies causes different iteration. The two bodies can stay in small contact (situation shown in the left), push away from each other (situation shown in the middle), or generate large penetration (situation shown in the right). Iteration value is the results of applying iterative method. Iterative method helps increasing surface converge ability when solving FE problems. More details of this method can be found in Oysu (2007).

All the contact nodes generate their own pinball regions. However, the contacts in the FE only calculate one pinball region when the two nodes are close. When "contact" is detected between two parts, one of the 'contact bodies' will be assigned to the 'target body', and the other will be assigned to the 'contact body'. The solver system only recognizes the contact when the nodes or interaction points on the 'contact bodies' are close to the surface of the 'target bodies' rather than the other way around.

A stiffer body (aortic wall) should be assigned as the target and the softer body (aortic leaflets) should be set as the contact for non-linear problems that include two different kinds of stiffness (e.g., aortic leaflets and aortic wall). One of the reasons for this assignment is the softer body having a larger deformation during the simulation. The movement of two contacting bodies may generate a small penetration because the contact detection is not achieved in real time. Allowing penetrate between large movement bodies enhances the model converge.

Moreover, we should ensure that the coarse mesh surface is the target when looking for the target surface assignment. This method reduces the penetration of the contact. The larger surface, such as the aortic wall, is preferred to be the target surface.

The aortic wall is assigned as the target surface in this study because it is stiffer and has a coarser mesh and a larger face. During the contact assignment of the leaflets, we should ensure that each leaflet has one contact face and one target face. Three 'contacts' exist between three leaflets, and each 'contact' has one 'target face' and one 'contact face.' Hence, the total number of contact faces is six faces. Each leaflet involves two contacts.

Moreover, when we looking for the assignment of the target surface, we should take care that ensuring the coarse mesh surface be the target. This method reduces penetrate of contact. The larger surface such as aortic wall prefers to be target surface. In this model, the aortic wall has a coarse mesh of 5mm, while aortic leaflets have mesh size of 1mm. Therefore, the aortic wall is more suit for assign to 'Target body'.

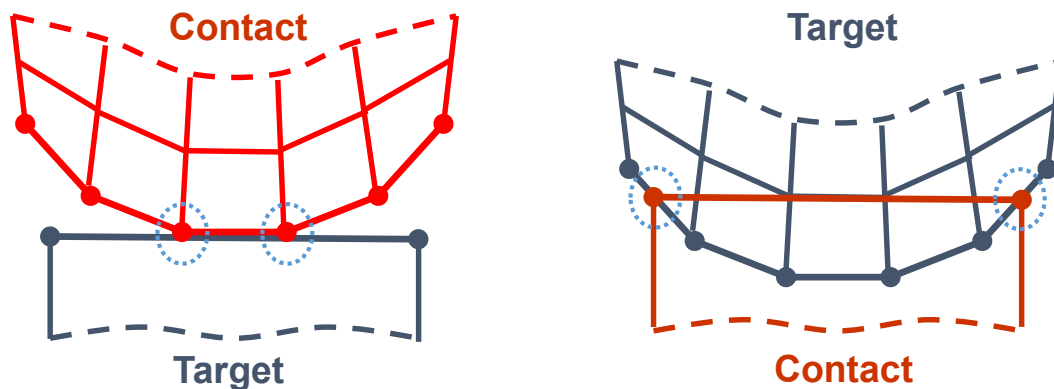


Figure 65 when coarse mesh body be the target body (left), the 'contact' is recognized properly. When the coarse mesh body be the contact body (right), the 'contact' dose not be detected properly.

Hence, the aortic wall is assigned as target surface in this study, since it is stiffer, coarser mesh, and larger face. During contact assignment of the leaflets, we should ensure that each leaflet has one contact face and one target face (there are three 'contact' between three leaflets, and each 'contact' have one 'target

face' and one 'contact face', so the whole contact faces are six faces, each leaflet involve in two contacts)

- Algorithm for two types of contact of aortic root simulation

Aortic leaflets move to contact in the diastole and dis-contact in the systole. The large movement of aortic leaflets generates penetration during simulation. Solver provides two types of algorithm to solve penetration problems, which are Penalty-based method and Augmented Lagrangian method. Those two methods both compute contact matrix by the depth of penetration.

In the penalty-based method, contact matrix is:

$$p = k_n x_n$$

Where k_n is contact stiffness matrix and x_n shows the penetration of two parts. Calculation need value of x_n to solve unknown p . The penetration X_n could be positive value, negative value, or zero, which result in push force, push-back force and zero force.

Augmented Lagrangian is developed on Penalty-base method, but an additional distance term λ , so full formulation becomes:

$$p = k_n x_n + \lambda$$

Introducing λ reduces the penetration sensitivity. Thus, this algorithm ensures that the simulation converges even though the penetration is above the maximum allowance.

The penalty-based method is widely used in linear problems, whereas the Lagrangian method is suited for non-linear problems, such as the aortic root simulation. Therefore, the augmented Lagrangian method is recommended for a large deformation.

The aortic leaflets and the aortic wall have a rigid bond contact. Instead of the penalty-based method, the normal language and multi-point constraint (MPC) methods are utilized for the rigid bond contacts with a nearly zero-penetration property. However, these two methods achieve almost a non-penetration state in two different ways.

The normal language method obtains almost zero penetration by increasing the degree-of-freedom of the contact elements. This method alleviates the addition of an extra stiffness matrix, thereby obtaining more accurate results after the simulation. However, this method dramatically adds extra computational effort and has high potential leading to convergence problems.

Figure 66 shows that no transition state exists between the 'contact' and the 'non-contact' when the normal language formulation is applied in the model. The model experiences a large deformation during the simulation, and is not appropriate for this approach.

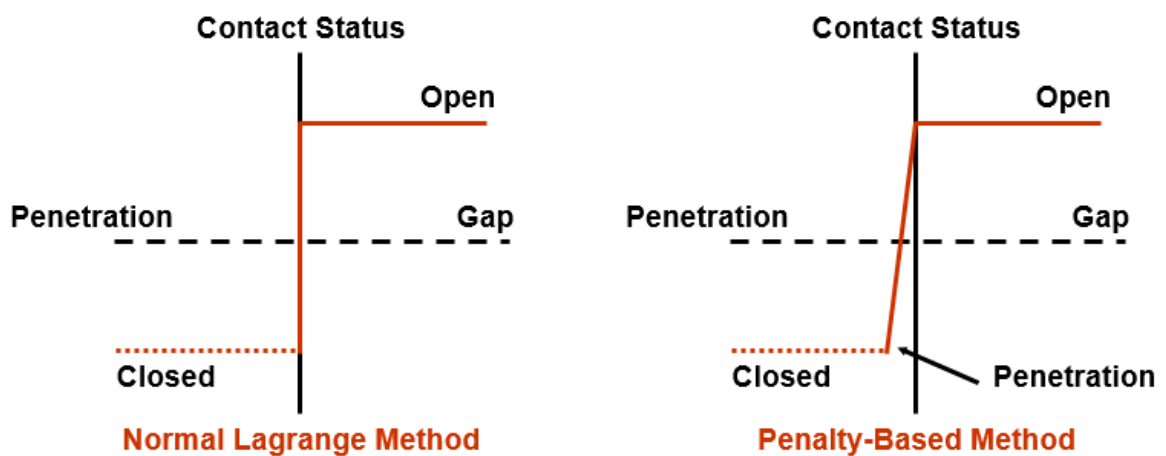


Figure 66 Different methods use different gap algorithm

Alternatively, MPC method shows a good performance in huge degeneration models. Basically, additional equations are assigned to bond the nodes that inside the contact pinball region. This approach is most suit for face contact and large deformation contact of bonding bodies.

- Contact detect point assignment

Contact simulation algorithms use vastly different contact determination methods during a simulation. The penalty-based method detects the integration points of elements, whereas the normal language and MPC methods are built on node detection. Nodes are the points created in the mesh process, and interaction points are generated between the nodes.

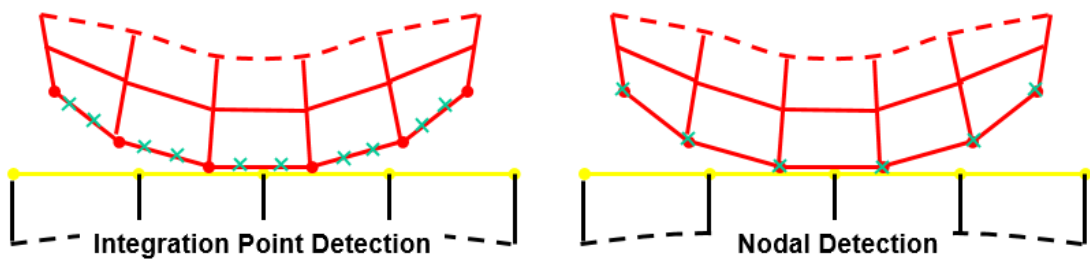


Figure 67 Integration detection method detect contact from integration points (left) while nodal detection method detect contact by the nodes at mesh (right)

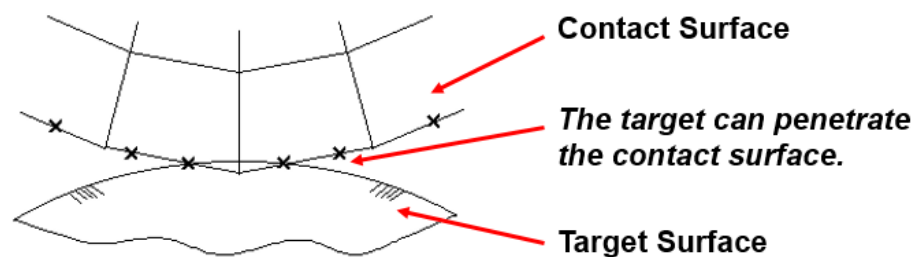


Figure 68 contact is detected when the contact body close to the target body

Our model is a pure surface model. Hence, we only considered the surface contact. Three types of surface contact are utilized in ANSYS—face-to-face, face-to-edge, and edge-to-edge. The face-to-face contact has the highest priority in ANSYS. The face-to-edge contact is not recommended because of the high strain energy that is well generated in the joint (a detail discussion can be found in the “Limitation of shell element” section). However, our model requires this type of connection. Hence, instead of avoiding the weld joint

contact, we are looking for a method to decrease the high stress at the joint. High stress can be reduced in two ways.

There are several methods to decrease high stress at the joint.

At first, refining mesh can help the distribution of stress. A fine mesh includes more nodes to propagate stresses rather than concentrates large stresses on few nodes. Secondly, the normal stiffness can be decreased. The default value of contact normal stiffness is 1, which is too large regards to pure soft tissue connection. ANSYS tutorial suggests using 0.1 and 0.01 for bending problems (ANSYS, 2013). Grande (1997) use value 0.002 without explain details, and it is merely mentioned normal stiffness factor value assignment in other people's studies. Therefore, the value of stiffness for contact matrix factor between leaflets and aortic wall was reduced to 0.002.

Finally, the assignment of the whole aortic root is as table 3.

4.2.2 Fixing

The aortic root is fully fixing at cylinder coordinate X and Y orientation. Moreover, the lowest layer of the aortic root given 'fixed support' to ensure that the whole body do not move away during the loading process. Ranga et al. (2007) constrain both the bottom and the top of the model. In this study, the Z orientation of aortic root allows extension undergoing loading. There is no special constrain for leaflets.

Table 3 Assignment of aortic root in ANSYS scope and definition part

Object Name	Bonded - LC fitting leaflet To Aortic Wall	Bonded - NC fitting leaflet To Aortic Wall	Bonded - RC fitting leaflet To Aortic Wall	Frictionless - LC fitting leaflet To NC fitting leaflet	Frictionless - NC fitting leaflet To RC fitting leaflet	Frictionless - RC fitting leaflet To LC fitting leaflet
Scope						
Contact Bodies	LC fitting leaflet	NC fitting leaflet	RC fitting leaflet	LC fitting leaflet	NC fitting leaflet	RC fitting leaflet
Target Bodies	Aortic Wall	Aortic Wall	Aortic Wall	NC fitting leaflet	RC fitting leaflet	LC fitting leaflet
Shell Thickness Effect	No					
Definition						
Type	Bonded	Bonded	Bonded	Frictionless	Frictionless	Frictionless
Formulation	MPC	MPC	MPC	Augmented Lagrange	Augmented Lagrange	Augmented Lagrange
Constraint Type	Inside Pinball, Couple U to ROT	Inside Pinball, Couple U to ROT	Inside Pinball, Couple U to ROT			
Pinball Radius	1 mm	1 mm	1 mm	1 mm	1 mm	1 mm
Detection Method				Nodal-Projected Normal From Contact	Nodal-Projected Normal From Contact	Nodal-Projected Normal From Contact
Normal Stiffness Factor				2.00E-03	2.00E-03	2.00E-03
Update Stiffness				Each Iteration	Each Iteration	Each Iteration
Interface Treatment				Add Offset, No Ramping	Add Offset, No Ramping	Add Offset, No Ramping

4.2.3 Loading

Howard, Patterson, and Yoxall (2003) and Carmody et al. (2006) proved that blood pressure changes in different leaflets locations, but the influence of this change could be ignored during the simulation. These results were verified by later researches (Koch et al., 2010, Soncini et al., 2009b, Conti et al., 2010b). Therefore, the uniform pulse pressure can be applied at the aortic leaflets and aortic root model to perform a normal cardiac cycle.

Aortic root pressure is increased to the end-systole pressure before loading pressure at the inner side of the aortic leaflets. The bottom of the aortic root is then loaded with ventricular pressure. The whole loading circle is simplified from Grande et al. (1997). Figure 69 shows the details.

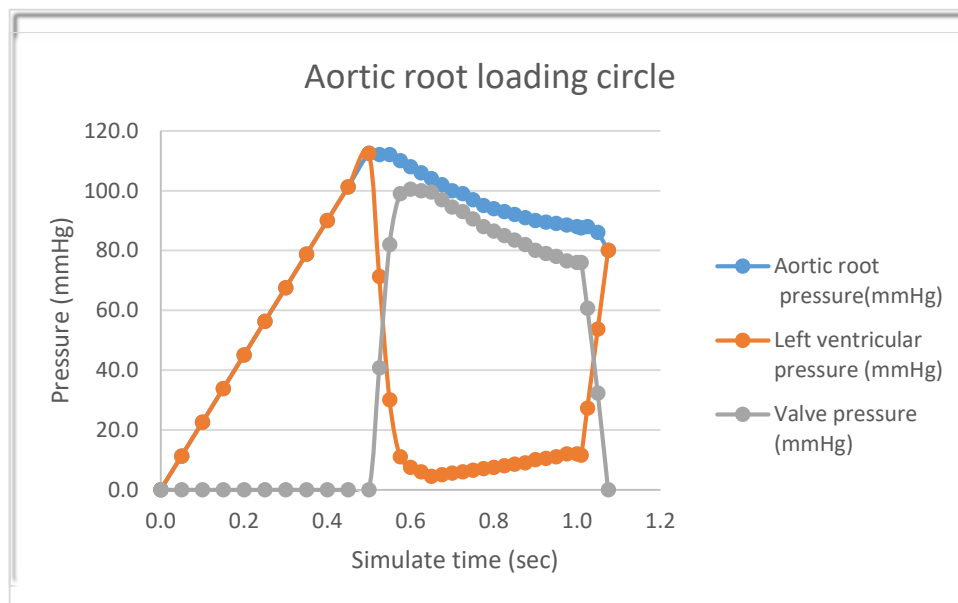


Figure 69 Loading circle of aortic root (modified from Grande et al, 1997)

4.3 Mesh refinement

Mesh quality highly affects the performance of models simulation process and results. A good mesh response accurate catch the geometry feature of the model as well as fine mechanical properties propagation. A poor mesh results in high strain energy at sharp corners and connections. In this study, we

adjust the total mesh relevance to 7 and mesh type to 'Mechanical' to ensure the mesh quality at medium level.

4.3.1 Intensive mesh in important place

The aortic leaflets should have higher mesh density than the aortic wall surface, since aortic leaflets are expected to have a large movement. Moreover, the force propagation at aortic leaflet is more complex. Study assign mesh element size to 0.7mm at aortic wall and 0.5 mm at aortic leaflets.

4.3.2 Topology capture

Initially, the more specific mesh gives more integral geometry feature. However, the intensive mesh couples with large computation. In terms of our model, original 3-D model from Scan IP is not smooth ideal since the resolution of CT image. Therefore, instead of applying intensive mesh to capture curvature and proximity, we increase smoothing and defeaturing tolerance (set as 0.5mm).

Smooth and defeaturing elevate the sharp transient in initial mesh information.

4.3.3 Sizing and Mapping

'Sizing' constrains element number at the edge. 'Mapping' pronounces an equally mesh element from one edge to another. Combination of these two methods preforms a uniform mesh at surface. Uniform mesh improves strain and stress distribution at the surface. This factor extremely important to leaflets, since studies shows the mesh alignment at leaflets regards to the fibers of leaflets. These fiber orientations represent the strain stress distribution at the leaflets during filling with blood.

For the aortic leaflets, we sizing left and right boundary with 50 elements at each side. Then, applying mapping to leaflets to create uniform mesh.

Moreover, to increase element contact quality, we constrain the element size of aortic wall is 0.3 mm. This reduces the difference of element size at contact edges.

4.2.4 Mesh connection

Mesh connection help the model to observe the continuous mesh between large surface and the other small surfaces which connecting the large surface with edge. The vales connecting aortic wall is similar to the describe situation above.

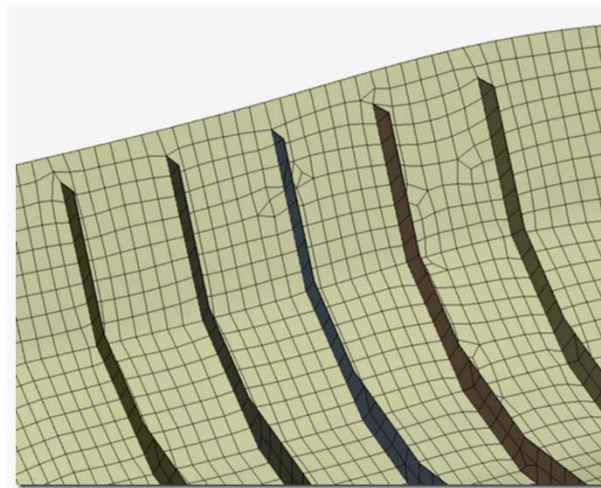


Figure 70 Typical mesh connection

During mesh connection, edge/faces detection is the primary method to detect the connection and the software adjust the mesh in the large surface to match the edge of mesh at small surface. Mesh connection also can combine two geometries with gap in the tolerance. Because our model has a fitting leaflets and the leaflets are not fully attached to the aortic wall. Mesh connection method were introduced to enhance the connection between leaflets edge to aortic wall.

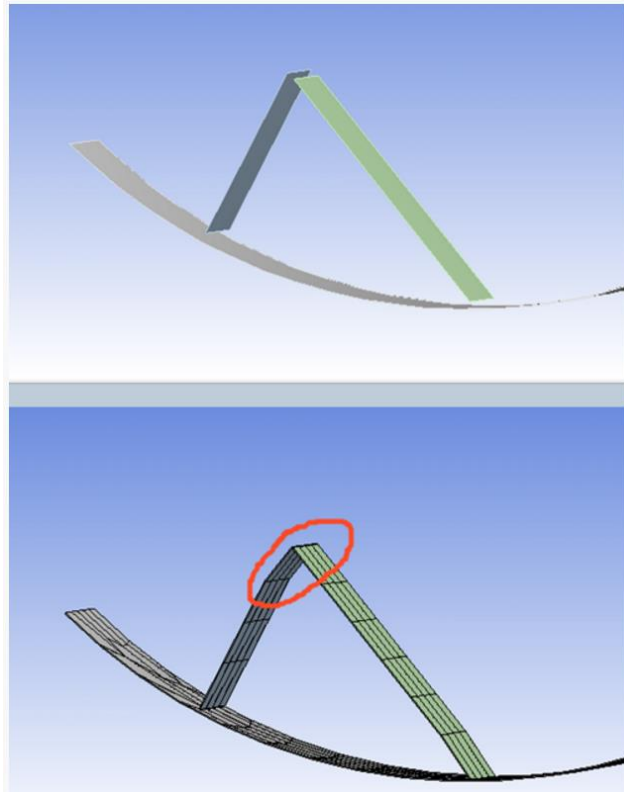


Figure 71 Mesh connection method combine two separated geometries when meshing

Chapter 5 Results

5.1 Results of model building

5.1.1 Image processing validation

- Smooth change validation

Smoothing process is very important to this mode. Since the limitation of the resolution, the surface of the model is not smooth enough. However, the smooth process will change the geometry of the initial model. We should ensure the geometry variation, especially the change of surface of the three leaflets parts, are in the tolerance lower than 5%.

Table 4. Data comparison of before and after soothing

		RC	LC	NC	Aortic wall
Surface area (mm ²)	Before smooth	2850	2560	2850	10400
	after smooth	2890	2650	2870	10400
	area error	1.40%	3.52%	0.70%	0.00%
Volume (mm ³)	Before smooth	4930	4450	4750	30500
	after smooth	5540	5060	5280	32200
	volume error	12.37%	13.71%	11.16%	5.57%
Voxel count	Before smooth	55546	50141	53460	343863
	after smooth	62399	56977	59448	362870
	voxel error	12.34%	13.63%	11.20%	5.53%
Mean greyscale (Original)	Before smooth	501	529	505	489
	after smooth	487	519	491	465
	greyscale error	2.79%	1.89%	2.77%	4.91%

RC: Right Coronary Leaflet (have cups)

LC: Left Coronary Leaflet (have cups)

NC: Non-coronary Leaflet (have no cups)

The volume of solid model changing significant during smoothing, but surface variation is not extreme. The volume change in the left coronary leaflet is the most significant. All the difference for volume change at leaflets is higher than 10%. The smooth process in 3D model tries to reduce the extreme value and

constrain uniformed body to sphere body. Thus, the change of volume increase significantly, but the surface area of solid body did not change that much.

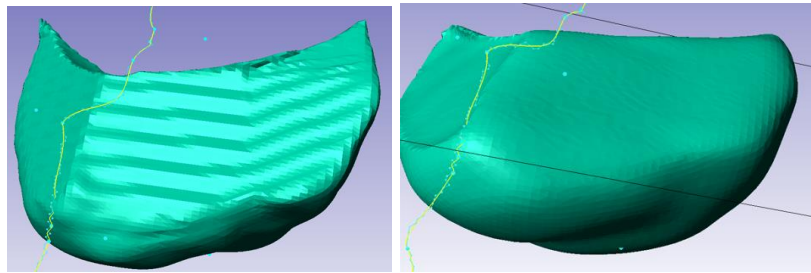


Figure 72 The leaflet volume that connecting to commissure is reduced significant during smoothing

5.1.2 Geometry validation

- Aortic valve validation diameter

The special anatomy feature of aortic root makes that normal measurement method does not suit for it. The STJ is ellipse ring. The long direction and short direction of STJ should be measured separately and the average data of them are the value of STJ diameter. Generally, there are two ways used for the diameter measurement of the aortic sinus (Freeman et al., 2013, Matura et al., 2007). The first method determines the diameter of the aortic root by measure the distance from one cups to the other cups, while the second way access diameter from the distance of cups and commissure (Figure 73). Freeman et al. (2013) suggested to measure the distance by both method and Rajiah (2013) suggested that each diameter measure three times.

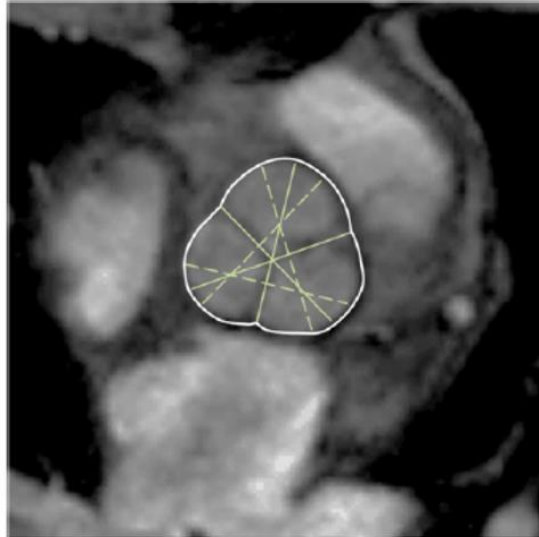


Figure 73. Position of Cusp- Commissure (solid line) and Cusp- Cusp measurement (dash line)

(Kawel-Boehm et al., 2015)

The mean of this aortic root is in table 5. Kunzelman et al. (1994) state the aortic root, the patient's annulus is more than double of normal value. The similar enlargement can be also found in the aortic sinus. It means this patient has dilatation at aortic root and the dilatation is almost 100%.

Table 5 Aortic root measurement

Position	Annulars (mm)	Cup - Commissure(mm)			Cup - Cup(mm)			STJ long Axis (mm)	STJ short Axis (mm)
		RC - commissure	LC - commissure	NC - commissure	RC - LC	LC - NC	NC - RC		
Measurement 1	34.61	40.91	38.12	41.68	42.37	40.52	44.14	28.30	28.30
Measurement 2	36.61	40.62	37.81	40.79	43.60	39.58	43.88	28.97	28.97
Measurement 3	35.84	41.84	38.51	40.63	42.88	41.36	43.63	29.13	29.13
Average	35.69	41.12	38.15	41.03	42.95	40.49	43.88	28.80	28.80

RC : Right sinus(connecting right coronary)

LC : Left sinus(connecting light coronary)

NC: Non-coronary

STJ: Sinutubular junction

In medicine, dilated artery is defined 50% larger than the normal diameter of artery, so this patient has dilated aortic root. It is recommended to take a surgery when the aneurysms larger than 5.5 cm. For some special high risk cases, a surgery is recommended after increasing of aortic root more than 6 cm (Isselbacher, 2005).

Since the aortic root already dilatation, parameter in the aortic root is hard to compare to the value at normal aortic root. Therefore, we use the method that refers different diameter to sinutubacular junction diameter to justify model reconstruction (Swanson and Clark, 1974).

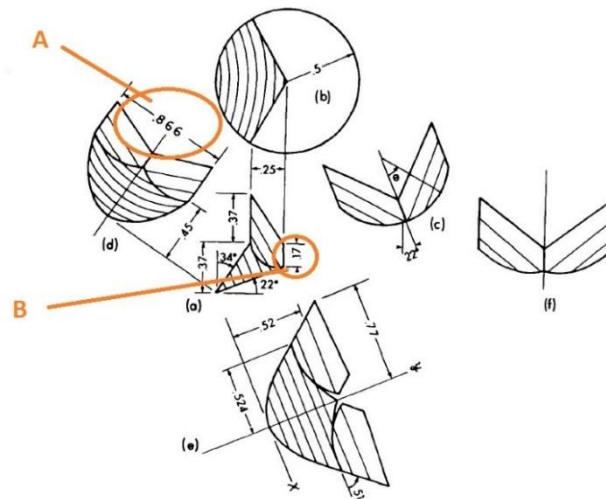


FIGURE 10
 a: Side profile through attachment plane. b: View from left ventricular side. c: Section through cylindrical leaflet profile. d: Projected attachment line profile. e: Developed surface of leaflet. f: Planar layout of coapting surfaces. Dimensions are relative to $d_s^* = 1.0$.

Figure 74 Relative value at aortic leaflet when STJ diameter is 1 (note where is the value A, and B)(Nataf and Lansac, 2006)

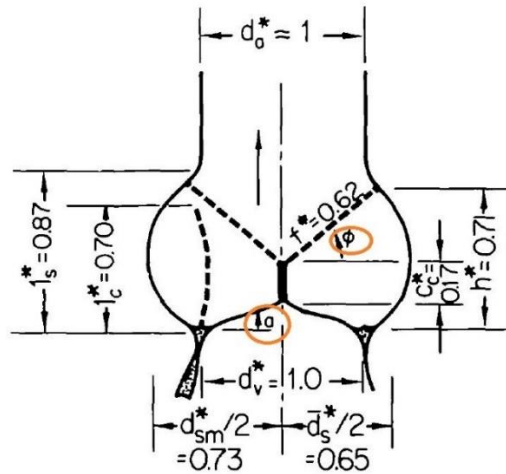


FIGURE 2

Geometry and relative dimensions of aortic valve region.
See text for abbreviations.

Circulation Research, Vol. 35, December 1974

Figure 75 Relative value at aortic root when STJ diameter is 1 (note where is α and ϕ , those two angles are measured in the table 6) (Nataf and Lansac, 2006)

Average values are recorded in table 6. All the value is given from geometry measurement of STJ, diameter A and B in figure 74, and angle α and ϕ in figure 75.

Table 6 Aortic root geometry validation

	STJ (mm)	A (mm)	B (mm)	Annulus (mm)	α (degree)	ϕ (degree)
reference value	31.33	26.94	5.30	31.33	17.00	46.20
Average of real value	31.33	27.81	5.43	30.12	16.30	49.69
error	0.00%	3.23%	2.45%	3.84%	4.12%	7.55%

The STJ has 0 error because the diameter is represented as a reference value. The angle ϕ has the largest error 7.55% and all the rest errors are lower than 5%. If we take the STJ 31.33 as a reference value, it is reasonable to have diameter A and B in this large. The error at angles is more significant than that in diameter. The smallest error in angle group is 4.12% at angle α , while this

number still larger than the maximum error of diameter group: diameter annulus 3.84%.

- Aortic leaflet surface area validation

<i>Table 7. Surface area of aortic root</i>			
Aortic wall	LC leaflet	NC leaflet	RC leaflet
4937.3 mm ²	579.9 mm ²	568.58 mm ²	620.98 mm ²

It can be found the largest surface is right coronary leaflet and the area of the left coronary leaflet and non-coronary leaflets have similar value (Poutanen et al., 2006). Moreover, A normal aortic leaflet has surface area $2.7 \text{ cm}^2 \pm 0.5 \text{ cm}^2$ (Poutanen et al., 2006). The rise of the annulus is positive corresponding to the size of the aortic leaflet. The diameter of the annulus is pronounced has twice larger comparing to normal aortic root. The surface area of the leaflet in this study is twice as the normal leaflets.

5.1.3 Mesh quality checking

The undesired mesh causes the model hard to converge in the simulation, since the bad mesh at aortic root domains strains distribution of model. The high strain concentrates in small spot causes model stop running automatically.

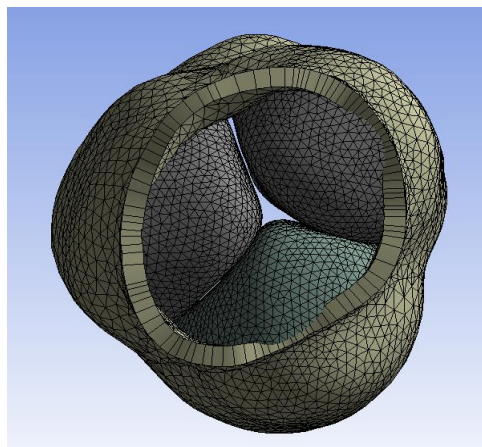


Figure 76 Button view of the aortic root. The aortic wall is outside body and the three leaflets are inside bodies

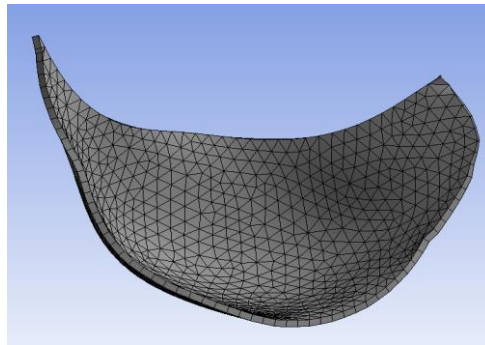


Figure 77 Front view of aortic leaflets

There are some embedded methods in ANSYS 15.0 to justify the mesh quality. In this study, we pick three measurements to justify the model mesh quality. (details are shown in table 8)

- Jacobian ratio

The Jacobian ratio shows deviation that encountered to measured mesh and unreformed shape. The scale can vary from 0 to 1. The increasing of Jacobian ratio represents that the mesh is similar to shell original geometry, while the decrease of the Jacobian ratio means shell elements have large deformation after meshing. The deformation is generated by extension and compression of local elements in order to match the global geometry. However, large deformation causes elements reducing ability to transfer strain and stress energy, which generates errors in the numerical calculation.

Jacobian Matrix is A X A dimension matrix related to the integration points of elements as follows:

$$J(x_1, \dots, x_n) = \begin{bmatrix} \frac{\partial f_1}{\partial x_1} & \dots & \frac{\partial f_1}{\partial x_n} \\ \vdots & \ddots & \vdots \\ \frac{\partial f_n}{\partial x_1} & \dots & \frac{\partial f_n}{\partial x_n} \end{bmatrix}$$

Where the function $f = (f_1(x_1, \dots, x_n), \dots, f_n(x_1, \dots, x_n))$

Third party software packages obtain Jacobian value by all the integration points. For instance, an element has 5 integration point will give determinant 5 X 5 Matrix. Jacobian ratio measured the deviation between the smallest number and the largest number in the Jacobian matrix. When the results of deviation closing to 1, the mesh is proved to have high quality. This mesh checking method can be applied to all the solid and plate elements, which is suitable for element in this study (shell 181) as well. (results details are in table 8)

- Element quality

This selection returns the shape difference of real mesh elements and ideal elements. Unlike Jacobian ratio, the difference is not given from deviation. Element quality accessing the change is directly given from the change of points that from the shell elements. For instance, 8 nodes shell element gain 'element quality' from the displacement at 8 nodes, while 4 nodes shell element has 'element quality' from change at 4 nodes.

- Aspect ratio

Aspect ratio returns the value of largest dimension over the smallest dimension of elements.

$$Aspect\ ratio = \frac{\text{largest dimension}}{\text{smallest dimension}}$$

Therefore, the increasing of aspect ratio means the quality of mesh decrease. The larger aspect ratio causes a large error in the displacement (figure 78).

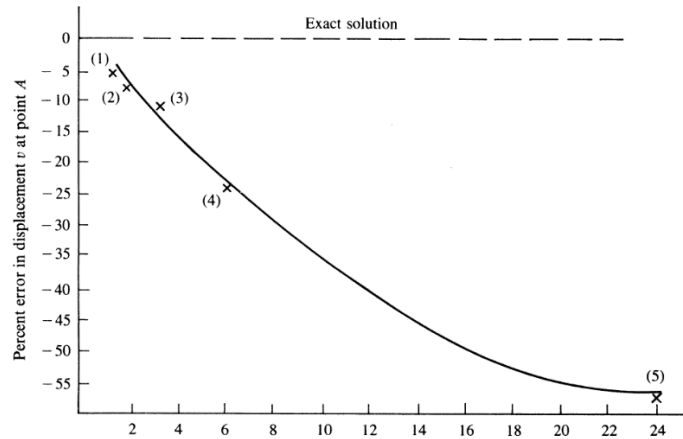


Figure 78 Error increase as aspect ratio far away from 1

The increasing of mesh density in this model do not affect Aspect ratio and Jacobian ratio during testing. Moreover, Element quality does not change after mesh density increased to a certain level. Therefore, the mesh density of model is adjusted to the value which maintains the element quality and is not too aggressive in order to reduce computational complex. (results details are in table 8)

Table 8 showed that a good performance in Jacobian Ratio since all the Jacobian Ratio is 1. Element quality can be adjusted by manually changing mesh density, so tolerance is controllable. Aspect Ratio has the largest stander deviation among those three values.

Table 8 Aortic root mesh quality checking

	Total Aortic root			Aortic wall			LC leaflet			NC leaflet			RC leaflet		
Nodes	4136			2275			667			659			718		
Elements	8143			4369			1229			1211			1334		
Mesh Metric	Element Quality	Aspect Ratio	Jacobian Ratio	Element Quality	Aspect Ratio	Jacobian Ratio	Element Quality	Aspect Ratio	Jacobian Ratio	Element Quality	Aspect Ratio	Jacobian Ratio	Element Quality	Aspect Ratio	Jacobian Ratio
Min	5.31E-02	1.00E+00	1.00E+00	2.11E-01	1.00E+00	1.00E+00	6.23E-01	1.00E+00	1.00E+00	5.31E-02	1.00E+00	1.00E+00	5.36E-01	1.01E+00	1.00E+00
Max	1.00E+00	3.68E+01	1.00E+00	1.00E+00	8.95E+00	1.00E+00	1.00E+00	2.58E+00	1.00E+00	1.00E+00	3.68E+01	1.00E+00	1.00E+00	3.17E+00	1.00E+00
Average	9.53E-01	1.25E+00	1.00E+00	9.39E-01	1.30E+00	1.00E+00	9.71E-01	1.17E+00	1.00E+00	9.70E-01	1.21E+00	1.00E+00	9.68E-01	1.18E+00	1.00E+00
Standard Deviation	7.83E-02	5.49E-01	0.00E+00	9.73E-02	4.75E-01	0.00E+00	3.06E-02	1.18E-01	0.00E+00	5.66E-02	1.08E+00	0.00E+00	3.47E-02	1.35E-01	0.00E+00

5.1.4 Element normal checking

Element normal is the main parameter to check whether material properties were assigned to the correct position. Aortic root has cylinder coordinate system and it is assigned with orthotropic material properties, so the element normal is an important value to check in this model.

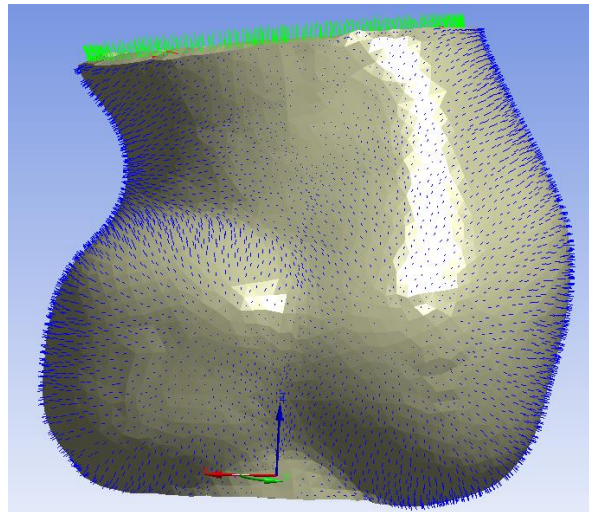


Figure 79 Small blue arrows show element normal. All the element normal point to the outside of the aortic root

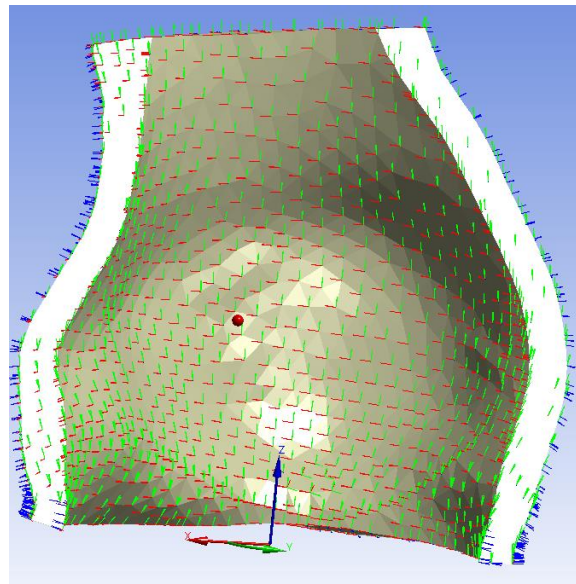


Figure 80 Inner alignment of element normal at the aortic root model (cutting half view). Small green arrows represent element Y axis and small red arrow point to element X axis. Element normal aligns uniform along the aortic root.

An element in aortic root aligns to the ideal orientation. All the element X axis aligns to the circumferential orientation. Since the leaflets are not uniform

geometry, the alignment of the element normal at leaflet surface is not as good as it is at the aortic root. However, the layered element coordinate system arrangement still can be observed at the aortic leaflet.

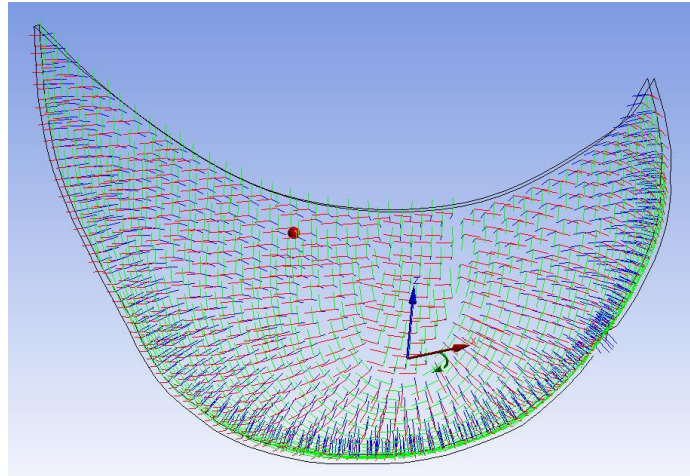


Figure 81 The alignment of aortic leaflet shows that the main orientation of small red arrows along at circumferential orientation

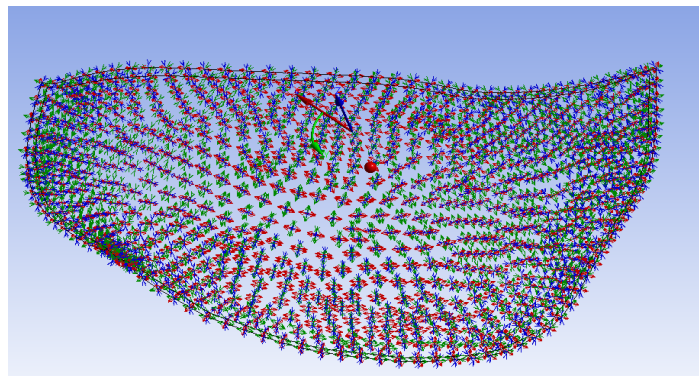


Figure 82 Vector of element shows similar alignment as in element normal

5.1.5 Contact

Table 9 initial contact table

For additional options, please visit the context menu for this table (right mouse button)

Name	Contact Side	Type	Status	Number Contacting	Penetration (mm)	Gap (mm)	Geometric Penetration (mm)	Geometric Gap (mm)	Resulting Pinball (mm)	Normal Stiffness (N/mm ²)	Real Constant
Bonded - LC fitting valve To Aortic Wall	Contact	Bonded	Closed	61.	0.	0.	0.	0.20786	1.	N/A	5.
Bonded - LC fitting valve To Aortic Wall	Target	Bonded	Inactive	N/A	N/A	N/A	N/A	N/A	N/A	N/A	0.
Bonded - NC fitting valve To Aortic Wall	Contact	Bonded	Closed	62.	0.	0.	0.	0.	1.	N/A	7.
Bonded - NC fitting valve To Aortic Wall	Target	Bonded	Inactive	N/A	N/A	N/A	N/A	N/A	N/A	N/A	0.
Bonded - RC fitting valve To Aortic Wall	Target	Bonded	Inactive	N/A	N/A	N/A	N/A	N/A	N/A	N/A	0.
Bonded - RC fitting valve To Aortic Wall	Contact	Bonded	Closed	62.	0.	0.	0.	0.40326	1.	N/A	9.
Frictionless - LC fitting valve To NC fitting valve	Target	Frictionless	Closed	3.	7.8886e-031	0.	0.	0.	1.	1.377e-002	12.
Frictionless - LC fitting valve To NC fitting valve	Contact	Frictionless	Closed	3.	7.8886e-031	0.	7.8886e-031	0.23673	1.	1.377e-002	11.
Frictionless - NC fitting valve To RC fitting valve	Contact	Frictionless	Closed	3.	7.8886e-031	0.	0.	0.	1.	1.377e-002	13.
Frictionless - NC fitting valve To RC fitting valve	Target	Frictionless	Inactive	N/A	N/A	N/A	N/A	N/A	N/A	N/A	0.
Frictionless - RC fitting valve To LC fitting valve	Contact	Frictionless	Closed	1.	7.8886e-031	0.	0.	0.	1.	1.377e-002	15.
Frictionless - RC fitting valve To LC fitting valve	Target	Frictionless	Inactive	N/A	N/A	N/A	N/A	N/A	N/A	N/A	0.

Color Legend

Red	The contact status is open but the type of contact is meant to be closed. This applies to bonded and no separation contact types.
Yellow	The contact status is open. This may be acceptable.
Orange	The contact status is closed but has a large amount of gap or penetration. Check penetration and gap compared to pinball and depth.
Gray	Contact is inactive. This can occur for MPC and Normal Lagrange formulations. It can also occur for auto asymmetric behavior.

This table shows the all the contact of the aortic root simulation model. LC, RC, and NC fitting leaflet represent Left coronary leaflet, right coronary leaflet, and Non-coronary leaflet separately. The top six contacts are 'bonded contact' which define the connection of the three aortic leaflets and the aortic wall. The last six contacts are 'frictionless contact' which define the connection of the three leaflets. Different colours show the states of this contacts. Red colour shows that the contact is not good defined. Colour yellow and orange illustrate the status of contact not ideal, but errors are acceptable. Contacts in the grey colour are not active in current geometry situation. This table also illustrate information such as nodes that in the contact status, parameters of penetration, and gap value of this contact and geometries

Table 9 shows the 'contact' of the leaflet to aortic wall is assigned properly and the gaps between leaflets are in the tolerance.

There is no 'contact' in the red status. The only warning (orange colour) appears in the connection between RC leaflet and aortic wall. Since the initial surface of the aortic root is curved, the fitting leaflets are not attaching to the aortic wall perfectly. However, the penetration gap 0.40326 mm is small than the pinball region 1 mm. Hence, the model supposes the bonded contact valid.

During simulation, the contact of the aortic root is detected by pinball region of each element. Moreover, the leaflets loading process needs to divide into small steps and let the computer checking 'contact' state and contacting nodes at the end of each step. The physiology pressure of the aortic leaflets ramped very slowly at the beginning (figure 83) to ensure the model converged.

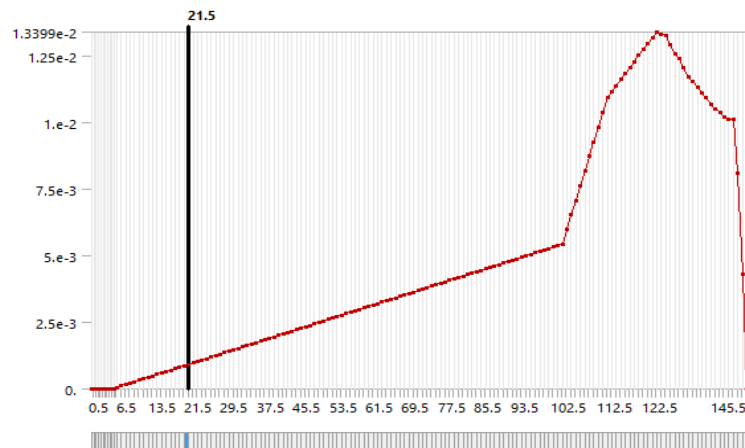


Figure 83. Real loading process in the model simulation

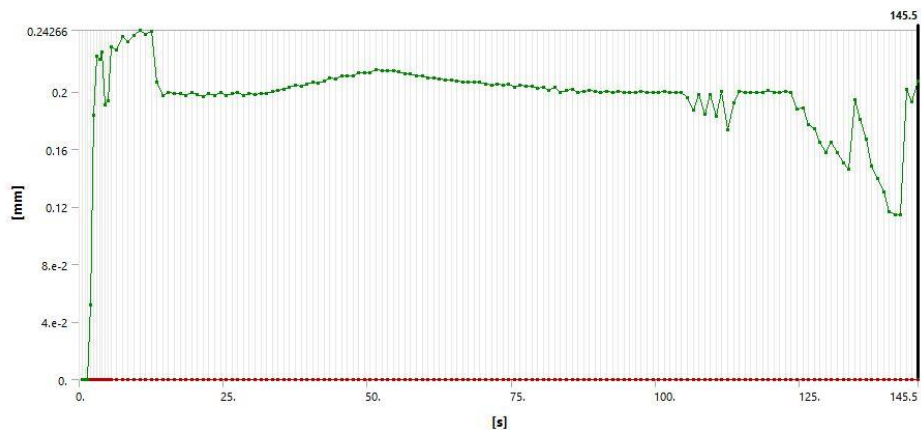


Figure 84. Penetration over the whole process

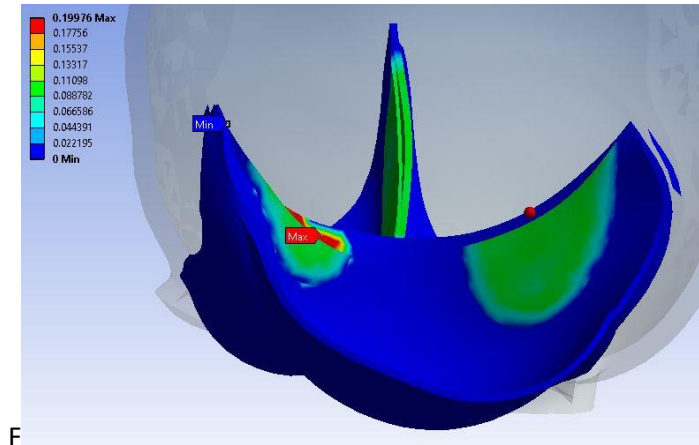


Figure 85 Penetration when the loading achieves maximum (at 125.5s)

Penetration of this model increases rapidly during the first few steps (figure 84), since the dramatic change of pressure at the aortic root at this time. The penetration traces almost stay in 0.2 mm after the contact of the leaflet has all been recognized and contacted. This figure shows the leaflets contact process finished at near 65s, which still at the slow loading region as talked above.

Table 10 Overall process contact checking

	Gap (mm)	Penetration (mm)	Pressure (MPa)
Minimum	-0.99858	0	0
Maximum	0	0.18083	0.0012938
Minimum occur	LC fitting leaflet	Aortic Wall	Aortic wall
Maximum occur	Aortic Wall	RC leaflet	RC leaflet

The maximum gap of the process is very close to the pinball region 1 mm.

5.2 Mechanical results checking

5.2.1 Converge

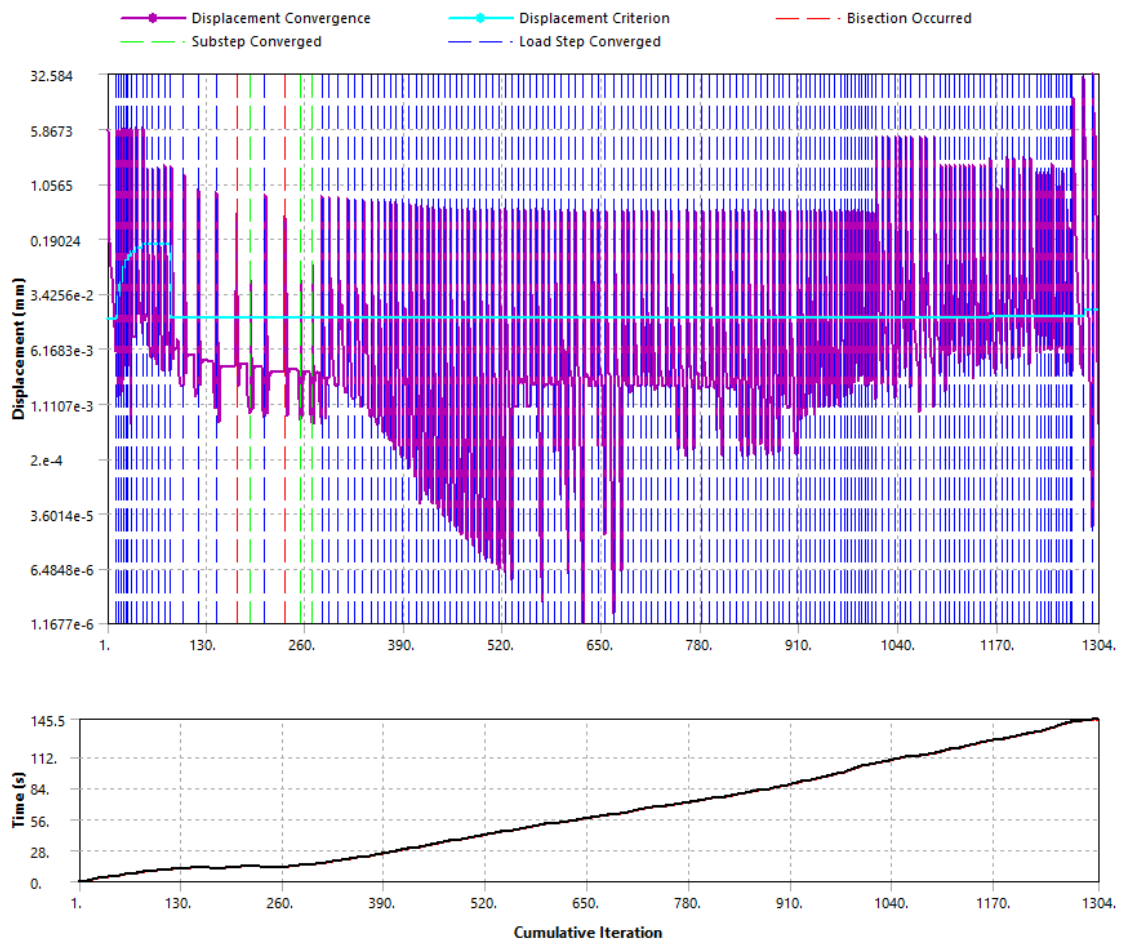


Figure 86 Overall process displacement residual converge

The whole steps of this model process are 151, so residual converge plot includes massive information. The whole process shows the converge has high oscillation. The model residual increase at beginning of each step since the force at aortic root rise at most steps. On the other hand, one leaflet pushes the other two leaflets and it also being push back from the other two leaflets with different orientations at the same time. The model is nonlinear since the area of the aortic wall and aortic leaflets are all different, which causes the push forces and push back forces between leaflets are different. Therefore, it is normal to have an oscillation results in all the residual figures.

To have a clear view of the converge, we only export the last 50 steps of model running.

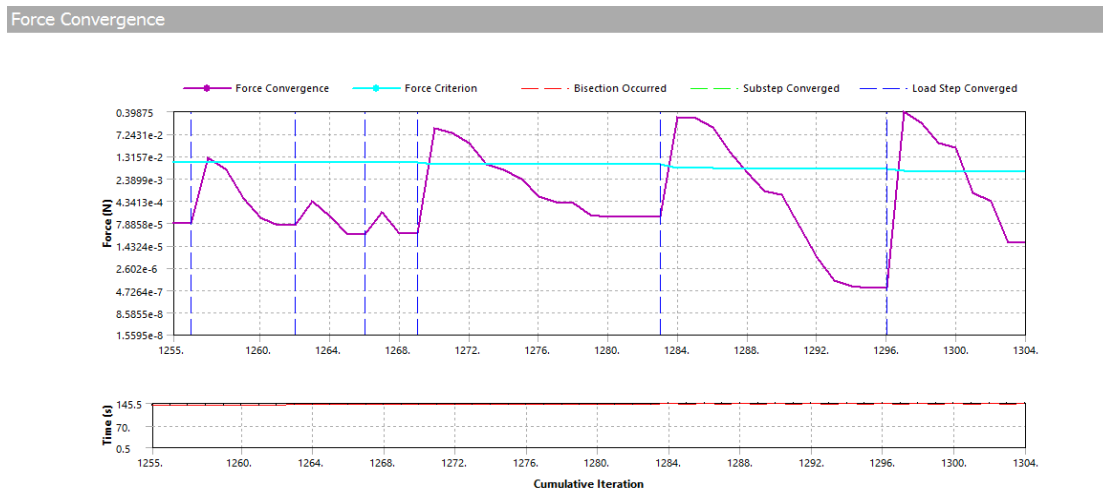


Figure 87 Force residual converge of aortic root model in 50 points view

The forces converge figure shows that force converges line fluctuated up and down with the force criterion, and it converges at every step. All the information between two blue dash line illustrates the converge situation at this steps. Substeps converge can not observe at most of the steps, but it appears during few steps at first half period which are hard to converge (from vivo simulation, this part is the model contacting process).

'fully iteration' option is required. This model has large numbers of iteration, which means converge process is computationally expensive. The model's iteration growth at each converges step, which is the key thing to force the residual (such as force, displacement) curve back under the criterion. Finally, the model achieves marginally converged with residual oscillated at a certain range.

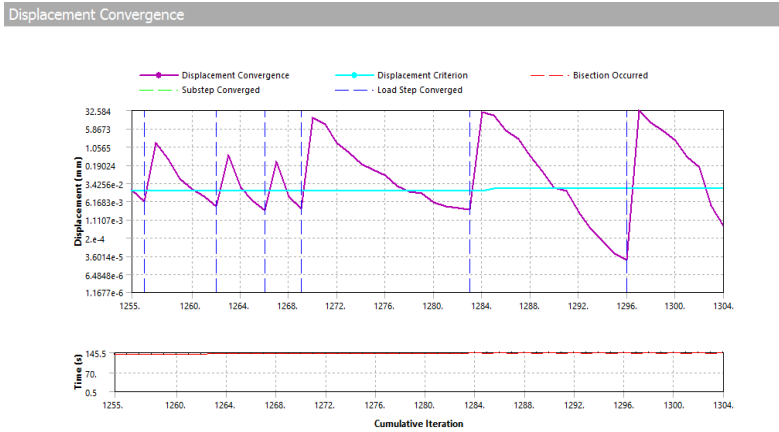


Figure 88 Displacement residual converge of aortic root model in 50 points view

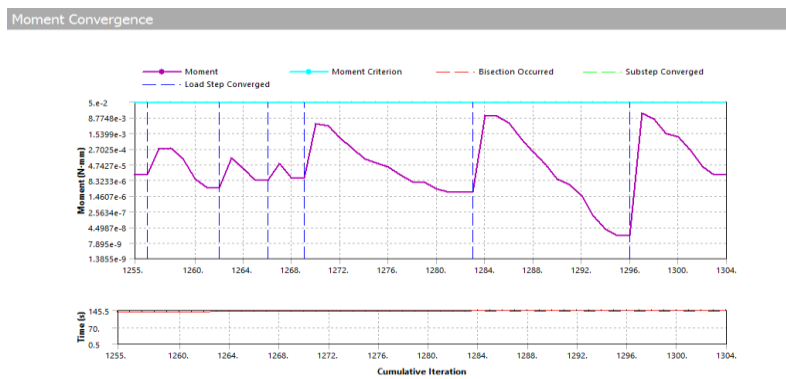


Figure 89. Moment residual converge of aortic root model in 50 points view

It can be observed that model converge line fluctuated at the same time, which means the figure converge line has the same feature in different types of converge figure. However, different converge figure has different criterions. The aortic root model only can converge with all the criterion are satisfied.

5.2.2 Maximum stress and strain

Table 11 Maximum and minimum aortic leaflet stress and strain value						
	RC Leaflet		LC Leaflet		NC Leaflet	
	Max	Min	Max	Min	Max	Min
Strain	4.04E-01	9.85E-05	2.28E-01	1.56E-04	2.73E-01	1.91E-04
Stress (MPa)	0.864	1.32E-04	1.03	2.93E-04	1.19	1.40E-04

The maximum stress and strain value (highlight in the red) located at the different leaflets and the location. The maximum strain for RC leaflet and LC leaflet is at the point that leaflets connecting to commissure, while the peak value for NC leaflet addressed in connection of hinge line. The three maximum stress value of leaflets are located at the attachment region of leaflets. All the maximum stresses and strains are given from the step or one step later of the highest pressure.

It can be found maximum strain value happen in a different location depending on leaflets (Figure 91), but the minimum value all appear close to the free margin. Strains can be found uniform distributed at the belly and contact face. Strain concentrates at the connection of free margin and hinge line. This concentration area has large displacement, since leaflet permits large deformation at the circumferential orientation (Vesely and Noseworthy, 1992).

Belly area has higher strain value than the contact area. The aortic pressure at belly area has a higher value than the ventricular pressure at this moment and there is no object to stop belly moving, so tissue at belly area stretches to the ventricular side and generates displacement.

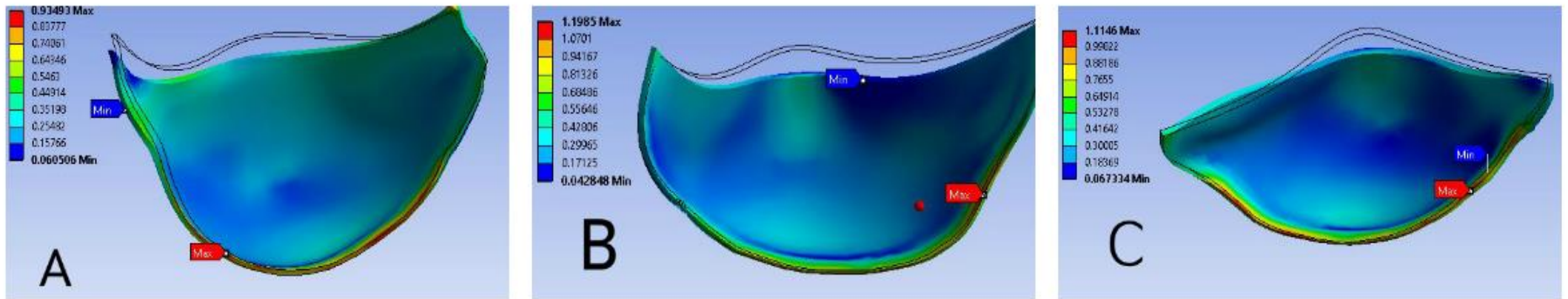


Figure 90 Aortic leaflets and their maximum stresses (A. RC leaflet B. NC leaflet C. LC leaflet Unit: MPa)

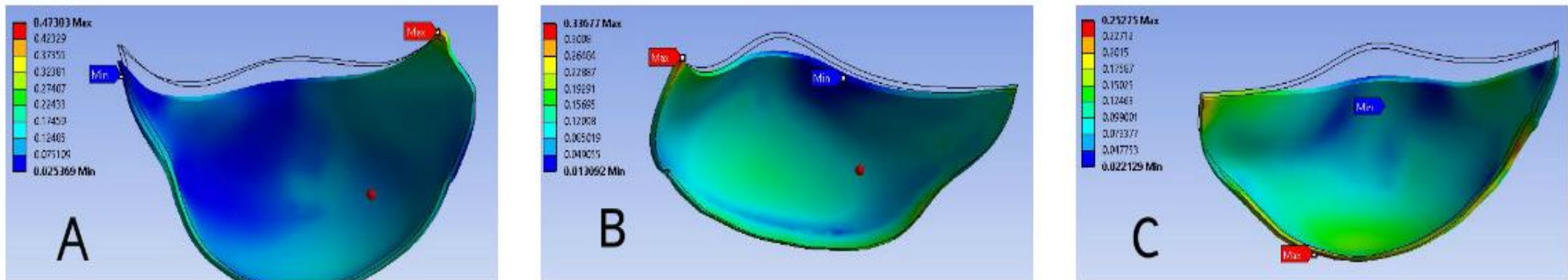


Figure 91 Aortic leaflets and their maximum strains (A. RC leaflet B. NC leaflet C. LC leaflet)

Table 12 Maximum stress and strain value of aortic wall

	Stress (MPa)		Strain	
	Maximum	Minimum	Maximum	Minimum
Value	0.12193	1.28E-05	0.26444	3.05E-05
Location	Button of NC leaflet	Button of LC leaflet	Commissure of NC to RC	Button of LC leaflet

The minimum value of stress and strain data appears at the similar places for aortic wall simulation results. The maximum value of stress is given in different address. Stress and strain representation is asymmetric in the three sinuses of the aortic wall. The maximum stress occurs in the non-coronary leaflet and closes to commissure. However, the distribution of the stress and strain in the aortic three sinuses looked very similar.

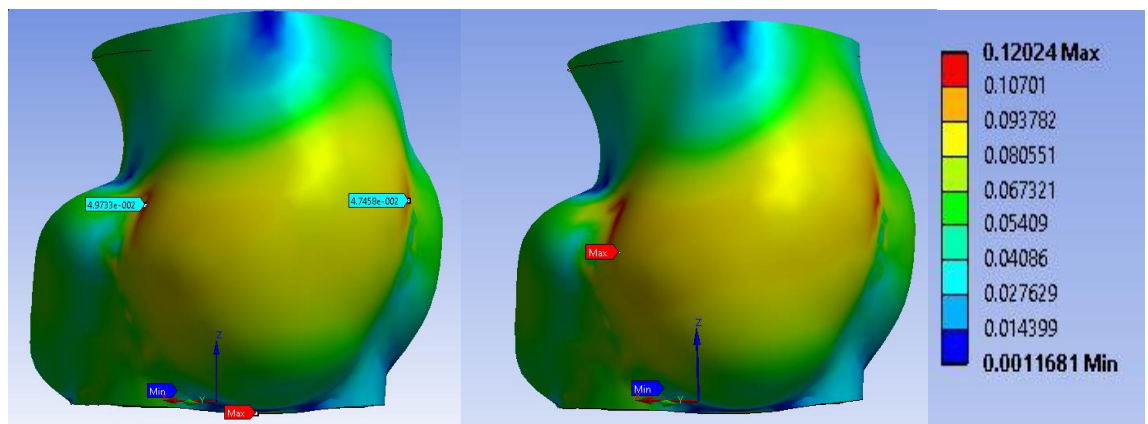


Figure 92 Stress (left) and strain (right) distribution at the surface of the non-coronary sinus

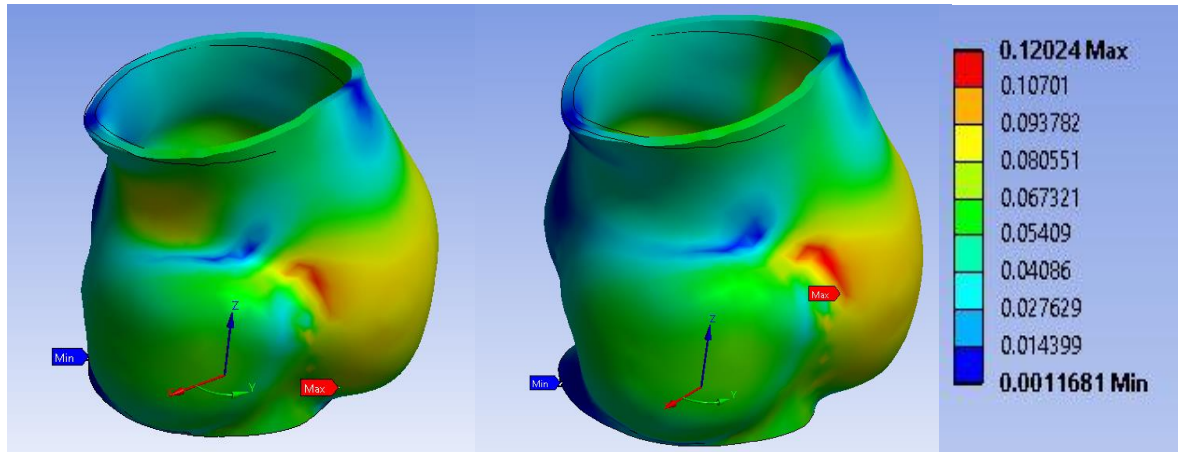


Figure 93 Stress (left) and strain (right) distribution at the surface of the right coronary sinus

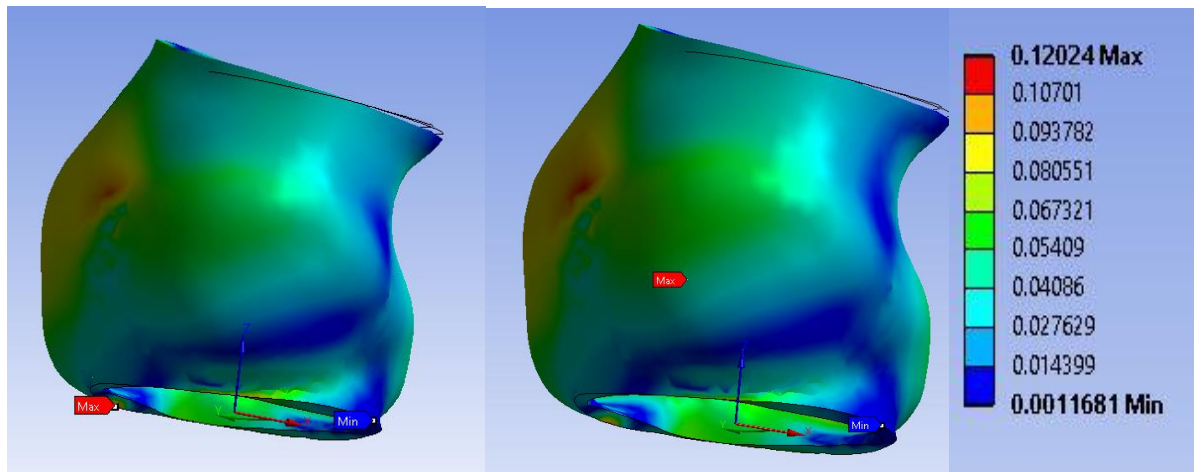


Figure 94 Stress (left) and strain (right) distribution at the surface of the left coronary sinus

Chapter 6 Discussion

6.1 Geometry

Geometry in this model is given by CT image, but the leaflets are given by fitting surface. The limited resolution of CT image increases manual effort during image processing. This manual process may introduce extra errors. The model is verified by taking the diameter of sino-tubular junction as a reference value and comparing other potential numbers corresponding to the length of sino-tubular junction.

Results showed the dilatator aortic root almost matched the ideal reference parameters from Swanson and Clark (1974).

In terms of angle measurement, the average value of angles is close to the ideal model (De Hart et al., 2002), but individual angles exhibited large variation at different leaflets. This is because that the geometry in three sinuses of aortic root model is not uniformed and the dilatation disease accelerated the distortion of geometry (Grande et al., 2000).

Non-coronary leaflet normally is the smallest leaflet, and the other two leaflets are expected to have similar area values from each other and less area than the non-coronary leaflet (Poutanen et al., 2006). In this study, the right coronary leaflet has a dramatically larger area compared to the other two leaflets. Disease at aortic root may be the cause of this issue.

6.2 Material property and boundary condition

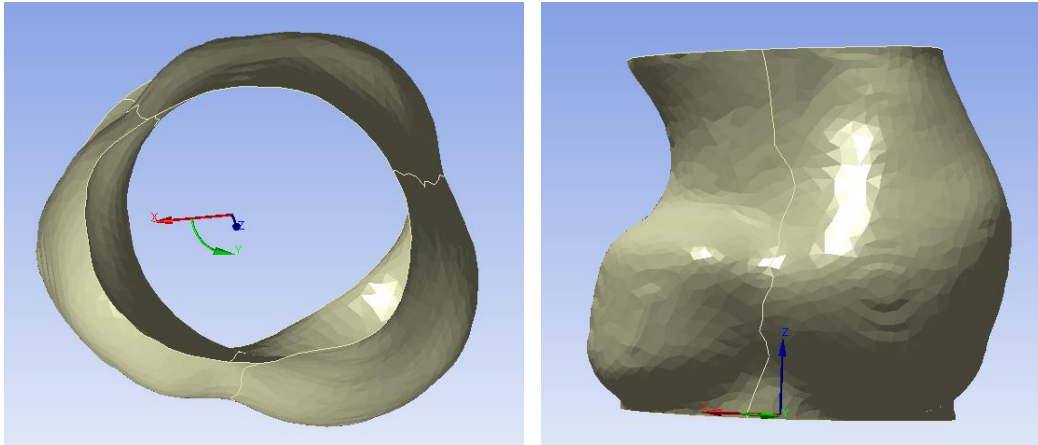


Figure 95 Aortic root with cylinder coordinate system. The original point of the aortic root is located at the central point of button plane of the whole aortic root.

The material property of aortic leaflet is well aligned at the desired orientation. It has been widely acknowledged that the leaflets module value is highly different in circumferential and radial orientation.

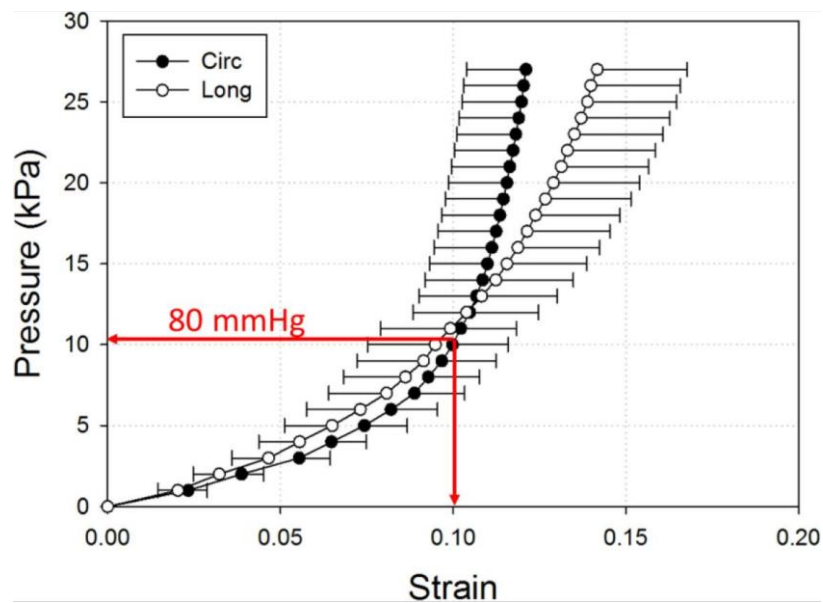


Figure 96 Stress – strain curve in aortic leaflet (Wang et al., 2012)

The tissue is linear elastic tissue. This model established a model in the almost contact position, which means stress-strain curve is near the elastic material performance. As mentioned before, studies showed the material properties of aortic leaflets are non-linear and anisotropic. Even through tissue properties is

given from circumferential and radial orientation separately, the real aortic leaflets are multi-layer tissues (Bäck et al., 2013). Lamina model with more than one layer and having different material properties in each layer can better represent the characteristics of the aortic leaflet (Kim, 2009). Further studies are expected to have a multi-layer tissue at aortic leaflets.

The geometry of aortic root is close to cylinder tube, so the cylindered coordinate system is beneficial for assigning material properties and mesh alignment. The vertical direction of the aortic leaflet is called 'radial orientation' and the horizontal direction of aortic root named 'circumferential orientation'.

The inherent shell contact results in a high strain in the contacts between aortic leaflets and aortic wall; however, this does not affect the results of this simulation.

6.3 Model convergence

Multi-contact increases the complexity and effort for model convergence.

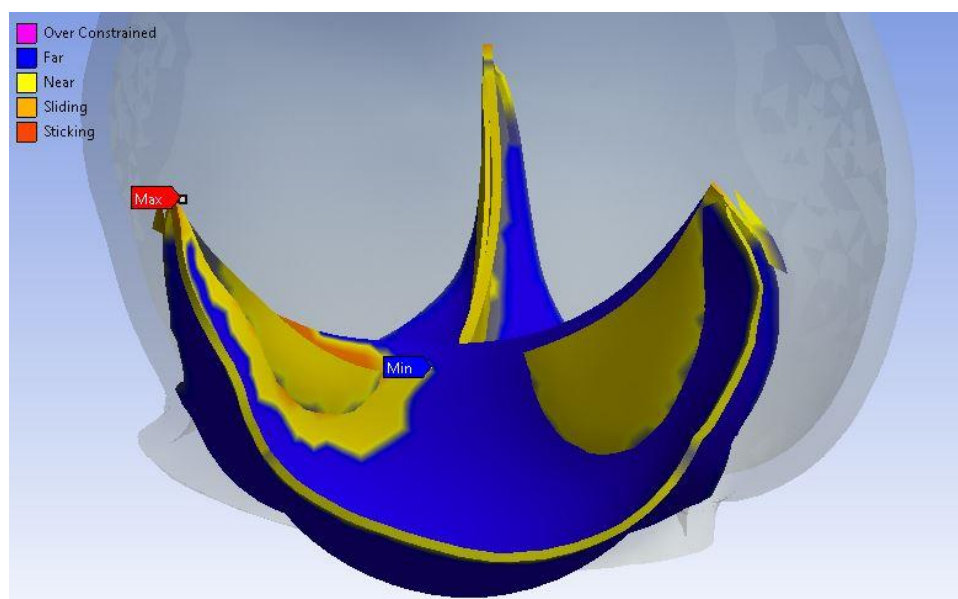


Figure 97 Contact status at leaflet including three leaflets view

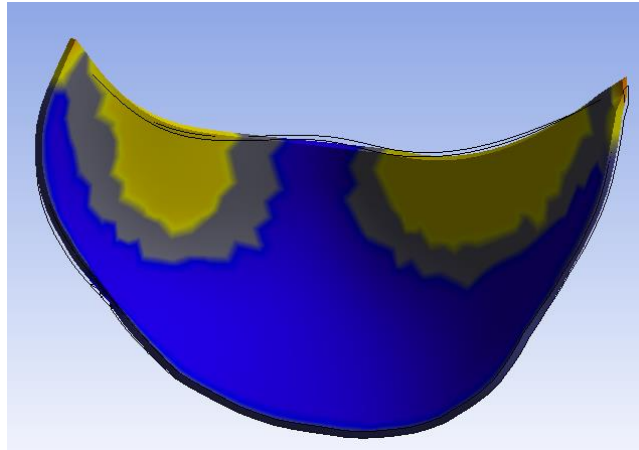


Figure 98 Contact status of single leaflet view

Yellow parts at leaflets are the contact areas that detected and areas that sliding against each other (figure 97). Contact status in single leaflet view shows a similar status to the situation in Grande et al. (1997). Coaptation region is located in the top half of the three leaflets.

It can be clearly seen penetration in the three leaflets view (figure 97). The results showed the penetration is stable at 0.2 mm (consider the thickness of leaflet is 0.5mm), but the penetration in figure 97 shows more extreme penetration when visualisation. The reason for this visual error may come from 'no shell thickness consideration' assignment, so they counting the penetration will use the distance to shell mid surfaces.

Moreover, it can be observed that most of the low quality mesh are located at mesh connection parts (figure 90), which is hinge line and leaflet attachment.

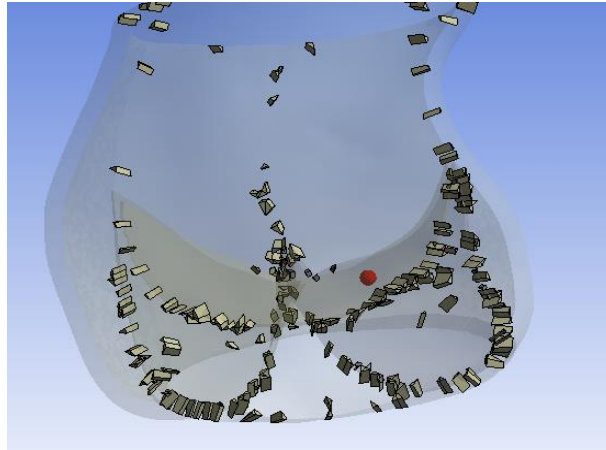


Figure 99 Low quality mesh located at leaflet attachment and the hinge line of aortic root

It turns out that mesh connection distorts mesh geometry to match the connection at the aortic root to the aortic leaflets.

In the second type of model geometry generation, the model cannot converge when contact at the edge was recognized. High stresses occurred at contact free edge of leaflets. However, a single leaflet can have a simulation running from closed state to the open state. The whole simulation cannot converge since the leaflets contact area is too small, so the overlaps (most overlaps appears at the top edge of leaflets) between leaflets generates high stress. This method normally used in an ideal model generation (Mohammadi et al., 2009), since overlap problem can be excluded by a proper parameter assignment.

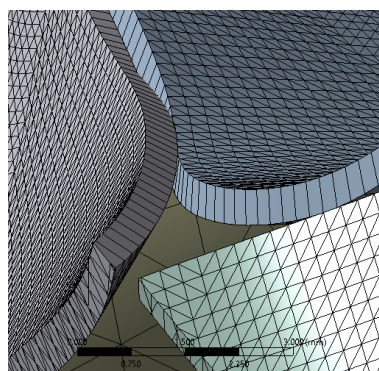


Figure 100 initial overlapping body in the second model

The leaflet contact initial data in the second model reconstruction has a large number of warning information compare to the third model. This is mainly because all the leaflets are hard to match the fitting leaflet to the curve surface of the aortic root. It is hard to ensure that the surface of leaflets has nice mapping mesh and that leaflets attach to the aortic wall properly at the same time.

The mesh at leaflets is easy to control and adjust when using virtual leaflets, but the model is hard to converge with rough contact. Therefore, this method is good for building an ideal model (De Hart et al., 2002), but poorer performance in the patient specific model establishment.

Name	Contact Side	Type	Status	Number Contacting	Penetration (mm)	Gap (mm)	Geometric Penetration (mm)	Geometric Gap (mm)	Resulting Pinball (mm)	Normal Stiffness (N/mm ²)	Real Constant
Frictionless - NC Virtualvalve To LC Virtualvalve	Contact	Frictionless	Near Open	0.	0.	0.82659	0.	N/A	1.	0.	5.
Frictionless - NC Virtualvalve To LC Virtualvalve	Target	Frictionless	Near Open	0.	0.	0.9179	0.	N/A	1.	0.	6.
Frictionless - LC Virtualvalve To RC Virtualvalve	Contact	Frictionless	Closed	19.	9.2166e-002	0.	0.	0.73522	1.	6.885e-003	7.
Frictionless - LC Virtualvalve To RC Virtualvalve	Target	Frictionless	Closed	11.	0.24334	0.	0.	1.1707	1.	6.885e-003	8.
Frictionless - RC Virtualvalve To NC Virtualvalve	Contact	Frictionless	Near Open	0.	0.	6.7205e-002	0.	0.56721	1.	0.	9.
Frictionless - RC Virtualvalve To NC Virtualvalve	Target	Frictionless	Near Open	0.	0.	8.8918e-002	0.	0.58892	1.	0.	10.
Bonded - RC Virtualvalve To Aortic Wall	Contact	Bonded	Closed	31.	7.8886e-031	0.	0.80762	0.	1.	N/A	11.
Bonded - RC Virtualvalve To Aortic Wall	Target	Bonded	Inactive	N/A	N/A	N/A	N/A	N/A	N/A	N/A	0.
Bonded - LC Virtualvalve To Aortic Wall	Contact	Bonded	Closed	31.	7.8886e-031	0.	0.2558	0.	1.	N/A	13.
Bonded - LC Virtualvalve To Aortic Wall	Target	Bonded	Inactive	N/A	N/A	N/A	N/A	N/A	N/A	N/A	0.
Bonded - NC Virtualvalve To Aortic Wall	Contact	Bonded	Closed	31.	7.8886e-031	0.	0.47322	2.2997e-003	1.	N/A	15.
Bonded - NC Virtualvalve To Aortic Wall	Target	Bonded	Inactive	N/A	N/A	N/A	N/A	N/A	N/A	N/A	0.
Bonded - RC Virtualvalve To Aortic Wall	Contact	Bonded	Closed	31.	7.8886e-031	0.	0.24411	0.	1.	N/A	17.
Bonded - RC Virtualvalve To Aortic Wall	Target	Bonded	Inactive	N/A	N/A	N/A	N/A	N/A	N/A	N/A	0.
Bonded - LC Virtualvalve To Aortic Wall	Contact	Bonded	Closed	31.	7.8886e-031	0.	0.45176	0.	1.	N/A	19.
Bonded - LC Virtualvalve To Aortic Wall	Target	Bonded	Inactive	N/A	N/A	N/A	N/A	N/A	N/A	N/A	0.
Bonded - NC Virtualvalve To Aortic Wall	Contact	Bonded	Closed	31.	7.8886e-031	0.	0.77432	0.	1.	N/A	21.
Bonded - NC Virtualvalve To Aortic Wall	Target	Bonded	Inactive	N/A	N/A	N/A	N/A	N/A	N/A	N/A	0.

Color Legend

Red	The contact status is open but the type of contact is meant to be closed. This applies to bonded and no separation contact types.
Yellow	The contact status is open. This may be acceptable.
Orange	The contact status is closed but has a large amount of gap or penetration. Check penetration and gap compared to pinball and depth.
Gray	Contact is inactive. This can occur for MPC and Normal Lagrange formulations. It can also occur for auto asymmetric behavior.

Figure 101 Initial contact body assignment in second geometry model have a lot of warnings. Even though all the warning is accessible, the figure shows the assemble are not in a desire contact status.

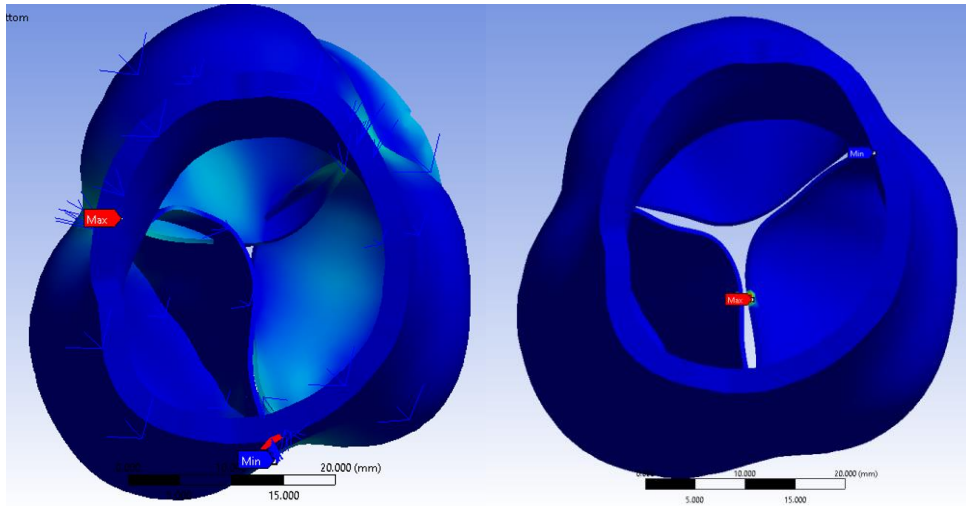


Figure 102 Second model can run when leaflets do not detect contact (left) and the aortic leaflet simulation failed with high stress at contact parts of two leaflets (right)

6.4 Mechanical results

6.4.1 Aortic leaflet

Strains and stresses value in the leaflets and aortic root are much higher than that of the normal value in Grande et al. (1997). However, Grande et al. (1997) proved that the stress peak increasing dramatically as the dilatation of aortic root become serious. The most significant increasing is at leaflet attachment area. According to Grande et al. (1997), 50% dilatation aortic root has peak stress value over 1.2 MPa at the attachment while normal aortic root only has peak stress near 0.3 MPa. Peak stress value increases four times than normal when the diameter of aortic root only increases 50%. In terms of this study, the initial model has almost two times diameter of annulus than normal aortic root, the peak stress is 1.19 MPa at the attachment of Non- Coronary leaflet.

The maximum strain value appeared at commissure. From Grande et al. (1997), the maximum strain value is expected to located at coaptation area and the peak strain at 50% dilatation aortic root is close 0.35. The peak strain value for this model is 0.4, which is reasonable considering the situation of dilatation is more than 50%. The maximum strain may be caused by the distorted mesh.

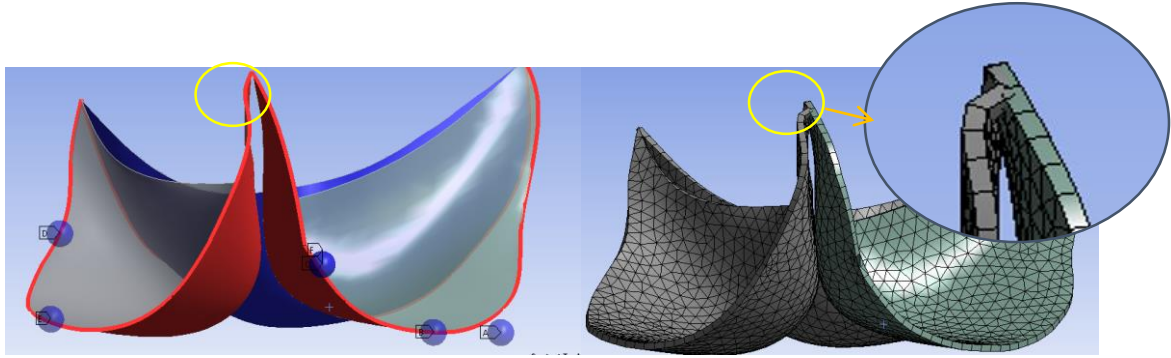


Figure 103 The initial geometry of commissure(left) and the meshed bodies at commissure (right)

The mesh distortion may result in leaflets too closed, so mesh defeature automatically changes geometry position. To avoid this, mesh quality can be developed by increasing reference value and reduce defeature tolerance.

6.4.2 Aortic root

This results of maximum stress 0.12193 MPa is close to value in Grande et al. (1997), which is near 0.13 MPa, but strain value 0.26444 does not match. From the distribution of stresses and strains at three leaflets, it can be found that right coronary leaflet has highest stress and strain. These results match the study from Grande. Moreover, the maximum strain is observed at the commissure. The non-coronary leaflet has maximum stress and strain distribution since it does not have ostium. Ostium has the ability to release to strain value.

The maximum stress value located at the bottom of the non-coronary leaflet, which may be caused by model rebuilding and distorted mesh.

Strain value at the aortic root is highly variable with location and surface curvature (Clark and Finke, 1974b). This patient has highly asymmetric aortic leaflets and non-uniform geometry of the aortic root. Therefore, it is possible to have difference value in strain. Moreover, Grande assigned material to diversity thicknesses values at a different parts of leaflets and aortic root, while our model reduces thickness to a constant value. Thickness has been proved that has effects to strain value as well (Clark and Finke, 1974a).

Chapter 7 Conclusion

Patient specific model in the cardiovascular simulation is a new area to explore. To apply this method in aortic root aneurysm researches, a fully repeatable model establishment is required. This study using different aortic root model establishment method to build patient specific aortic root model, and explore the optional assignment to ensure the converge of model simulation.

7.1 Method of geometry reconstruction

Patient specific model is given from CT image data. Due to the inherent feature of CT image theory and the resolution of the image, aortic root reconstruction can not be given directly by segmenting aortic leaflet from the CT image. However, this problem has been faced by most of the patient specific modelling of the aortic root. Instead of having high quality image data from processed real aortic root and scan in MRI image, most of the studies choose to have a fitting leaflet and a real feature of aortic wall geometry (Wang et al., 2012). Leaflet fitting method varies as simulation environment changing and software choosing.

In this study, three geometry construction methods are explored and compared. The first method generated a model from the solid multi-faces surface. This model can precisely repeat the main feature of leaflet surface, but this model need a large amount of manual effort to modify, and geometry in the multi-faces surface is hard to generate meshes in the ANSYS 15.0. The second method created a surface from several key points of aortic leaflets. This method provides uniform edges at leaflets, which makes leaflets are easy to be modified and meshed. However, the virtual leaflet is too ideal, and the leaflet straight line edge is hard to attach to the aortic wall. The large gap increases the computation effort and leads to model unconverted. Apart from the undesired gap at the contact between the aortic leaflet and aortic wall, this fitting method also hard to detect contact with the contact face in initial geometry is too small. The final method is given leaflet from the spline line. This method combines the advantage of the other two methods. The feature of leaflets is more patient specific and the generated leaflet is more easy to modified.

Geometry validation measured STJ annulus and other important angles from 3-D image data. Then, comparing those measurement value from method from Swanson and Clark (1974). The geometry is valid.

7.2 Method of simulation assignment

The simulation process in FE problem only converges when the material properties and boundary conditions were assigned properly. This study includes more than one contact faces and each leaflet contact to three different bodies with distinct formulation (MPC formula for a leaflet to aortic wall contact and Augmented Lagrange for a leaflet to leaflet contact). Moreover, the full shell faces asymmetric contact increases the difficulty of converging. Projection normal detected method is enquired in this study and mesh connection method is introduced to increase the stability of constrain.

The model assignment is valid by comparing the simulation results to the previous maximum stress and strain value at aortic leaflets and aortic root.

Reference

- ANSYS 2013. ANSYS Mechanical APDL Basic Analysis Guide. *ANSYS® Academic Research*, 15.
- ASTORINO, M., GERBEAU, J.-F., PANTZ, O. & TRAORÉ, K.-F. 2009. Fluid–structure interaction and multi-body contact: Application to aortic valves. *Computer Methods in Applied Mechanics and Engineering*, 198, 3603-3612.
- ASTORINO, M., HAMERS, J., SHADDEN, S. C. & GERBEAU, J. F. 2012. A robust and efficient valve model based on resistive immersed surfaces. *International journal for numerical methods in biomedical engineering*, 28, 937-959.
- BÄCK, M., GASSER, T. C., MICHEL, J.-B. & CALIGIURI, G. 2013. Biomechanical factors in the biology of aortic wall and aortic valve diseases. *Cardiovascular Research*, 99, 232-241.
- BICKERSTAFF, L. K., PAIROLERO, P. C., HOLLIER, L. H., MELTON, L. J., VAN PEENEN, H. J., CHERRY, K. J., JOYCE, J. W. & LIE, J. T. 1982. Thoracic aortic aneurysms: a population-based study. *Surgery*, 92, 1103-8.
- BROWN, J. M., O'BRIEN, S. M., WU, C., SIKORA, J. A. H., GRIFFITH, B. P. & GAMMIE, J. S. 2009. Isolated aortic valve replacement in North America comprising 108,687 patients in 10 years: Changes in risks, valve types, and outcomes in the Society of Thoracic Surgeons National Database. *The Journal of Thoracic and Cardiovascular Surgery*, 137, 82-90.
- CARMODY, C. J., BURRIESCI, G., HOWARD, I. C. & PATTERSON, E. A. An approach to the simulation of fluid–structure interaction in the aortic valve. *Journal of Biomechanics*, 39, 158-169.
- CHONG, W.-Y., WONG, W. H., CHIU, C. S. & CHEUNG, Y.-F. 2006. Aortic root dilation and aortic elastic properties in children after repair of tetralogy of Fallot. *The American journal of cardiology*, 97, 905-909.
- CLARK, R. & FINKE, E. 1974a. Scanning and light microscopy of human aortic leaflets in stressed and relaxed states. *The Journal of thoracic and cardiovascular surgery*, 67, 792-804.
- CLARK, R. E. & FINKE, E. H. 1974b. Scanning and light microscopy of human aortic leaflets in stressed and relaxed states. *J Thorac Cardiovasc Surg*, 67, 792-804.
- CONTI, C. A., DELLA CORTE, A., VOTTA, E., DEL VISCOVO, L., BANCONE, C., DE SANTO, L. S. & REDAELLI, A. 2010a. Biomechanical implications of the congenital bicuspid aortic valve: a finite element study of aortic root function from in vivo data. *The Journal of Thoracic and Cardiovascular Surgery*, 140, 890-896. e2.
- CONTI, C. A., VOTTA, E., DELLA CORTE, A., DEL VISCOVO, L., BANCONE, C., COTRUFO, M. & REDAELLI, A. 2010b. Dynamic finite element analysis of the aortic root from MRI-derived parameters. *Medical Engineering & Physics*, 32, 212-221.
- DE HART, J., PETERS, G., SCHREURS, P. & BAAIJENS, F. 2002. Fluid-Structure Interaction in the Aortic Heart Valve: a three-dimensional computational analysis.
- DELLIMORE, K., KEMP, I., SCHEFFER, C., WEICH, H. & DOUBELL, A. 2013. The influence of leaflet skin friction and stiffness on the performance of bioprosthetic aortic valves. *Australasian Physical & Engineering Sciences in Medicine*, 36, 473-486.
- FREEMAN, L. A., YOUNG, P. M., FOLEY, T. A., WILLIAMSON, E. E., BRUCE, C. J. & GREASON, K. L. 2013. CT and MRI assessment of the aortic root and ascending aorta. *American Journal of Roentgenology*, 200, W581-W592.

- GNYANESHWAR, R., KUMAR, R. K. & BALAKRISHNAN, K. R. 2002. Dynamic analysis of the aortic valve using a finite element model. *The Annals of thoracic surgery*, 73, 1122-1129.
- GRANDE-ALLEN, K., COCHRAN, R., REINHALL, P. & KUNZELMAN, K. 2001a. Mechanisms of aortic valve incompetence: finite-element modeling of Marfan syndrome. *The Journal of thoracic and cardiovascular surgery*, 122, 946-954.
- GRANDE-ALLEN, K. J., COCHRAN, R. P., REINHALL, P. G. & KUNZELMAN, K. S. 2000. Re-creation of sinuses is important for sparing the aortic valve: a finite element study. *The Journal of Thoracic and Cardiovascular Surgery*, 119, 753-763.
- GRANDE-ALLEN, K. J., COCHRAN, R. P., REINHALL, P. G. & KUNZELMAN, K. S. 2001b. Finite-element analysis of aortic valve-sparing: influence of graft shape and stiffness. *IEEE Transactions on Biomedical Engineering*, 48, 647-659.
- GRANDE, K. J., COCHRAN, R. P., REINHALL, P. G. & KUNZELMAN, K. S. 1997. Stress Variations in the Human Aortic Root and Valve: The Role of Anatomic Asymmetry. *Annals of Biomedical Engineering*, 26, 534-545.
- GRANDE, K. J., COCHRAN, R. P., REINHALL, P. G. & KUNZELMAN, K. S. 2000. Mechanisms of aortic valve incompetence: finite element modeling of aortic root dilatation. *The Annals of Thoracic Surgery*, 69, 1851-1857.
- HE, C. M. & ROACH, M. R. 1994. The composition and mechanical properties of abdominal aortic aneurysms. *Journal of vascular surgery*, 20, 6-13.
- HELSEN, J. A. & MISSIRLIS, Y. 2010. *Biomaterials: a Tantalus experience*, Springer Science & Business Media.
- HIRATZKA, L., BAKRIS, G., BECKMAN, J., BERSIN, R., CARR, V., CASEY JR, D., EAGLE, K., HERMANN, L., ISSELBACHER, E. & KAZEROONI, E. 2010. Guidelines for the diagnosis and management of patients with thoracic aortic disease: a report of the American College of Cardiology Foundation/American Heart Association Task Force on Practice Guidelines, American Association for Thoracic Surgery, American College of Radiology, American Stroke Association, Society of Cardiovascular Anesthesiologists, Society for Cardiovascular Angiography and Interventions, Society of Interventional Radiology, Society of Thoracic Surgeons, and Society for Vascular Medicine. *Circulation*, 121, e266-e369.
- ISSELBACHER, E. M. 2005. Thoracic and Abdominal Aortic Aneurysms. *Circulation*, 111, 816-828.
- JERMIHOV, P. N. 2013. Biomechanical implications of congenitally bicuspid aortic valves: a finite element analysis of patient-specific geometry.
- KAWEL-BOEHM, N., MACEIRA, A., VALSANGIACOMO-BUECHEL, E. R., VOGEL-CLAUSSEN, J., TURKBEY, E. B., WILLIAMS, R., PLEIN, S., TEE, M., ENG, J. & BLUEMKE, D. A. 2015. Normal values for cardiovascular magnetic resonance in adults and children. *J Cardiovasc Magn Reson*, 17, 29.
- KERENDI, F., GUYTON, R. A., VEGA, J. D., KILGO, P. D. & CHEN, E. P. 2010. Early Results of Valve-Sparing Aortic Root Replacement in High-Risk Clinical Scenarios. *The Annals of Thoracic Surgery*, 89, 471-478.
- KIM, H. S. 2009. Nonlinear multi-scale anisotropic material and structural models for prosthetic and native aortic heart valves.
- KOCH, T. M., REDDY, B. D., ZILLA, P. & FRANZ, T. 2010. Aortic valve leaflet mechanical properties facilitate diastolic valve function. *Computer Methods in Biomechanics and Biomedical Engineering*, 13, 225-234.
- KRUMMEN, D. E., OSHODI, G. & NARAYAN, S. M. 2010. Integrating State-of-the-Art Computational Modeling with Clinical Practice: The Promise of Numerical Methods. *Patient-Specific Modeling of the Cardiovascular System*. Springer.

- KUNZELMAN, K. S., GRANDE, K. J., DAVID, T. E., COCHRAN, R. & VERRIER, E. D. 1994. Aortic root and valve relationships: impact on surgical repair. *The Journal of Thoracic and Cardiovascular Surgery*, 107, 162-170.
- LABROSSE, M. R., BELLER, C. J., ROBICSEK, F. & THUBRIKAR, M. J. 2006. Geometric modeling of functional trileaflet aortic valves: development and clinical applications. *Journal of biomechanics*, 39, 2665-2672.
- LANSAC, E., LIM, H.-S., SHOMURA, Y., LIM, K. H., RICE, N. T., GOETZ, W. A. & DURAN, C. 2005. Aortic root dynamics are asymmetric. *J Heart Valve Dis*, 14, 400-407.
- LEYH, R. G., FISCHER, S., KALLENBACH, K., KOFIDIS, T., PETHIG, K., HARRINGER, W. & HAVERICH, A. 2002. High Failure Rate After Valve-sparing Aortic Root Replacement Using the "Remodeling Technique" in Acute Type A Aortic Dissection. *Circulation*, 106, I-229-I-233.
- LI, J., LUO, X. Y. & KUANG, Z. B. 2001. A nonlinear anisotropic model for porcine aortic heart valves. *Journal of Biomechanics*, 34, 1279-1289.
- LIM, K. H., CANDRA, J., YEO, J. H. & DURAN, C. M. 2004. Flat or curved pericardial aortic valve cusps: a finite element study. *J Heart Valve Dis*, 13, 792-7.
- MATURA, L. A., HO, V. B., ROSING, D. R. & BONDY, C. A. 2007. Aortic dilatation and dissection in Turner syndrome. *Circulation*, 116, 1663-1670.
- MEIRELLES, G. V., MANTOVANI, M., BRAILE, D. M., ARAÚJO FILHO, J. D. & ARAÚJO, J. D. 2007. Prevalence of abdominal aortic dilatation in patients aged 60 years or older with coronary disease. *Jornal Vasculiar Brasileiro*, 6, 114-123.
- MOHAMMADI, H., BAHRAMIAN, F. & WAN, W. 2009. Advanced modeling strategy for the analysis of heart valve leaflet tissue mechanics using high-order finite element method. *Med Eng Phys*, 31, 1110-7.
- NATAF, P. & LANSAC, E. 2006. Dilation of the thoracic aorta: medical and surgical management. *Heart*, 92, 1345-1352.
- NICOSIA, M., KASALCO, J., COCHRAN, R., EINSTEIN, D. & KUNZELMAN, K. 2002. Biaxial mechanical properties of porcine ascending aortic wall tissue. *The Journal of heart valve disease*, 11, 680-6; discussion 686-7.
- OYSU, C. 2007. Finite element and boundary element contact stress analysis with remeshing technique. *Applied Mathematical Modelling*, 31, 2744-2753.
- POUTANEN, T., TIKANOJA, T., SAIRANEN, H. & JOKINEN, E. 2006. Normal Mitral and Aortic Valve Areas Assessed by Three- and Two-Dimensional Echocardiography in 168 Children and Young Adults. *Pediatric Cardiology*, 27, 217-225.
- RAGHAVAN, M., WEBSTER, M. W. & VORP, D. A. 1996. Ex vivo biomechanical behavior of abdominal aortic aneurysm: assessment using a new mathematical model. *Annals of biomedical engineering*, 24, 573-582.
- RAJIAH, P. 2013. CT and MRI in the Evaluation of Thoracic Aortic Diseases. *International journal of vascular medicine*, 2013.
- RANGA, A., MONGRAIN, R., BIADILAH, Y. & CARTIER, R. A compliant dynamic FEA model of the aortic valve. 12th IFToMM World Congress, Besançon, France, 2007.
- ROMAN, M. J., DEVEREUX, R. B., NILES, N. W., HOCHREITER, C., KLIGFIELD, P., SATO, N., SPITZER, M. C. & BORER, J. S. 1987. Aortic root dilatation as a cause of isolated, severe aortic regurgitation: prevalence, clinical and echocardiographic patterns, and relation to left ventricular hypertrophy and function. *Annals of Internal Medicine*, 106, 800-807.
- SAREMI, F. 2011. *Revisiting cardiac anatomy: a computed-tomography-based atlas and reference*, John Wiley & Sons.
- SCHWARTZ, M. L., GAUVREAU, K., DEL NIDO, P., MAYER, J. E. & COLAN, S. D. 2004. Long-term predictors of aortic root dilation and aortic regurgitation after arterial switch operation. *Circulation*, 110, II-128-II-132.

- SIEVERS, H.-H. & SCHMIDTKE, C. 2007. A classification system for the bicuspid aortic valve from 304 surgical specimens. *The Journal of Thoracic and Cardiovascular Surgery*, 133, 1226-1233.
- SMUTS, A. N., BLAINE, D. C., SCHEFFER, C., WEICH, H., DOUBELL, A. F. & DELLIMORE, K. H. 2011. Application of finite element analysis to the design of tissue leaflets for a percutaneous aortic valve. *J Mech Behav Biomed Mater*, 4, 85-98.
- SONCINI, M., VOTTA, E., ZINICCHINO, S., BURRONE, V., MANGINI, A., LEMMA, M., ANTONA, C. & REDAELLI, A. 2009a. Aortic root performance after valve sparing procedure: A comparative finite element analysis. *Medical Engineering & Physics*, 31, 234-243.
- SONCINI, M., VOTTA, E., ZINICCHINO, S., BURRONE, V., MANGINI, A., LEMMA, M., ANTONA, C. & REDAELLI, A. 2009b. Aortic root performance after valve sparing procedure: a comparative finite element analysis. *Med Eng Phys*, 31, 234-43.
- SWANSON, W. M. & CLARK, R. E. 1974. Dimensions and geometric relationships of the human aortic valve as a function of pressure. *Circulation research*, 35, 871-882.
- TRIMARCHI, S., NIENABER, C. A., RAMPOLDI, V., MYRMEL, T., SUZUKI, T., MEHTA, R. H., BOSSONE, E., COOPER, J. V., SMITH, D. E., MENICANTI, L., FRIGIOLA, A., OH, J. K., DEEB, M. G., ISSELBACHER, E. M. & EAGLE, K. A. 2004. Contemporary results of surgery in acute type A aortic dissection: The International Registry of Acute Aortic Dissection experience. *The Journal of Thoracic and Cardiovascular Surgery*, 129, 112-122.
- TU, J., INTHAVONG, K. & WONG, K. K. L. 2015. *Computational Hemodynamics—Theory, Modelling and Applications*, Springer.
- VESELY, I. & NOSEWORTHY, R. 1992. Micromechanics of the fibrosa and the ventricularis in aortic valve leaflets. *Journal of Biomechanics*, 25, 101-113.
- WANG, Q., SIROIS, E. & SUN, W. 2012. Patient-Specific Modeling of Biomechanical Interaction in Transcatheter Aortic Valve Deployment. *Journal of Biomechanics*, 45, 1965-1971.
- WONG, K. K., TU, J., KELSO, R. M., WORTHLEY, S. G., SANDERS, P., MAZUMDAR, J. & ABBOTT, D. 2010. Cardiac flow component analysis. *Med Eng Phys*, 32, 174-88.